organics

MDPI

Review

Architecture of Molecular Logic Gates: From Design to Application as Optical Detection Devices

Gleiston G. Dias * and Francielly T. Souto

Departamento de Química, Universidade Federal de Santa Catarina, UFSC, Florianópolis 88040-900, SC, Brazil; f.t.souto@posgrad.ufsc.br

* Correspondence: gleiston.dias@posgrad.ufsc.br

Abstract: Three decades after A. P. de Silva's seminal paper introduced the concept of logic gates at the molecular level, the field of molecular logic gates (MLGs) has witnessed significant advancements. MLGs are devices designed to perform logical operations, utilizing one or more physical or chemical stimulus signals (inputs) to generate an output response. Notably, MLGs have found diverse applications, with optical detection of analytes emerging as a notable evolution of traditional chemosensors. Organic synthesis methods are pivotal in crafting molecular architectures tailored as optical devices capable of analyte detection through logical functions. This review delves into the fundamental aspects and physical–chemical properties of MLGs, with a particular emphasis on synthetic strategies driving their design.

Keywords: molecular logic gates; chemosensors; chemodosimeters; lab-on-a-molecule; optical devices; analyte sensing; supramolecular analytical chemistry

1. Introduction

The investigation of the chemical composition of matter has long been a subject of broad interest. Nowadays, this interest has become more of a case of necessity. The constant threat of chemical contamination of soil, air, water, food, beverages, and cosmetics has threatened human security. In this context, scientists have devoted countless efforts to developing analytical tools capable of detecting and quantifying different chemical species. The efficiency of these tools is directly linked to their ability to detect and quantify analytes in low concentration (ppm or ppb) quickly, selectively, and inexpensively. The World Health Organization states that an optical detection device should be affordable, sensitive, specific, user-friendly, rapid/robust, equipment-free, and deliverable (ASSURED) [1,2].

Organic and analytical chemists have joined forces, in an interdisciplinary environment, to develop optical detection sensors for the selective recognition of an analyte. Organic synthesis plays a crucial role as a tool for the development of sensitive materials in chemical sensors [3–5]. These materials encompass functionalized polymeric materials, nanomaterials, or simply molecular ligands, as long as they exhibit affinity toward specific analytes and translate this affinity into analytically useful signals [6]. In the case of optical chemical sensors, it is evident that the chemical environment influences the optical properties of chromophores and fluorophores. Changes in pH, solvent composition, oxygen presence, and the introduction of analytes, which can be neutral, radical, cationic, or anionic, are some examples of perturbations that can induce significant alterations in the photophysical behavior of such devices [5,7,8]. Under this perspective, analytical chemistry addresses qualitative and quantitative analyses to process this sign and determine the chemical composition by recognizing these analytes [9,10].

The design of these compounds has evolved over the last few decades to increase their efficiency. One of the most modern approaches is the concept of molecular logic gates (MLGs)—molecules capable of performing logical operations based on one or more

check for updates

Citation: Dias, G.G.; Souto, F.T. Architecture of Molecular Logic Gates: From Design to Application as Optical Detection Devices. *Organics* **2024**, *5*, 114–162. https://doi.org/10.3390/org5020008

Academic Editor: Wim Dehaen

Received: 13 November 2023
Revised: 10 April 2024
Accepted: 30 May 2024
Published: 6 June 2024

physical or chemical stimulus signals (inputs) to produce an output response [11]. The study of MLGs is a new interdisciplinary field involving chemistry, physics, electronics, Boolean algebra, and computing concepts related to molecular structures [12].

We perceive logic gates as fundamental mathematical constructs that can be applied in different fields. This applicability extends to the field of chemistry, where notable advancements have been observed in recent years. Among the areas of particular interest, we highlight (1) the construction of nanodevices, especially nanoenzymes [13] or even functionalized carbon dots [14] used as MLGs. These systems are particularly interesting because of their increasingly small size, which lengthens the prediction of Moore's law. (2) Dynamic systems, which aim to generate a cascade system, are also exciting: a logical and modulable sensing output is responsible for subsequent movements/reactions. We envision such systems potentially resolving challenges in pharmacological or medical domains, such as managing pharmacokinetics for specific compounds [15,16]. (3) Regarding the application, MLGs focused on food security currently stand out not only because of the current global scenario and the growing concern about the indiscriminate use of pesticides and polluting agents but also because of the prospect of constructing multi-analyte detection systems. In this sense, detection systems based on combinatorial MLGs, such as lab-on-a-molecule [17], adders, and comparators [18], stand out.

Although the development of MLGs is structured in an interdisciplinary field, organic synthesis plays a primary role in elaborating most of these devices. In this sense, this review aims to discuss several synthetic strategies in planning MLGs associated with their applications and optical properties. Therefore, the examples discussed here were selected to bring a diversity of fluorescent cores, analytes, and optical responses. These examples were mainly selected based on the synthesis and diversity strategies in MLG classifications.

2. Analytes

2.1. Potential Toxic Metals

Exposure to potentially toxic metals, such as lead, cadmium, mercury, and aluminum, can result in severe health damage [19]. These exposures originate from different sources, mainly environmental pollution, contaminated air, soil, and water.

Among these toxic contaminants, mercury is notable for its damage to human health, even at low doses, compromising nervous, renal, cardiorespiratory, immune, and reproductive systems [20–22]. Its affinity with compounds containing thiol groups, present in proteins and enzymes, is the leading cause of the harmful effect on life [7–9]. Another example of a toxic metal is lead [23,24], whose prolonged exposure severely damages health, mainly through nerve system damage [25,26]. Cd^{2+} ions have a high affinity for metallothioneins in the liver, kidneys, intestines, and brain [27–29]. For this reason, this metal can also lead to several effects on the body. Despite aluminum's abundance in the earth's crust and its versatility in various applications [30,31], exposure to this metal may be associated with neurological disorders, such as Alzheimer's disease, osteomalacia, and breast cancer [32–34].

Other metals, such as nickel, copper, and zinc, are deemed essential micronutrients and play important roles in maintaining the healthy functioning of the human body [35]. Even so, the excessive accumulation of these substances can also compromise health. For instance, Ni^{2+} is crucial for biosynthesis and metabolism, but its excess may cause dermatitis, asthma, pneumonitis, disorders of the central nervous system, and cancer [36,37]. In excess, Cu^{2+}, fundamental in redox activity, can provoke amyloid precipitation and contribute to developing Wilson's, prion, and Parkinson's diseases [35,38–40]. Zinc accumulation in the human body can cause diabetes, epilepsy, brain, Alzheimer's, and Parkinson's disease [41–44].

2.2. Alkaline and Alkaline Earth Metals

Alkaline cations such as Na^{+} and K^{+}, predominantly found in saline water, are related to critical biological processes. These include regulating blood and body fluid homeostasis,

skeletal and smooth muscle, taste and pain sensation, and signal transduction in animals [45–50]. In excess in the human body, Na^+ is associated with various health issues, including water retention and hypertension [51]. Alteration of K^+ ions in the human system can provoke effects such as muscle cramps or weakness, diarrhea, dehydration, changes in heart rhythms, and others [52–56]. The deficiency of Ca^{2+}, present in the composition of teeth and bones, can result in osteoporosis. However, excessive amounts of calcium intake can result in muscle relaxation, kidney stones, and bone pain [57–59].

2.3. Anionic Species

Anions such as cyanide, fluoride, acetate, and phosphate, among many others, can also significantly interfere with different aspects of life. For instance, cyanide displays toxic effects by forming complexes with ferric ions in some enzymes' active sites. This reaction interferes with the electron transport chain, compromising the tissue's ability to utilize oxygen effectively [60,61]. Therefore, this anion can cause acute and systemic toxicity, leading to rapid cardiovascular collapse [60,62–64].

The fluoride (F^-) ion, added in toothpaste and drinking water to prevent dental caries, is associated with healthy bones, hair, and nails. However, excessive F^- intake can result in dental or skeletal fluorosis, renal lithiasis, and other disorders [65].

The acetate (AcO^-) anion is highly important due to its application as an indicator of organic decomposition in marine sediments [66,67], in controlling microbial growth, and as an additive in foods to extend shelf life and also to improve sensory properties [68,69]. Phosphates, used as fertilizer for agriculture, may exhibit risks to communities when used excessively [70], leading to the growth of algae and plants, hampering their use [71]. Consequently, excessive algae growth can decrease dissolved oxygen, ultimately resulting in the death of aquatic organisms.

Despite their relevance, the detection of anions poses greater complexity than cations. Designing anionic recognition sensors requires considering molecular geometry, stereochemistry, and energy-related properties, such as enthalpy, entropy, Gibbs free energy, and solvation [72,73]. In addition, anions such as HCO_3^-, NO_3^-, PO_4^{3-}, and HSO_4^- can exhibit different sizes and charges at various pH values, impacting their recognition and detection [74].

2.4. Neutral Species

The detection of ionic species by optical sensors relies on the interaction between electron-rich and electron-poor sites, involving or not chemical reaction. Therefore, detecting electrically neutral species represents a challenge in the sensing field [75]. Still, many sensors have been developed to identify and quantify neutral species, such as amines, warfare agents, and toxic volatile compounds, among many others [75–77]. Examples of target-neutral analytes include amino acids, which are essential for various metabolic processes and biological functions. Lysine (Lys), fundamental in the Krebs–Henseleit cycle and polyamine synthesis, plays a vital role in animal development [78,79]. Histidine (His) is essential for the active sites of many enzymes and functional proteins, and it controls the transmission of metallic elements in biological systems [80,81]. Tryptophan (Trp) is crucial for protein biosynthesis, animal growth, and plant development. The deficiency of certain amino acids can lead to various abnormalities [82].

Biogenic amines, which bear biologically active nitrogen, exhibit essential physiological functions, such as increased DNA, RNA, and protein synthesis and membrane stabilization [83,84]. However, their high concentration in food may indicate microbial contamination [85]. Chemical warfare agents, used to incapacitate people during conflict, threaten society's safety [86]. One example of these agents is phosgene ($COCl_2$), a gas capable of irritating the respiratory tract and even causing death [87,88].

3. Optical Detection Devices

From the pioneering studies of Pedersen [89,90], Lehn [91], and Cram [92], a new era emerged in the development of receptors capable of identifying and selectively forming complexes with various substrates, some of which are mentioned above, through non-covalent interactions. These advances led to the development of the field known as *Supramolecular chemistry*, initially conceptualized by Lehn as "*chemistry beyond the molecule*". Based on concepts of molecular recognition and stored information within molecules, along with planning through self-assembly and preorganization, it has become essential to redefine supramolecular chemistry as the "chemistry of informed systems" [93–96].

The integration of analytical sciences into supramolecular chemistry has dramatically expanded our understanding of molecular recognition, self-assembly, and other fundamental processes. The construction of macrocycles and their interaction with substances form the basis of molecular recognition, understood as the energy and information involved in binding a substrate by a receptor molecule [97–99]. The combination of supramolecular chemistry and optical detection has paved the way for numerous applications, including chemical sensors, biosensing, drug delivery systems, and materials science.

IUPAC defines chemical sensors as devices that convert chemical information into an analytically useful signal [6,100]. Sensors can be designed as electrical, magnetic, optical, or colorimetric devices, depending on the type of signal they present [4,101–103]. Optical detection devices respond to specific analytes and can be created by connecting a molecule with intrinsic signaling behavior to a recognition system, which may be either molecular or supramolecular [99,104]. In a simplified manner, optical devices can be categorized based on their interaction with the corresponding substance being detected. When optical devices interact with the analyte reversibly, they are known as *Chemosensors* (Scheme 1a). On the other hand, if their interaction is irreversible, they are referred to as *Chemodosimeters* (Scheme 1b).

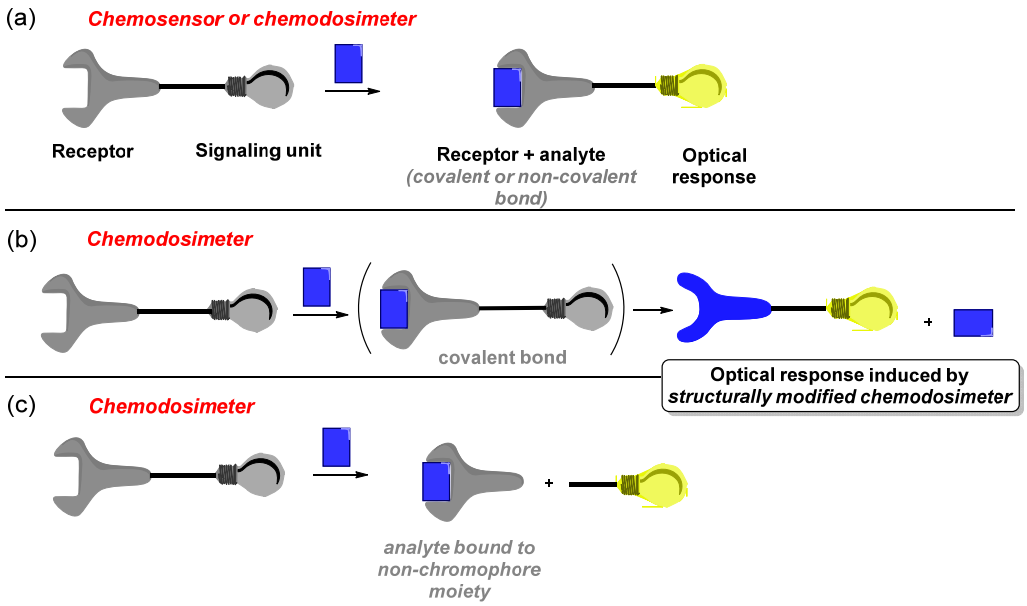

Scheme 1. General representation of (**a**) a chemosensor building strategy and strategies for building chemodosimeters, considering: (**a**) the covalent bond of the analyte with the chemodosimeter inducing an optical response, (**b**) the analyte binding to the chemodosimeter and catalyzing a chemical reaction and (**c**) the reaction of the analyte with the chemodosimeter capable of cleaving part of the molecule.

Scheme 1 shows the main strategies used when considering the development of a chemodosimeter: (a) the analyte can covalently bind to the chromogenic or fluorogenic chemosensor, leading to a variation in its optical properties; (b) the analyte can interact with

the chemodosimeter and catalyze a chemical reaction that generates changes in color or fluorescence emission; and finally, (c) the analyte reacts with the chemodosimeter, releasing a leaving group with chromogenic or fluorogenic properties [104,105].

4. Planning Optical Devices Based on Sensing Mechanism

Comprehending the connection between the molecular structure and photophysical phenomena is crucial in designing fluorescent and colorimetric-based detection systems. The design of fluorescent devices employs several sensing mechanisms, including photoinduced electron transfer (PET), intramolecular charge transfer (ICT), fluorescence resonance energy transfer (FRET), chelation-enhanced fluorescence (CHEF), excited state intramolecular proton transfer (ESIPT), and aggregation phenomena.

4.1. Photoinduced Electron Transfer (PET)

Photoinduced electron transfer (PET) occurs when an electron is transferred to or from an electronically excited state of a molecule. An orbital in a portion of the molecule may possess energy between the energy levels of the highest occupied molecular orbital (HOMO) and the lowest unoccupied molecular orbital (LUMO) of the fluorophore [106]. Electron-donating groups possess an outer orbital that is filled with electrons, and during electronic excitation, PET can occur from this orbital to the previously highest occupied molecular orbital (HOMO) of the fluorophore. Conversely, regions of the molecule with empty orbitals can accept electrons via PET from the fluorophore's lowest unoccupied molecular orbital (LUMO) [105,107].

4.2. Intramolecular Charge Transfer (ICT)

Intramolecular charge transfer (ICT)-based chemosensors contain an acceptor directly connected, via a π-system, to an electron-donating fluorophore. This design allows efficient electron transfer from the electron-rich donor moiety to the electron-poor acceptor moiety, both located within the same molecule. The donor and acceptor groups are connected through a π electron bridge [108].

4.3. Fluorescence Resonance Energy Transfer (FRET)

Fluorescence resonance energy transfer (FRET) is a non-radiative energy transfer process between a donor and an acceptor molecule. For FRET to occur, the donor and acceptor molecules must be in close proximity, and the emission spectrum of the donor molecule must overlap with the emission spectrum of the acceptor molecule to which it provides the energy transfer. Unlike PET, no electrons are transferred between the molecules [109,110].

4.4. Chelation-Enhanced Fluorescence (CHEF)

Chelation-enhanced fluorescence (CHEF) involves complexing a metal cation by a ligand within a fluorophore. During this process, the heteroatoms within the fluorophore form a chelate complex with cation, enhancing fluorescence [111].

4.5. Metal-to-Ligand Charge Transfer (MLCT)

Metal-to-ligand charge transfer (MLCT) transitions are prevalent in coordination complexes and organometallic compounds that feature π-acceptor ligands, where the metal exists in a lower oxidation state, indicating an electron-rich state. Upon light absorption, electrons residing on the metal orbitals become energized, transitioning to the $\pi*$ orbitals of the ligand [112,113].

4.6. Excited State Intramolecular Proton Transfer (ESIPT)

Excited state intramolecular proton transfer (ESIPT) occurs in molecules containing proton donors and acceptors that allow the exchange of a hydrogen atom upon excitation. This process is often associated with the formation of isomers, such as tautomeric (keto-

enol) equilibrium (Scheme 2) [114,115], similar to an acid-base reaction. The ESIPT process primarily occurs in systems where the proton donor is usually a hydroxyl and the acceptor group is carbonyl or nitrogen. However, donor and acceptor groups are nitrogen-based, and other similar configurations have also been described [116–119].

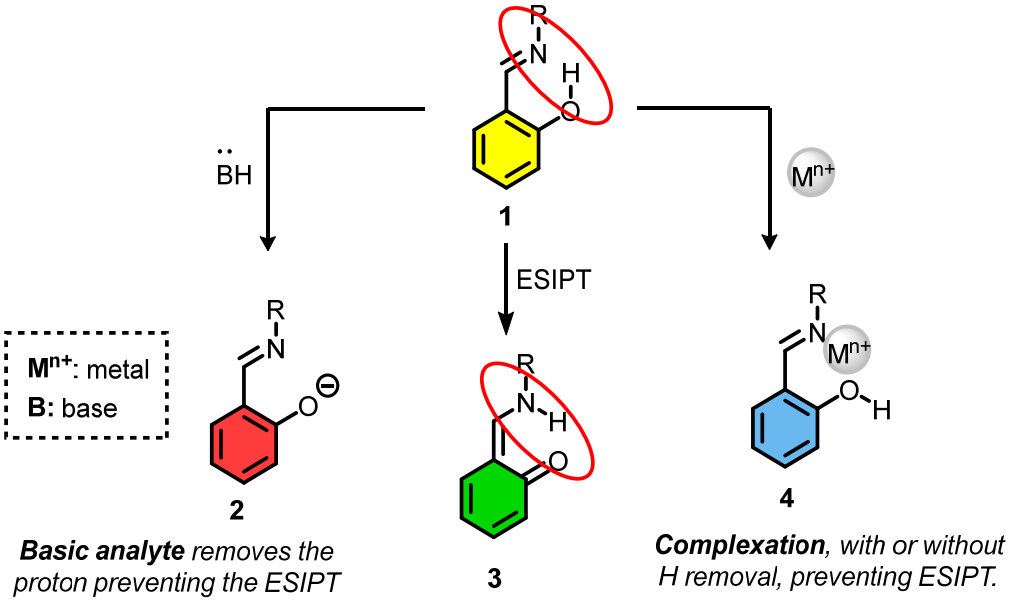

Scheme 2. Generic representation of the ESIPT process and its prevention by basic and metallic species in case of analyte detection.

An analyte can interfere with the ESIPT process (Scheme 2). A basic analyte, for instance, can remove this acid proton (**3**), or a cation can coordinate to this site (**4**), preventing, in both cases, the ESIPT from occurring. Once this phenomenon is prevented, the optical properties of the sensor will be modified, and consequently, the presence of the analyte can be confirmed.

The interruption of ESIPT by an analyte as a strategy in developing optical detection devices has been widely used. Therefore, different molecular architectures have been designed to contain proton donor groups close to proton acceptor groups. This is an efficient strategy, as it enables the detection of both basic and acidic analytes. This review describes some chemical reactions that have made this molecular architecture possible in developing MLGs.

4.7. Aggregation

Aggregation-caused quenching (ACQ) occurs when strong intermolecular interactions in an aggregated state result in fluorescence quenching [120]. Conversely, aggregation-induced emission (AIE) is a phenomenon where weakly fluorescent chromophores emit light upon aggregation. These effects may be attributed to phenomena that reduce the non-radiative relaxation pathways, such as intramolecular rotation restriction (RIR) and J-aggregate formation (JAF), which are influenced by mechanical and thermal factors [121].

5. Architecture of Optical Sensor Devices

The typical molecular architecture of an optical sensor consists of at least one detector unit and at least one signaling unit, although these distinctions are blurred in some cases. The detector unit is designed to interact specifically with an analyte, while the signaling unit consists of a molecular structure that causes an optical response upon interacting the receptor unit with the analyte (Scheme 1a). Generally, this response is associated with changes in the electronic density of the optical sensor. For example, an interruption of

electronic flow between a donor unit and a receptor unit due to interaction with an analyte can cause a change in color or fluorescence, allowing analyte recognition.

The design of an optical sensor relies on the combination of detector and signaling units. With numerous groups already discovered or developed, there are countless possibilities for combinations. In addition, there are cases of planning more than one signaling unit in the same device, so that after detection, more than one response is given—for example, a change in color and electrochemical potential [17]. In other cases, more than one molecular or supramolecular group receptor can be installed in the signaling unit to obtain a device capable of detecting different chemical species [122–126]. This last scenario is a classic strategy for planning optical and multi-analyte sensors.

The diversity in optical responses and the richness of structural possibilities demonstrate that the architecture of optical sensors offers a wide array of opportunities. In this context, organic synthesis is vital in designing sensor molecules.

The following topics illustrate typical examples of signaling and detector units with different molecular arrangements involving electron density donor and acceptor units. Examining each component of the structure is crucial in designing an optical sensor. The process entails connecting one or more receptors (molecular or supramolecular) to a signaling unit, either with a spacer or directly.

5.1. Choosing the Signaling Unit

The structural features of a molecule influence the dissipation of absorbed energy in the form of fluorescence. For instance, rigid and flat molecules bearing conjugated systems, such as aromatic groups, are inclined to exhibit fluorescent properties [127,128]. The planar structure of a molecule enhances the interaction and conjugation within the π electron system, resulting in absorption through $\pi \rightarrow \pi^*$ transitions (between antibonding π orbital and bonding π orbital). Absorption may also occur less frequently through $n \rightarrow \pi^*$ transitions (between antibonding π orbital and non-bonding orbital) [120].

In this regard, aromatic hydrocarbons and heterocycles have been intensely investigated due to their potential application as fluorescent and colorimetric signaling units (Figure 1). For instance, polydiacetylenes have been elaborated as supramolecular scaffolds in analyte sensing [129,130]. Classical condensation reactions have been employed in synthesizing fluorescent heterocycles. For instance, highly conjugated imidazoles (**5**) can be synthesized through a multicomponent reaction between an aldehyde, an ammonium salt, and 1,2-dicarbonyl compounds [131–137]. Furthermore, this last substrate can also be used for the preparation of fluorescent phenazine (**6**), quinoxaline (**7**), and oxazoles (**8**) [138,139]. Other examples of fluorescent heterocycles obtained in diverse synthetic strategies include quinoline (**9**) [140–144], pyrazine (**10**) [145,146], acridine (**11**) [147–152], BODIPy (**12**) [153–158], benzothiadiazoles (BTDs) (**13**) [159–166], coumarin (**14**) [167–170], fluorescein (**15**) [171–178], rhodamine (**16**) [179–183], auramine O (**17**) [184–186], proflavine (**18**), phenoxazine (**19**), xanthene (**20**) [187,188]. Examples of aromatic hydrocarbons include naphthalene (**21**) [189–193], anthracene (**22**) [194–198], and pyrene (**23**) [199–202].

The scientific community is making intensive efforts to continuously develop new classes of chromophores and fluorophores using numerous synthetic methodologies [203]. For instance, more recently, metal-catalyzed C−H activation [204], particularly through annulation, has emerged as a powerful synthetic strategy in elaborating fluorescent building blocks [205,206]. This approach is especially noteworthy for the formation of chromophoric and fluorophoric groups, as metal-catalyzed C−H activation represents an important innovation capable of directly connecting aryl halides to (hetero)arenes by metal-promoted activation of a C−H bond [207–209].

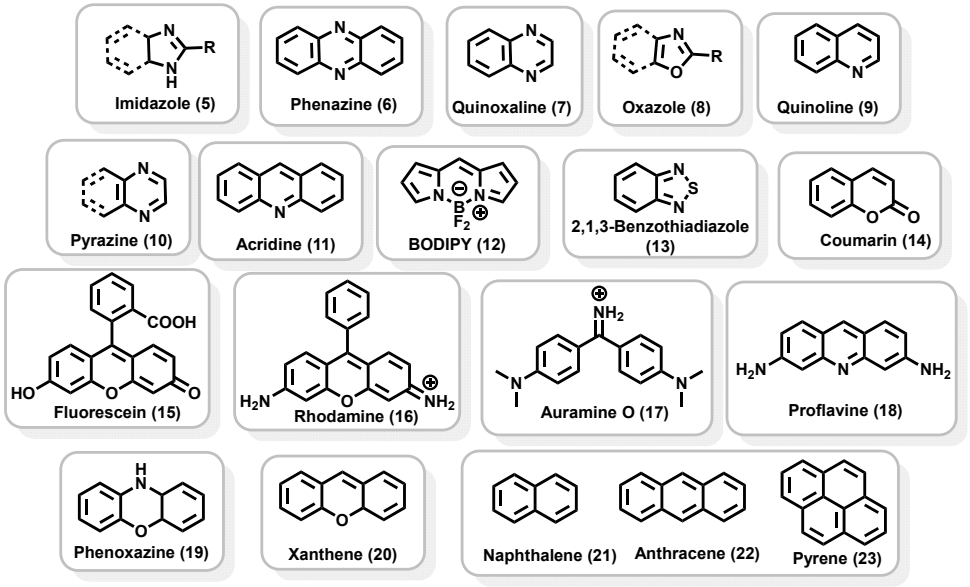

Figure 1. Examples of chromophores/fluorophores, which are usually used as building blocks for constructing optical devices.

5.2. Choosing the Receptor Unit

Regarding receptors, there are two approaches to constructing devices capable of identifying analytes, according to chemosensors and chemodosimeters definitions: association and chemical bonding.

Figure 2 shows some types of receptors commonly employed in the preparation of molecular/ionic recognition devices. Crown ethers (**24**) [210,211] can vary in their heteroatom composition (**25**), thus influencing the selectivity for a particular analyte. More intricate macrocycles, like cyclodextrins (**26**) [212–218], calixarenes (**27**) [219–223], and calix[4]pyrroles (**28**) [223–226], can complex organic molecules, ions, and halides. In addition to macrocycles, simple organic molecules can be structurally and electronically modified to build receptors that respond to chemical, electrical, or optical inputs. Ligands containing pyridines or bipyridines (**29**) are known for their ability to interact with transition metal cations. Nitrogen-based receptors, such as ureas (**30**), amino acids (**Cys**; **31**), amines, and amides (**32**), are also extensively researched.

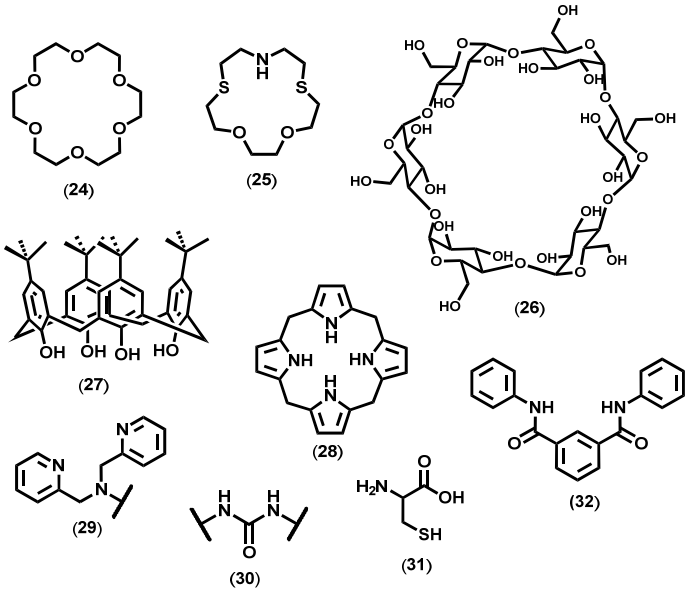

Figure 2. Receptors based on association with the design of chemosensors.

In all these instances, the hard–soft acid-base (HSAB) theory is frequently employed to elucidate the stability of the formed adducts. However, other factors may also be related, such as cavity size, ion charge, and solvent effects: polarity, polarizability, acidity, and temperature [227].

The recognition of analytes based on chemical reactions often considers the type of functional group on the receptor device. Mohr et al. compiled a list of functional groups and neutral analytes that could be detected by forming linkages (Scheme 3) [75,228].

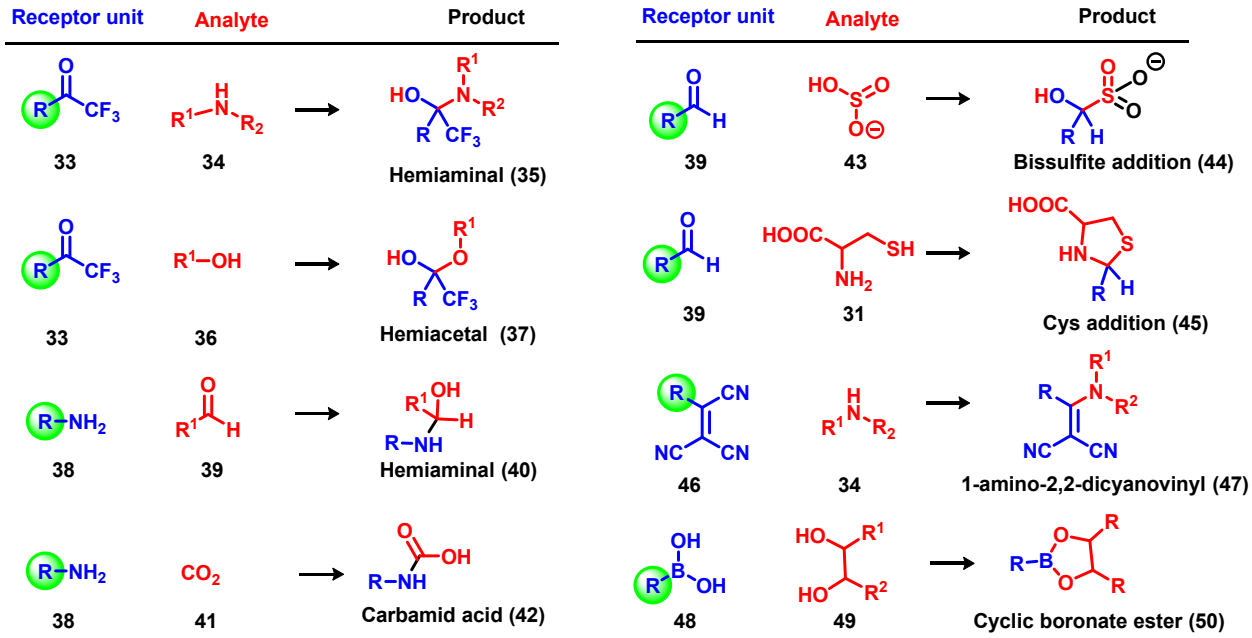

Scheme 3. Receptor functions can detect analyte molecules by forming a covalent bond.

5.3. Choosing the Assembly of the Device

To assemble an optical sensor, molecular devices can be engineered with various donor and acceptor group arrangements. For a molecule to operate as a sensor, it must efficiently transfer electrons and respond appropriately to the presence of the analyte. Therefore, some arrangements of donor and acceptor groups may include (a) **D–A** (donor–acceptor), (b) **D–A–D** (donor–acceptor–donor), and (c) **A–D–A** (acceptor–donor–acceptor) configurations, although other combinations are also possible. Figure 3 summarizes the order used to construct each arrangement, considering one, two, or more donor groups, depending mainly on the application to which the final molecule will be given.

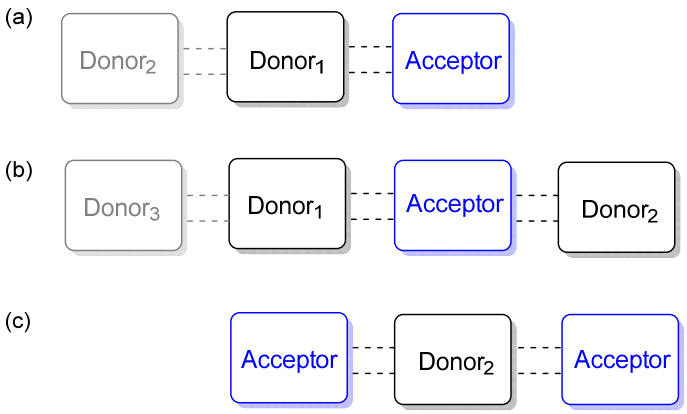

Figure 3. Summary of constructing (**a**) donor–acceptor, (**b**) donor–acceptor–donor, and (**c**) acceptor–donor–acceptor configurations.

D–A or **D–pi–A**: This configuration comprises the most straightforward system and the most predictable optical response. In this case, there is a transfer of charge from the donor region to the acceptor region when the molecule interacts with a specific analyte or even its surrounding environment. A conjugate spacer may separate donor and acceptor groups. It is commonly related to the PET and ICT mechanisms [229–231].

D–A–D: Combinational logic gates involving multiple logic operations can be conveniently prepared through more complex arrangements, such as D–A–D [232,233].

A–D–A: This configuration refers to opposite structures to D–A–D systems. In A–D–A arrangements, electron acceptor groups are introduced into the donor structure. Designing MLGs with an acceptor–donor–acceptor architecture also offers an intriguing platform for preparing optical devices [234–236].

5.4. Integrating the Molecular Architecture

So far, we have demonstrated that an optical detection device is built by signaling and detector units articulated to present structural combinations with donor and acceptor regions. The optical response of this device is related to changes in molecular electronic density, involving processes such as PET, ICT, FRET, CHEF, MLCT, ESIPT, and aggregation. In this context, the molecular structure of an optical detection device is elaborated through the observation and understanding of these critical aspects. In implementing this structural planning, numerous synthetic tools provided by organic chemistry have been fundamental in elaborating the architecture of such devices. These tools serve various purposes in sensor design. For instance, joining signaling units with detectors, associating donor and acceptor units, pre-functionalize the molecule for sequential modification, changing optical properties by altering molecular conjugation, and changing the sensors' physical–chemical properties (increasing solubility, stability, and restricting conformation, among others).

Although there are numerous synthetic methods for building these devices, we can mention classic methodologies, such as imine formation, Knoevenagel reaction, nucleophilic aromatic and aliphatic substitutions, and functionalization of arenes. Additionally, other successful methodologies that have been explored include multicomponent (MCRs), pericyclic, and coupling reactions.

Multicomponent reactions (MCRs) offer an efficient and versatile approach to synthesizing complex molecules, making them essential tools in modern organic synthesis [237]. In these reactions, three or more commercially available or readily accessible starting materials react to form a product, involving the contribution of essentially all or most of the atoms to the newly formed product, using a one-pot approach [238]. MCRs have been successfully employed in constructing fluorescent building blocks suitable for application as signaling units in an optical detection device [239–242].

Heterocycles and aromatic rings are frequently synthesized or modified through cycloaddition reactions involving breaking pi bonds and forming sigma bonds. Various cycloaddition methods are employed to construct both essential units (signaling unit or receptor), and they can be used to connect these units (spacers). The copper-catalyzed azide-alkyne cycloaddition (CuAAC), a 1,3-dipolar cycloaddition reaction, to afford 1,4-disubstituted 1,2,3-triazoles is an important synthetic methodology in constructing optical detection devices (Scheme 4a). The triazole unit can perform three functions: (a) it serves as a connector for different molecular groups (donors, acceptors, receptors); (b) due to its nature as an aromatic heterocycle, the triazole ring conjugates with aromatic systems of the fluorophores/chromophore, modifying the optical properties of the device; (c) the nitrogen atom of the triazole, in association with other molecular groups, can function as a detector unit for metallic species (Scheme 4b) [243–247].

Halogenation reactions, characterized by substituting hydrogen atoms with halogens, such as chlorine, bromine, and iodine, hold considerable importance in synthetic processes. They serve as precursors for more intricate transformations, including coupling reactions, and are also utilized in simple substitution and elimination reactions.

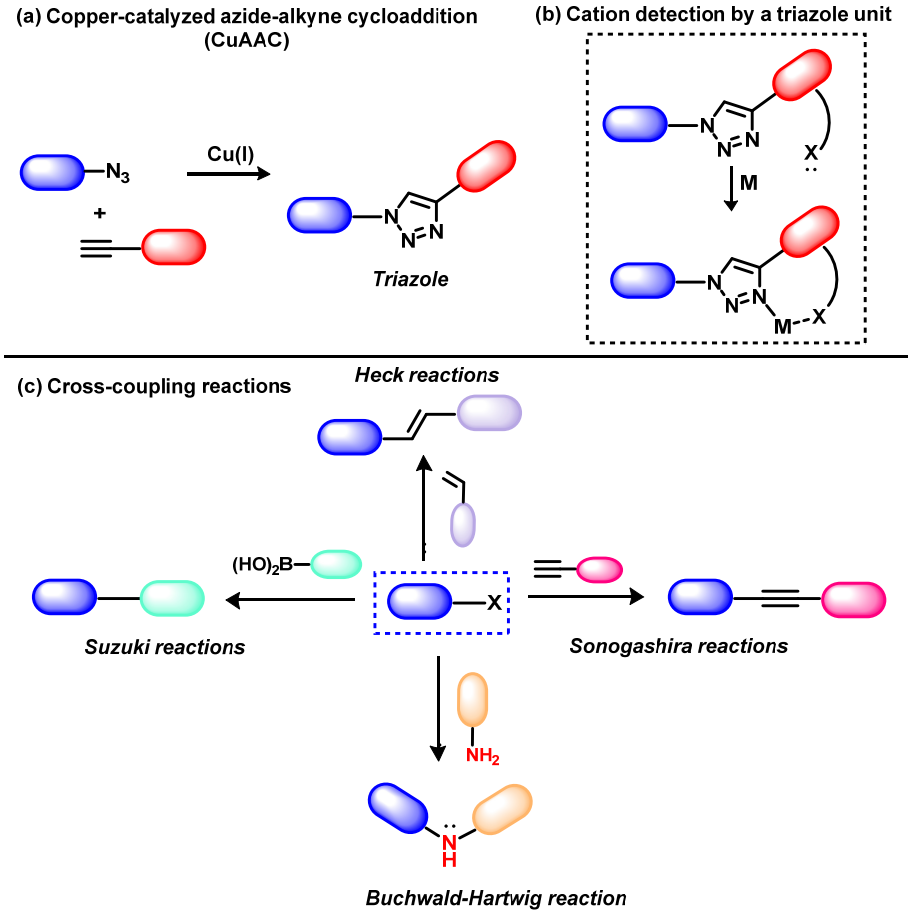

Scheme 4. (**a**) Generic representation of copper-catalyzed azide-alkyne cycloaddition (CuAAC) to afford 1,4-disubstituted 1,2,3-triazoles and (**b**) their application as sensors; (**c**) Representation of coupling reactions in obtaining and modifying optical detection devices.

The advent of coupling reactions, predominantly mediated by palladium, opened up an avenue of synthetic possibilities in the development of optical detection devices. Among these methodologies, noteworthy examples include Suzuki, Sonogashira, Heck, Stille, and Buchwald–Hartwig reactions (Scheme 4c). Using these synthetic methodologies in the construction of optical detection devices yields two fundamental effects: first, the extension of the molecular pi conjugation modulating optical properties, and second, the junction of units (donor, acceptor, fluorophore, chromophore, signaling, detector unit). The Buchwald–Hartwig reaction enables the formation of C–N bonds, and the NH group offers the possibility to unite two groups, afford a hydrogen atom that can interact with basic analytes, and be involved in ESIPT processes. Furthermore, the lone nitrogen electron pair can interact with cations and acid detector units. Conversely, Heck and Sonogashira reactions enable the formation of C–C bonds. In these reactions, the alkene and alkyne groups, respectively, join two molecular groups, contributing to the extension of pi conjugation.

6. Strategies for Building Optical Devices Based on Interaction Type

6.1. Acid-Base Reactions or Hydrogen Bonding (H-Bonds) Interactions

The principles related to acid-base reactions can be effectively applied in the development of optical devices. In this strategy, H-bonds-based chemosensors contain hydrogen donor groups, such as OH, NH, and SH, within their molecular structure. These groups can interact with a basic analyte and trigger an acid-base reaction, changing the behavior of the signaling unit and allowing the sensor to detect and quantify the analyte [248].

Ghosh et al. developed the chemosensor **53** (Scheme 5a), an azine-based molecule prepared from the coupling of 2-hydroxy-1-naphthaldehyde (**51**) using hydrazine ($N_2H_4 \cdot H_2O$;

52), designed for the recognition of acetate and Al^{3+} [249]. The interaction with Al^{3+} depends on inhibition of the ESIPT phenomenon, isomerization of the CH–N bond, and enhancement of fluorescence resulting from metal complexation. On the other hand, the detection of acetate anion is attributed to H-bond formation with hydroxyl hydrogens. Scheme 5b illustrates the H-bonds mechanism between the chemosensor and acetate anion, and Scheme 5c shows the proposed Al^{3+} sensing mechanism.

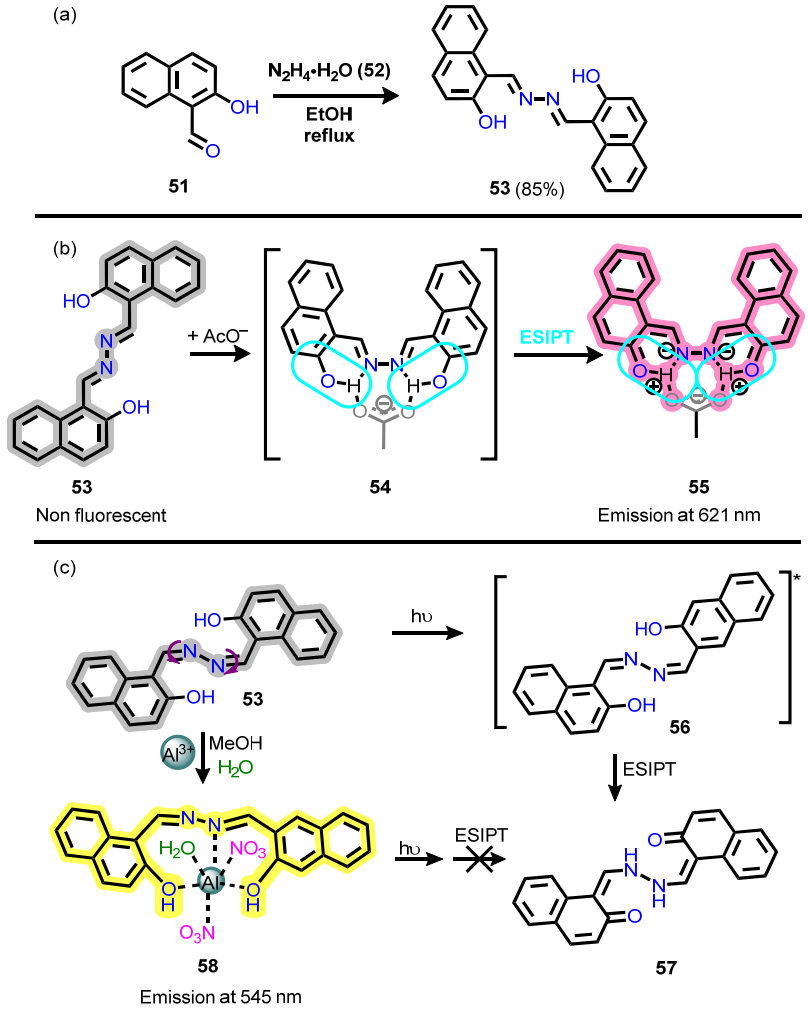

Scheme 5. Chemosensor prepared by Ghosh et al. [249]. (**a**) Synthetic route adopted by the authors. (**b**) The interaction mechanism between compound **30** and acetate anion and (**c**) the detection of Al^{3+} by 30 involving the ESIPT phenomenon and isomerization of the CH–N bond.

6.2. Displacement Assays

An alternative approach that has been used involves planning direct and indirect detection assays, working with a unique system containing molecular groups competing for a single receptor. In a simplified manner, a chromogenic or fluorogenic indicator (sensor–indicator) binds reversibly to a receptor, forming a receptor–indicator complex. This complex alters the optical properties of the system, either the change in the solution's color or the intensity of fluorescence emission. The indicator is displaced upon adding a competitive analyte, and the receptor and the new analyte form a new complex. This new complex has a stability constant of greater magnitude than the previous complex. Consequently, the free indicator in solution will again present the optical properties observed before adding the receptor to the medium [250].

For instance, Mawai et al. reported a dual-response OFF–ON–OFF system (**61**) prepared by condensing 2,6-diformyl-4-methylphenol (**59**) and 2-(1-phenylhydrazinyl)pyridine

(**60**) through refluxing in methanol (Scheme 6a) [251]. The weakly emissive compound **61** could selectively recognize zinc ions via a fluorescent ON response in a DMSO/water mixture (1:9, vol/vol). Subsequent investigations into the fluorescence emission behavior of the zinc complex (**62**) revealed significant suppression of emission upon the addition of pyrophosphate (PPi; **64**) (Scheme 6b). Furthermore, a bathochromic shift was observed in the emission band, shifting from λ_{max} = 521 nm to 526 nm.

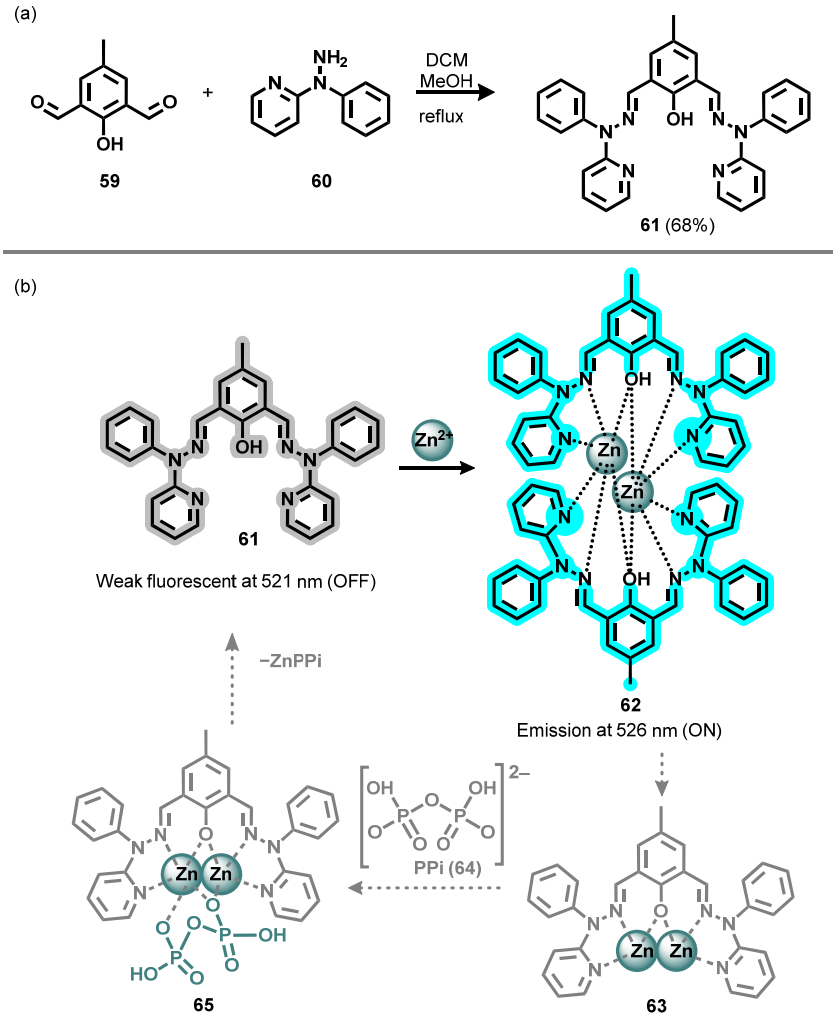

Scheme 6. (**a**) Synthetic route of chemosensor **61**. (**b**) Sensing mechanism of chemosensor based on displacement assay for detection of Zn^{2+} and PPi, presented by Mawai et al. [251].

6.3. Chromo- and Fluororeagents

In the chromo- and fluororeagent approaches, chemosensors establish a reversible covalent bond with the analyte, inducing significant changes in absorbance or fluorescence. The reaction between the chromoreagent and analyte builds the covalent bond, thereby altering the electronic delocalization of the chromophore and resulting in observable color changes. The reaction between an analyte and a fluorophore group, connected via a spacer with the receptor unit, frequently results in enhanced (or newly observed) fluorescence intensity by blocking the PET phenomenon [75,228]. Such chemosensor allows the optical detection of electrically neutral analytes like alcohols, amines, thiols, and aldehydes.

For instance, Nedeljko et al. devised an optical detection system for continuous determination of biogenic amines, such as isopentylamine (**67**), *n*-propylamine (**68**), and putrescine (**69**), based on a layer of a sensitive dye in its trifluoroacetyl form (**66**) immobilized in SiO_2 (Scheme 7) [252]. The commercial chromoreagent ETH4001 (**66**) was immobilized in sol–gel layers prepared by different combinations of hydrophilic precursors of tetraethoxysi-

lane and hydrophobic sol–gel. The response to primary amines was achieved through their reversible reaction with the chromoreagent. This reaction forms a covalent bond with the dye, transforming it into the hemiaminal form (**70**), whereby the color changes from red to yellow. According to the authors, the decrease in absorbance at 500 nm (red) can be attributed to the presence of **66**. Conversely, the increase in absorbance at 420 nm (yellow) results from the formation of several products: a hemiacetal form (resulting from the interaction between TFA and alcohols), a diol form (resulting from the interaction between TFA and water), and a hemiaminal form (resulting from the interaction between TFA and amines).

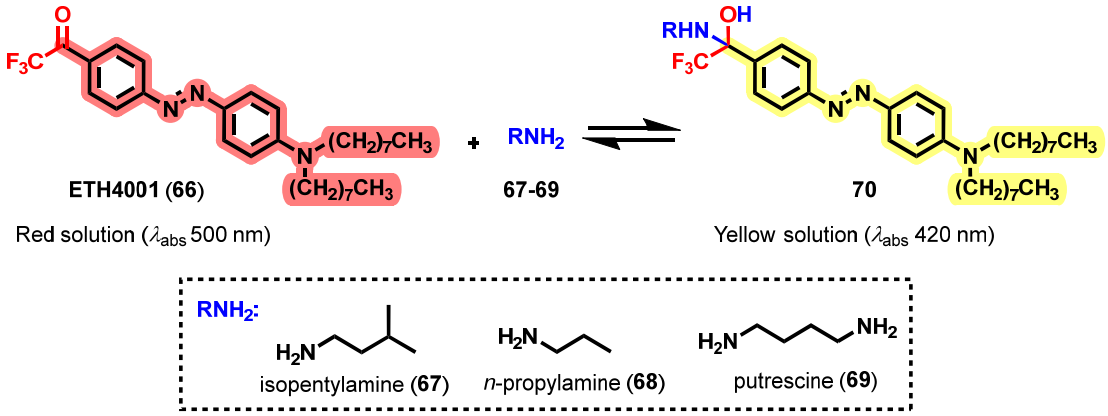

Scheme 7. Chromoreagent prepared by Nedeljko et al. [252] for detection of biogenic amines.

6.4. Chemosensor

Chemosensors are optical devices based on reversible interaction with the analyte [106]. For example, in some of these devices, a basic analyte can interact with proton donor groups (NH, OH, SH) via hydrogen bonding [248,253]. These interactions, regardless of the complete transfer of hydrogen ions, can induce changes in the color or fluorescence emission of the chemosensor, thereby enabling the detection and quantification of the analyte [254,255].

One example of a chemosensor was described by Bhaumik et al. via synthesis of the phenanthro[9,10-*d*]imidazole (**73**) for the detection of fluoride, Fe^{2+}, and Zn^{2+} (Scheme 8a) [256]. Compound **37** behaves as a solvatochromic chemosensor with different emission colors ranging from violet, blue, and green to yellow, which suggests that **73** could be used as a solvent polarity indicator. The colorless **73** solution (λ_{abs} 341–371 nm) becomes bright yellow (λ_{abs} 413 and 279 nm) upon adding F^- or HO^- (Scheme 8b; **74**). Furthermore, F^- induced a fluorescence quenching and a redshift in emission maximum from 475 to 485 nm. NMR investigation suggested that this phenomenon might be associated with the interaction or removal of the proton from NH groups. Adding Fe^{2+} modified the colorless solution of compound **73** into a deep violet solution (**75**), attributed to a strong MLCT band at 575 nm (Scheme 8c). The authors described that no color change was observed for Fe^{3+}, indicating that this cation did not interfere with the detection of Fe^{2+}. The progressive addition of $Zn(ClO_4)_2$ reduced the band's intensity centered at 370 nm, accompanied by a simultaneous increase in absorbance at 395 and 284 nm. Both Fe^{2+} and Zn^{2+} ultimately led to the complete quenching of emission at 475 nm. However, Zn^{2+} also induced a distinct linear emission enhancement at 600 nm. The synthetic strategy employed by the authors to obtain **73** is particularly interesting because the signaling unit (imidazole) is obtained by joining the detector unit (pyridine groups). This approach has been widely used in developing phenanthro[9,10-*d*]imidazole-based fluorescent and colorimetric sensors [124]. Generally, a substrate containing a formyl group is also designed to hold a detector unit, enabling the construction of an optical detection device in a single step.

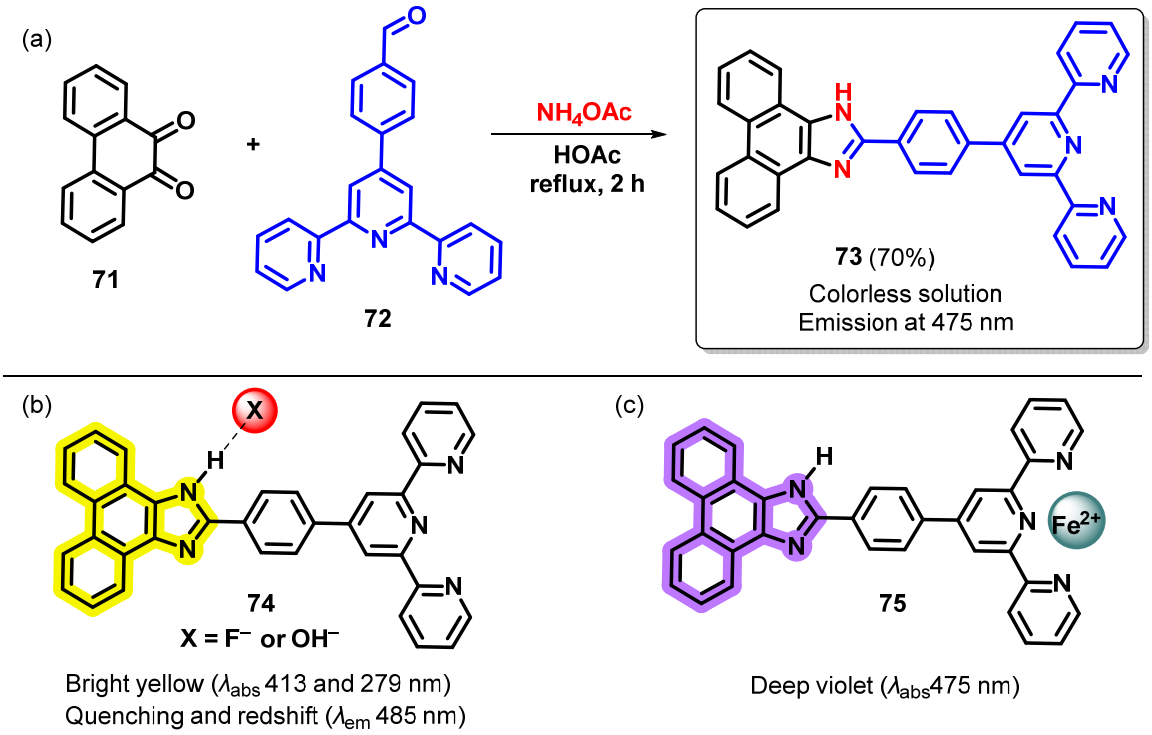

Scheme 8. (**a**) Synthesis of phenanthro[9,10-*d*]imidazole **73** described by Bhaumik et al. [256]. (**b**) Interaction of HO^- and F^- with NH in **74**. (**c**) Interaction with Fe^{2+} in **75**.

Designing molecules with energy gaps according to the substituents also presents opportunities for constructing chemosensors. For instance, Kim et al. prepared a series of pyrene-based molecules, 1,6-bis[(*N*,*N*-*p*-(R)-diphenylamine)phenyl]pyrene (**82–86**), containing *N*,*N*-bis(*p*-(R)-phenyl)aniline as an electron donor and pyrene as an electron acceptor by using the Suzuki cross-coupling reaction (Scheme 9) [257]. As previously discussed (Scheme 4), the Suzuki-coupling reaction is an essential synthetic tool in the general design of optical devices. In this instance, the authors devised a highly conjugated molecular system based on this coupling reaction. Compounds **82–86** were used as chemosensors to detect nitroaromatic explosives by controlling their energy gap decreasing the fluorescence due to the FRET mechanism. Sensor **82** exhibited the highest Stern–Volmer constant of all the compounds tested, measured to be 3171 M^{-1}.

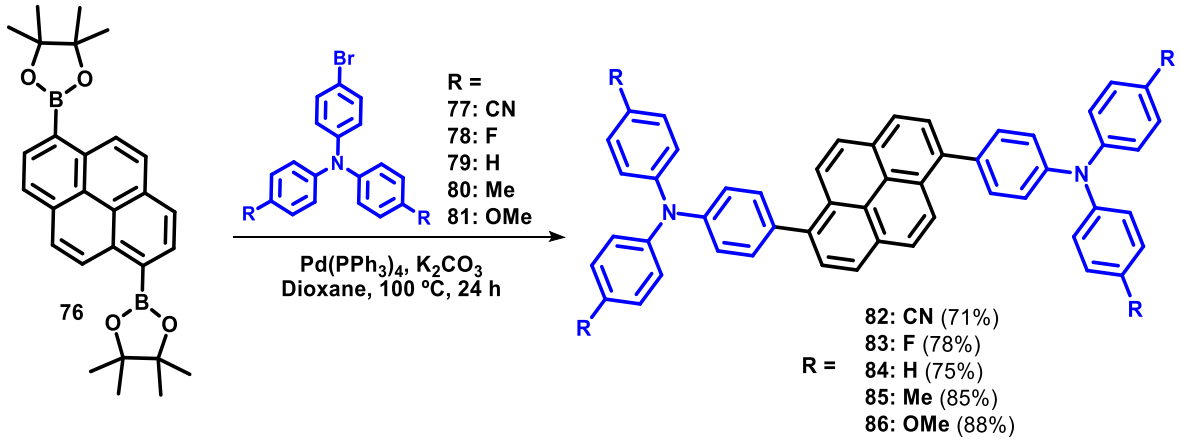

Scheme 9. Synthesis of 1,6-bis[(*N*,*N*-*p*-(R)-diphenylamino)phenyl]pyrenes (**82–86**) proposed by Kim et al. [257].

6.5. Chemodosimeters

A chemodosimeter is an optical device that does not consider intermolecular interactions as the driving forces of the analyte detection system. Instead, it involves the formation of irreversible covalent bonds between the analyte and the detection system [258,259].

An example of a chemodosimeter was described by Souto et al. via a new azo-silylated compound (**91**) derived from naphthol (**88**) for the selective detection of CN^- in acetonitrile/water and an aqueous micellar system (Scheme 10a) [260]. To synthesize **91**, 4-nitroaniline (**87**) was first diazotized and then condensed with 1-naphthol (**88**). The chemodosimeter **91** was obtained through nucleophilic substitution to introduce the tri-isopropylsilane group. In the sensing process, the CN^- anion breaks the Si–O bond in **91**, releasing the dye **92** and inducing a color change in the solution from yellow to blue (Scheme 10b).

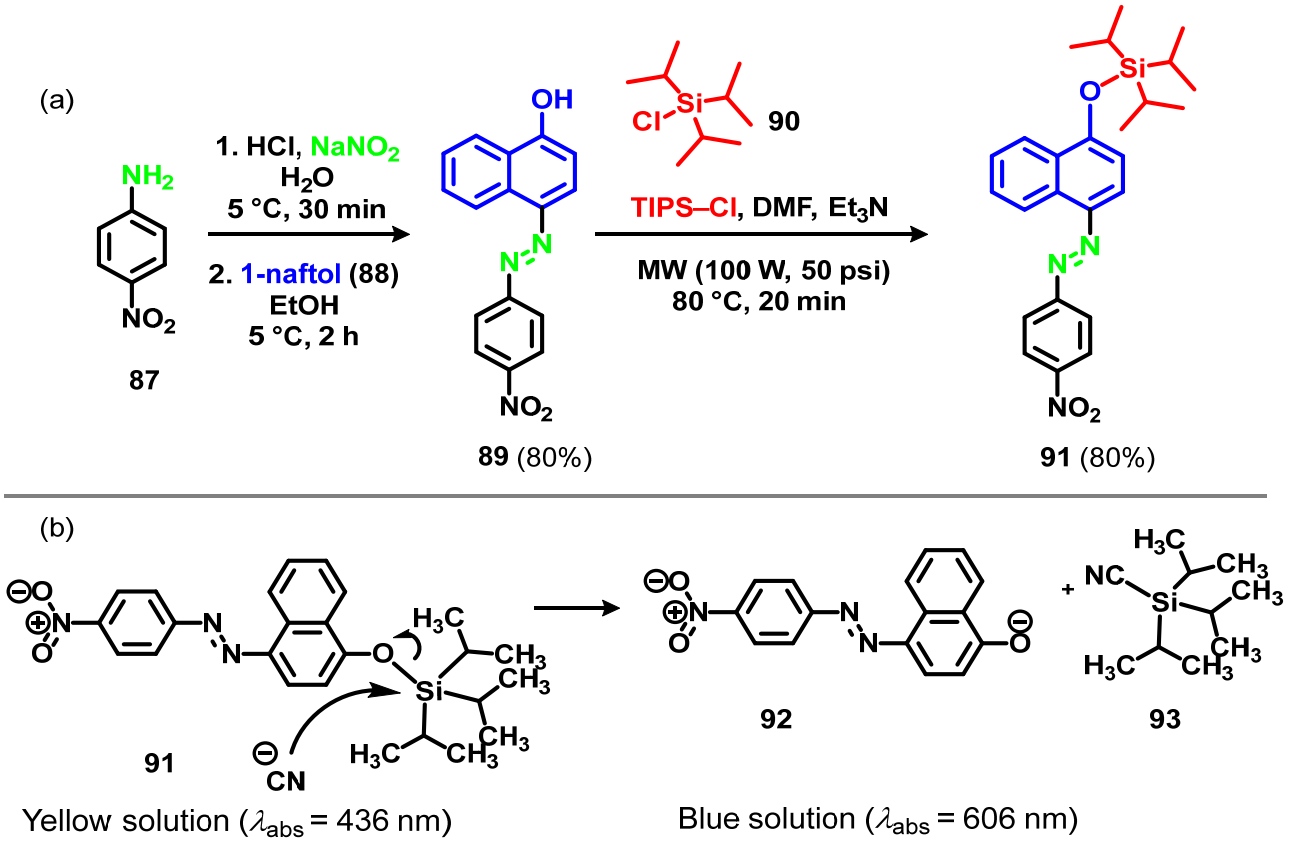

Scheme 10. (**a**) Synthetic route for preparation of compounds **89** and **91**. (**b**) Reaction of compound **91** with CN^-, generating the phenolate **92**, proposed by Souto et al. [260].

The development of sensors containing the Si–O bond is inspired by the high affinity of silicon for species such as CN^- and F^-, which leads to the breaking of the Si–O bond [261], as exemplified here by Souto et al. Thus, installing groups such as TIPS, tetramethylsilane (TMS), dimethylphenylsilane, and *tert*-butyldimethylsilane in the molecular architecture is a direct strategy to obtain devices capable of detecting chemical species such as CN^- and F^- [253,262–266].

Song et al. developed a fluorescence turn-on chemodosimeter benzimidazole-based (**98**) to detect cysteine (**31**). In their device, the benzimidazole (**96**) is linked to an acrylate group (**97**) and easily synthesized in two steps (Scheme 11a) [267]. The acrylate functional group controls the π-electron system and initiates the fluorescence turn-on effect-based ICT. However, when the -SH group in cysteine undergoes a Michael addition to the acrylate of **98**, followed by the elimination of a seven-membered ring (**100**), it disrupts the ICT process, leading to the fluorescence turn-on effect from signaling released moiety (**101**, Scheme 11b).

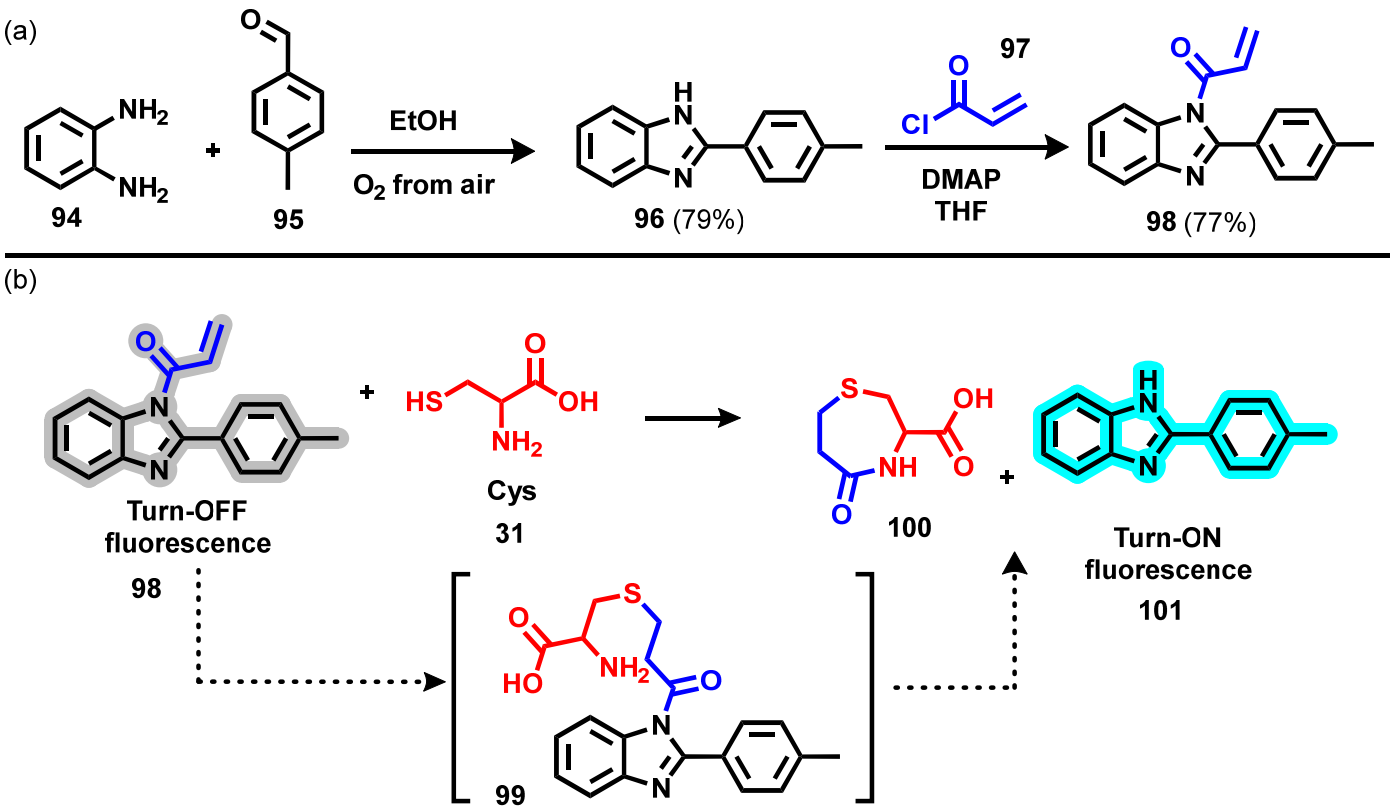

Scheme 11. (**a**) Synthesis of the D–A system **98** reported by Song et al. (**b**) Sensing mechanism of Cys detection [267].

7. Logical-Based Devices: Molecular Logic Gates (MLGs)

Thirty years ago, A. P. de Silva published the seminal work that revolutionized the field of supramolecular analytical chemistry [11]. By leveraging information science as an analytical tool, he introduced the molecular logic gates (MLGs) concept. These molecular devices could operate following binary logic and generate potential applications with significant promise in various fields.

The combinations of responses caused by perturbations of the pre-associated system can potentially be interpreted in terms of logical operations. In electronics, a logic gate (LG) corresponds to a model that performs a logic operation on one or more logic inputs and produces a logic output [268]. When this concept is transferred to supramolecular chemistry, the optical response of a perturbation (input) can be interpreted as an output, particularly in scenarios where more than one receptor is present in a supramolecular structure, enabling the recognition of more than one chemical species [269–272].

The researchers who continued the work of George Boole developed the control of information flow by formulating a language whose variables can assume one of two possible values, which can be denoted by [F, V] (false or true), [H, L] (high and low; high and low) or [0, 1]. This model performs a logic operation on one or more logic inputs and produces one or more logic outputs [273]. The combination of two inputs results in responses that characterize the three fundamental types of logic gates: NOT, AND, and OR. These gates can be combined to obtain more complex operations (XOR, XNOR, INH, NOR, etc.), whose logic is illustrated in Figure 4 through its truth tables and respective diagrams. All processors and digital equipment on the market are operated by systems comprising the combinations of those three basic LGs according to well-defined rules, receiving or generating signals compatible with the binary language [271,274,275].

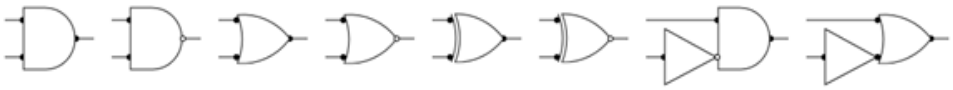

$Input_1$	$Input_2$	AND	NAND	OR	NOR	XOR	XNOR	INHIBIT	IMPLICATION
0	0	0	1	0	1	0	1	0	1
0	1	0	1	1	0	1	0	0	1
1	0	0	1	1	0	1	0	1	0
1	1	1	0	1	0	0	1	0	1

Figure 4. Symbolic representation of logic gates and their corresponding truth tables built from values of inputs and outputs.

In 1993, Prasanna de Silva et al. described an anthracene core attached to a crown ether (Figure 5) [11]. Although anthracenyl may exhibit fluorescent properties, compound **102** displayed a weakened fluorescence emission due to the PET process. Therefore, without additives (inputs "0"), **102** exhibited weak emission (output "0"). Upon adding acid ($input_1$ "1") to **102**, the protonation of the tertiary amine occurred; yet, this did not prevent the PET process, resulting in a low fluorescence response (output "0"). Another operation is adding Na^+ ($input_2$ "1"), in the absence of acid ($input_1$ "0"), allowing the crown ether to recognize this cation. However, this interaction also failed to prevent the occurrence of PET, and likewise, a low fluorescence response (output "0") was observed. Remarkably, the simultaneous addition of acid and Na^+ cation ($input_1$ "1" and $input_2$ "1") led to a six-fold increase in fluorescence intensity (output "1"). In this case, the two stimulus signals (H^+ and Na^+) were necessary for a response with a significant increase in fluorescence (output). Therefore, this MLG could be classified as type AND (Figure 5).

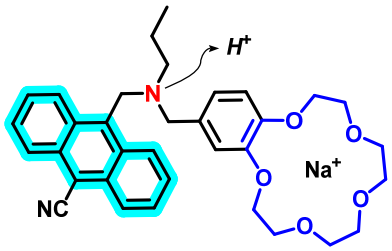

$Input_1$ (H^+)	$Input_2$ (Na^+)	Output (λ_{em} 446 nm)
0	0	0
1	0	0
0	1	0
1	1	1

Molecular Logic Gate - AND

Figure 5. Structure of the first MLG **102**, reported by Prasanna de Silva et al. [11].

8. The Architecture of MLGs Based on Truth Tables' Interpretation

So far, we have shown the importance of various analytes, provided examples of optical detection devices, their architecture involving signaling and detector units, elucidated the general arrangement comprising units serving as both electron density donors (D) and electron density acceptors (A), and expounded upon the fundamental concepts of MLGs. These concepts will be used to discuss different MLGs that can be constructed from a binary analysis of the responses generated as detection devices.

Similarly to a general optical detection device, the development of an MLG entails the integration of electron-donating and electron-accepting groups via a signaling unit connected to one or more analyte receptor groups. This architecture allows for interpreting chemical signals in terms of binary logic. A traditional chemical sensor can be transformed into a sophisticated logic gate capable of processing and responding to specific chemical inputs. For instance, we recently described several examples of MLGs that can be proposed from traditional sensors exploiting aspects of reversibility [276].

Most MLGs involve supramolecular systems in solution to respond to different stimuli, including chemical, light, and electrical inputs. Physical–chemical processes, such as the interaction of a cation with a chelating site, protonation–deprotonation of an acid-base

site, oxidation reduction, photochemical event, formation or breaking of chemical bonds, etc., can give rise to a spectroscopic response, such as changes in fluorescence emission or absorption in the UV–Vis region [268,277–283]. Thus, based on the concepts of conventional microelectronics, the stimuli transferred to a molecule are understood as inputs, and the changes in the emission/absorption of that medium as outputs. We presented below some commonly used logic functions in constructing optical detection devices.

8.1. "YES" Logic

YES logic is one of the most straightforward logic gates that require the output to follow the input, and most cases can be simplified as an "OFF–ON" switch [283–293]. Boolean YES logic can be described if the output signal increases with increasing stimulus, i.e., when an input is present, the output signal is increased.

A simple "OFF–ON" chemosensor (**109**) able to discriminate glutathione (GSH) from cysteine (Cys)/homocysteine (Hcy) was introduced by Li et al. (Scheme 12) [290]. First, the authors started with a formylation reaction of 3-(*N*,*N*-diethylamine)phenol (**103**) to afford **104**, followed by a reaction with ethyl acetoacetate (**105**) to generate **106**, formylated again by the Vilsmeier–Haack protocol. Finally, **107** reacted with malononitrile (**108**), producing **109** (Scheme 12a). The authors identified two potential reaction sites for the chemosensor: Site 1, the chlorine atom at the 3-position of the coumarin moiety as a leaving group, and Site 2, the α,β-unsaturated malononitrile as a Michael acceptor (Scheme 12b). The sensor **109** could discriminate between GSH and Cys/Hcy through fluorescence response. The proposed detection mechanism involves thiol-halogen substitution, where the chlorine atom is replaced by thiolates of the three evaluated thiols, leading to intramolecular rearrangements for Cys and Hcy. Then, an intramolecular Michael addition reaction between the α,β-unsaturated malonitrile and the thiol group interrupts the π conjugation system. GSH only leads to substitution due to its tripeptide structure, making it difficult for the amino group to attack. The structural modifications increased the fluorescence emission intensity up to 505 nm. The mechanism was investigated using fluorescence, UV–Vis, NMR, and ESI-MS techniques. In this case, an increased fluorescence intensity is only obtained in the presence of GSH. In other words, **109** generates an output "1" exclusively when the GSH input matches "1". Therefore, it can be described as a YES MLG.

8.2. "NOT" Logic

NOT logic causes the output to behave opposite to the input. Unlike YES gates, NOT logic devices respond to an input in an "ON–OFF" manner [280,281,291–293]. If the output signal decreases in the presence of an input, the NOT logic is the result.

Noushija et al. proposed the optical sensor **115** based on quinizarin dye for detecting acetate anions through the anion-induced deprotonation of phenolic-OH groups (Scheme 13) [294]. The fluorescence quenching of **115** can be attributed to the PET process from the oxygen atom to the π^* orbitals of anthraquinone. The authors applied the Stern–Volmer equation to analyze the fluorescence titration curve, which yielded a linear graph. Based on this analysis, the Stern–Volmer extinction constant was 2.3×10^3 M^{-1}. The turn-OFF behavior can be interpreted as a NOT gate.

In general, traditional sensors that exhibit optical signal intensification (ON, output "1") or suppression (OFF, output "0") responses can be classified, respectively, as YES and NOT MLGs. However, this is a very generic classification because there are no combinations of inputs in these cases, as these are generic systems. Hence, in numerous instances, as those described by Li et al. [290] and Noushija et al. [294], the sensors are not explicitly characterized as MLGs. Even so, these two classes of MLGs are essential to be discussed, as they are used to compose more complex systems.

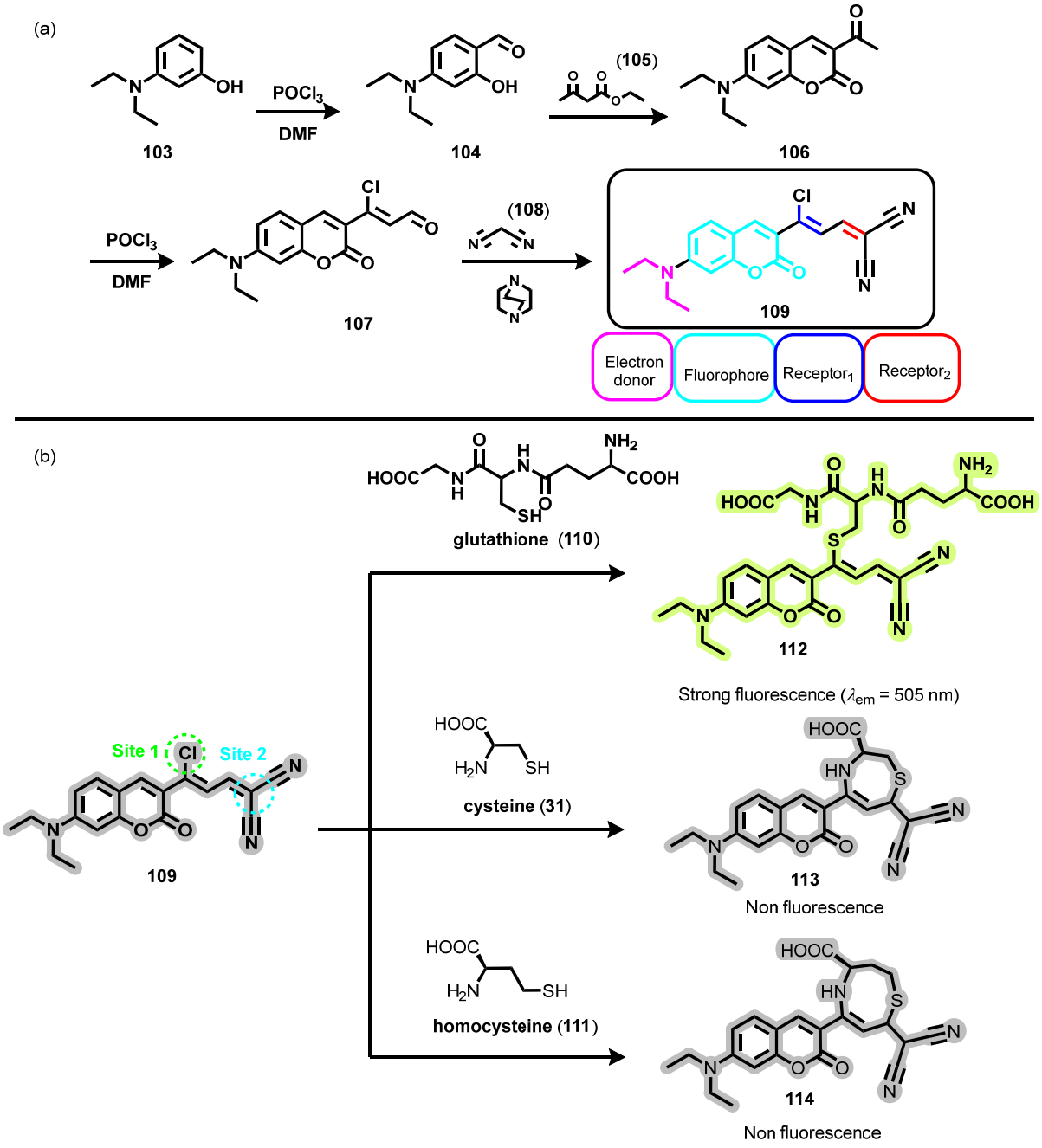

Scheme 12. (**a**) The synthetic route for obtaining chemosensor **109**, proposed by Li et al. [290]; (**b**) GSH, Cys, and Hcy structures and adducts (**112**–**114**) formed between them and the chemosensor **109**.

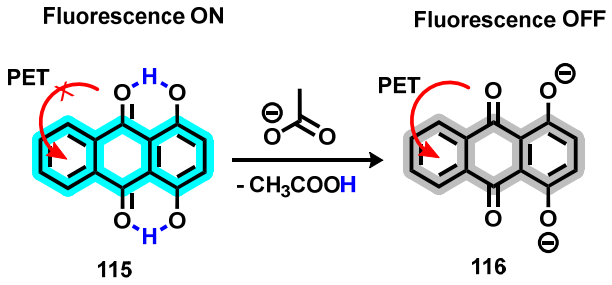

Scheme 13. The sensing mechanism of compound **115** and acetate anion, according to Noushija et al. [294].

8.3. "AND" Logic

AND logic produces an output "1" only when both inputs, designated as input$_1$ and input$_2$, correspond to "1" concurrently. In other words, it occurs when two or more inputs are present simultaneously and produce a single output value only obtained under these conditions. Since the first molecular AND logic gate was created in 1993 [11], the field of molecular-logic-based computation based on this particular logic gate has garnered significant attention. Recently, Gauci and Magri designed compounds based on crown-ether-fused 4-piperazino-N-aryl-1,8-naphthalimides (**121** and **122**) and investigated the effect of the polarity of the solvent on the reconfiguration of the identified logics, between the TRANSFER logic and the AND logic (Scheme 14) [295]. The 4-chloro-N-aryl-1,8-naphthalimides (**117**) reacted with piperazine (**118**) in *N*,*N*-dimethylformamide (DMF) to afford compounds **119**–**122**. The molecular structure exhibits dual interaction sites: the crown ether, engaging to binding with Na^+ (for compound **121**) or Ba^{2+} (for compound **122**), and a piperazine unit capable of undergoing protonation. The naphthalimide unit functions as a signaling moiety. The authors point out that the molecules correspond to two-input TRANSFER logic gates, activated by Na^+ or H^+ (**121**), triggered by Ba^{2+} (**122**), in water, and as logic gates of the two-input AND type, controlled by Na^+ or H^+ (**121**), activated by Ba^{2+} (**122**), when studied in methanol (Scheme 14b,c).

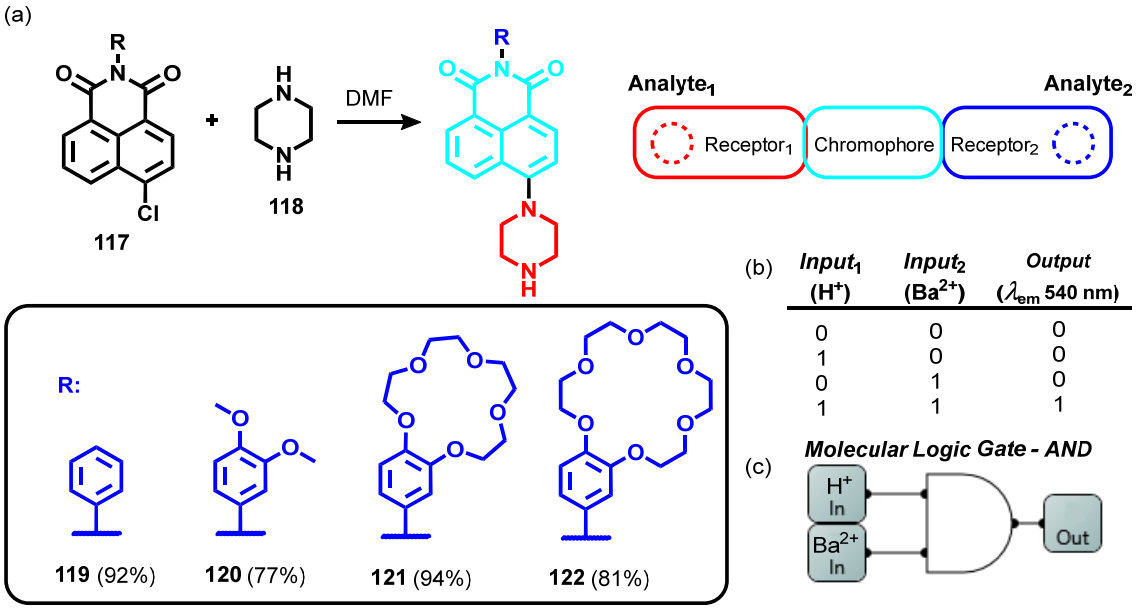

Scheme 14. (**a**) Synthetic route to obtain compounds **121** and **122** based on crown ether development by Gauci et al. [295]; (**b**) Corresponding truth table and (**c**) MLG diagram.

8.4. "NAND" Logic

NAND can be considered a combination of the NOT and AND gates. Precisely, the output of the AND gate is linked to the input of the NOT gate, which inverts the output of the AND gate [296]. Unlike the AND gate, the NAND gate does not generate an increased output signal if two analytes are present simultaneously; instead, it does so in all other conceivable situations: the absence of both inputs, the presence of input$_1$, or the presence of input$_2$ individually. Fang et al. synthesized examples of NAND MLGs (**128** and **129**) through the coupling of tetrathiafulvalene (**127**) and 5-methoxy-2-pyridylthiazoles (**123**–**124**; Scheme 15) [297]. Palladium-catalyzed coupling reactions offer a reliable and efficient approach to constructing carbon–carbon bonds, which is particularly useful when considering the requirements for building a fluorophore. Halogenated groups are important starting materials for such reactions. Using $Pd(PPh_3)_4$ as the catalyst, the authors achieved a 58% yield of both **128** and **129** by performing a Stille coupling reaction that joined 5-methoxy-2-pyridylthiazole (**125**–**126**) (a fluorophore) with Bu_3Sn substituted tetrathiafulvalene (**127**).

Due to the unique reversible and selective oxidation property of tetrathiafulvalene, the fluorescent emission of **128**–**129** can be switched ON and OFF based on the oxidation states of the tetrathiafulvalene unit. Therefore, the researchers noted that adding Fe^{2+} or $NOBF_4$ individually did not affect the emission, resulting in a high fluorescence output "1" from the gate. However, the presence of both Fe^{2+} and $NOBF_4$ resulted in fluorescence quenching. This phenomenon was attributed to the sequential quenching by Fe^{2+}, induced by the oxidation of Fe^{2+} by $NOBF_4$. This output pattern corresponds to the performance of an electronic NAND gate (Scheme 15b,c).

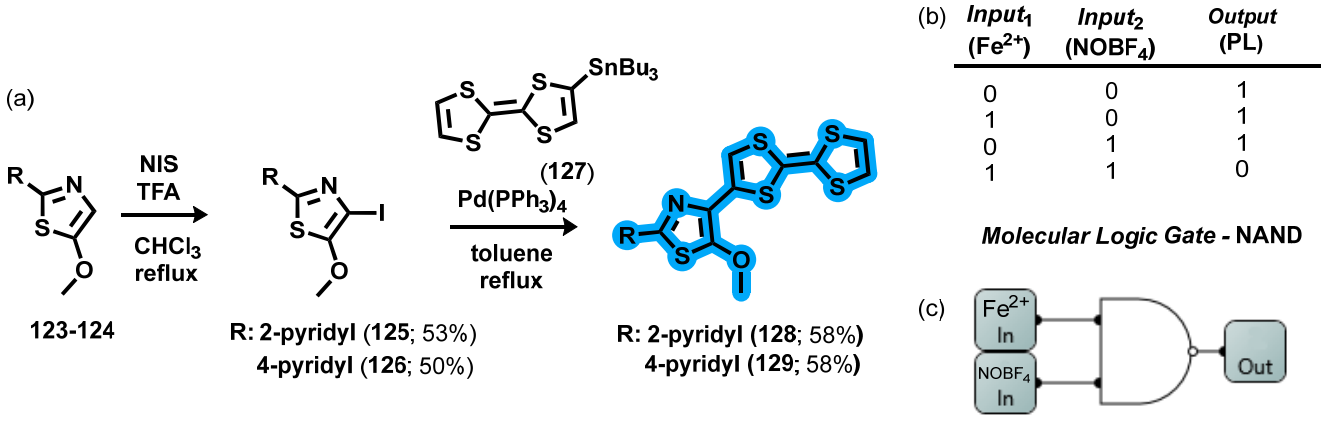

Scheme 15. (**a**) Synthesis of compounds **128** and **129** described by Fang et al. [297]; (**b**) Truth table for NAND logic and (**c**) the corresponding diagram.

8.5. "INHIBIT" Logic

The INHIBIT logic gate blocks or inhibits the output when a signal is present at a specific input, regardless of the other inputs. This behavior corresponds to AND gates with one of the inputs inverted through a NOT function, essentially acting as a veto power over an input [298].

This type of logic is recognized in detection systems based on displacement assays. Introducing a competitive analyte disrupts the binding/interaction between the chemosensor and the initial analyte, restoring the optical properties of the primary system [276]. In a simplified way, the presence of a second input inhibits the response of the first input.

A traditional approach for designing sensors for Hg^{2+} detection involves using rhodamine and naphthalimide bases via ring-opening reactions. These sensors can undergo rhodamine lactam ring opening upon exposure to Hg^{2+} ions, forming mercury–ion complexes [299]. For instance, Bai et al. designed a rhodamine-6G-based MLG (**135**) for colorimetric and fluorimetric recognition of Hg^{2+} and I^- (Scheme 16a) [300].

The colorless and non-fluorescent solution of MLG **135** submitted to $input_1$ of Hg^{2+} resulted in a yellow solution via a naked-eye perception, with fluorescence emission at 560 nm. This phenomenon was attributed to the spirolactam ring-opening amide induced by Hg^{2+} (Scheme 16b), investigated via FT-IR and HRMS spectra. The sequential $input_2$ of I^- to MLG **135** solution led to fluorescence quenching, indicating the recovery of the spirolactam form.

The authors have described that the reversibility of this process could be repeated up to eight times without significant loss in fluorescence efficiency. In this sense, $input_1$ (Hg^{2+}) enhanced fluorescence (YES operation), while the interaction of $input_2$ (I^-) with **135** resulted in fluorescence quenching (**135**), implementing the required NOT gate. MLG **135** operates parallel with the fluorescence output signals, which implements the necessary AND function. Therefore, when evaluating the fluorescence at 560 nm after introducing Hg^{2+}, I^- and an equimolar mixture of Hg^{2+} and I^-, **135** can be characterized as an INHIBIT logic gate (Scheme 16c,d). In other words, I^- inhibits the Hg^{2+} input.

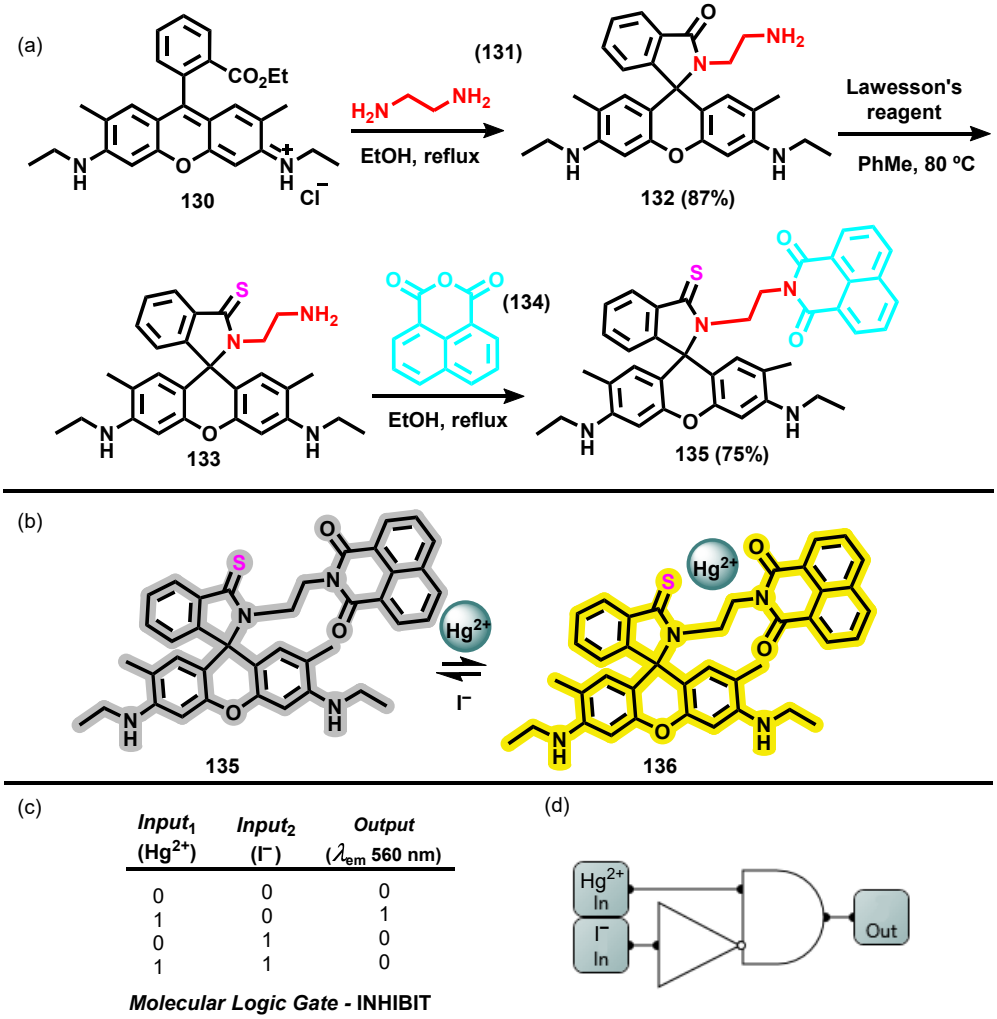

Scheme 16. (**a**) MLG rhodamine-6G-based (**135**) described by Bai et al. [300]; (**b**) Sensing mechanism for detection of Hg^{2+} and I^-; (**c**) Truth table and (**d**) the corresponding diagram.

Considering sensors designed for the primary detection of Hg^{2+}, complexing agents such as sulfides, EDTA, and other chelating agents can effectively decomplex the Hg^{2+} ions and reinstate the system's original properties [301,302].

For instance, Kumar et al. designed the MLG **140**, based on 2-amino pyrazine and phthalaldehyde, via a condensation reaction (Scheme 17a) [303]. Upon addition of Hg^{2+} ($input_1$ "1"), the initially non-fluorescent (output "0") **140** resulted in a turn-on response, displaying intense emission at 410 nm (**141**; output "1"). This phenomenon was attributed to the binding of **140** with Hg^{2+} interrupting the PET process, thereby inducing the chelation-enhanced fluorescence (CHEF) effect. Subsequent addition of EDTA ($input_2$ "1") to **141** solution led to fluorescence quenching (output "0") due to the formation of the EDTA–Hg^{2+} complex and the release of MLG **140** (Scheme 17b). The sequential increment of Hg^{2+} recovered the fluorescence emission, indicating the reversibility of the MLG **140**. Five more alternative cycles of additions of Hg^{2+} and EDTA were performed without affecting the process. The suggested sensing mechanism involves the coordinating Hg^{2+} with carbonyl groups. The CHEF effect increases the rigidity of the sensor, interrupting the PET process and leading to fluorescence emission. The reversibility of **140** induced by EDTA allowed the description of **98** as an INHIBIT molecular logic gate. Considering the $input_1$ (Hg^{2+}) and $input_2$ (EDTA) and emission at 410 nm as output, an INHIBIT logic gate may be established. The truth table and the MLG **140** are described in Schemes 17c and 17d, respectively.

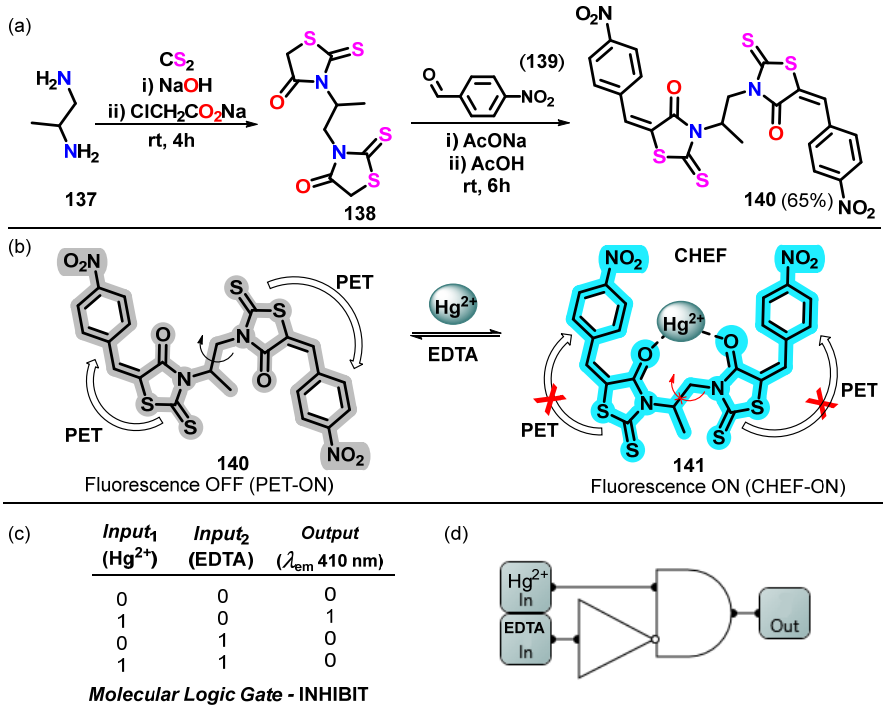

Scheme 17. (**a**) Molecular logic gate **140** for detection of Hg^{2+} described by Kumar et al. [303]; (**b**) The sensing mechanism and (**c**) corresponding truth table and (**d**) diagram.

INHIBIT gates can also be devised by introducing a suppressor to the system. In Scheme 18a, compound **145** features a dioxobenzene group (ether crown), an electron density donor via internal charge transfer (ICT), and the group bis(2-pyridin)pyridazine, an electron acceptor [304]. Logical operations can be constructed by adding K^+ and Zn^{2+} (Scheme 18b) cations as inputs and the fluorescence emission as an output (response). These operation outcomes are summarized in the truth table in Scheme 18c.

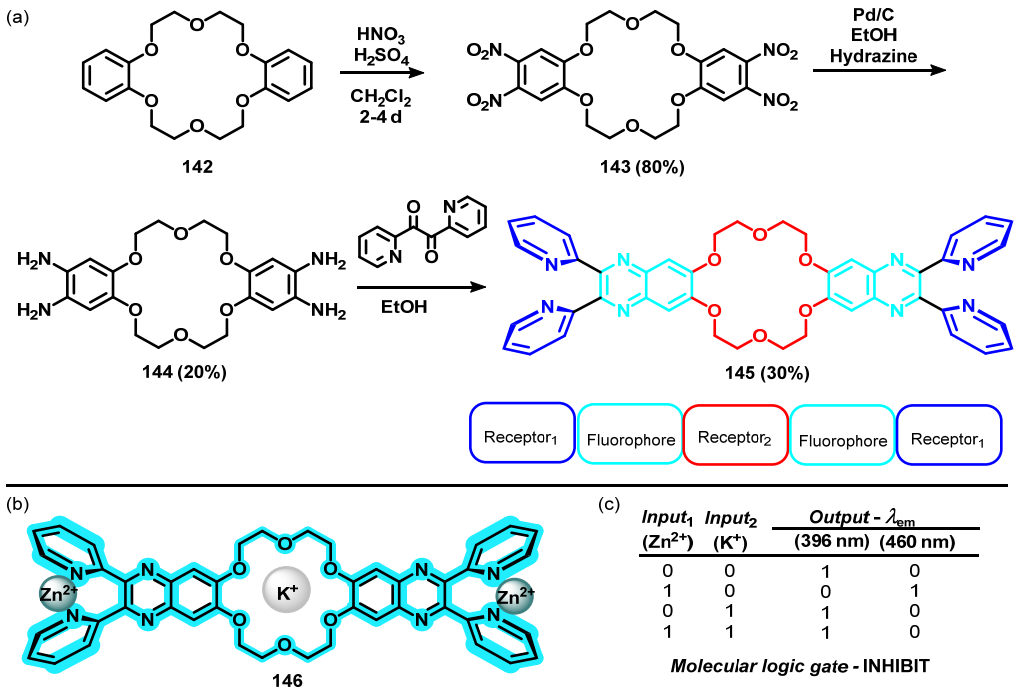

Scheme 18. (**a**) Molecular logic gate **145** for detection of K^+ and Zn^{2+} described by Li et al. [304] and (**b**) the corresponding truth table and (**c**) diagram associated.

In this example, in the absence of cations (input "0"), MLG **145** exhibits emission at 396 nm (output$_{396}$ "1"). However, when Zn^{2+} cation (input$_1$ "1") binds to the pyridinyl groups, the ICT intensifies, causing the emission to shift to 460 nm (output$_{460}$ "1"). In the absence of the Zn^{2+} cation (input$_1$ "0"), K^+ (input$_2$ "1") coordinates to the crown ether, leading to a reduction in ICT due to the diminished electron-donor effect in the ether crown. This coordination results in emission maintenance at 396 nm (output$_{396}$ "1"). The simultaneous addition of Zn^{2+} (input$_1$ "1") and K^+ (input$_2$ "1") preserves the emission at 396 nm (output$_{396}$ "1"). Conversely, the opposite operation (sequence) maintains the fluorescence emission unchanged at 460 nm.

As previously discussed, this MLG is classified as the INHIBIT type, an integration between the NOT and AND operations. In this case, the NOT operation is applied only to the second input (input$_2$–K^+ addition), which reduces the effect of the first input (Zn^{2+} addition input). In other words, adding Zn^{2+} (input$_1$) shifts the MLG emission from 396 nm to 460 nm, whereas adding K^+ (input$_2$) reduces this change, reverting to the emission value at 396 nm. Furthermore, **145** can be understood as an OFF–ON–OFF molecular device triggered by Zn^{2+} and K^+.

A remarkable example was introduced by Guo et al., wherein the authors explored an asymmetrical Receptor$_1$–Chromophore–Receptor$_2$ bis-condensed dicyanomethylene-4*H*-pyran (DCM)-type derivative as an MLG (**151**) [305]. Compound **151** was synthesized by the condensation of 4-dicyanomethylene-2,6-dimethyl-4*H*-pyran (**147**) with 4-hydroxybenzaldehyde (**148**) and then with 4-[bis(pyridin-2-yl-methyl)amino]benzaldehyde (**150**) with 35% yield (Scheme 19a). The two receptors of **151** display different spectral responses upon hosting the two guests: Zn^{2+} and OH^- (Scheme 19b). A noticeable hypsochromic shift from 442 to 415 nm is observed upon the incremental addition of Zn^{2+} to **151**. This shift is accompanied by a visible color change from orange-yellow to light green. These observations suggest that upon coordination with Zn^{2+}, the electron-donating character of the amine nitrogen atom within the chromophore group is reduced, resulting in a decrease in the efficiency of ICT. The authors observed a slight hypsochromic shift in emission spectra and an almost complete fluorescence quenching. Conversely, upon base being added to **154** in the presence of Zn^{2+}, a shift from 415 to 442 nm in the absorption spectrum is observed (**153**). The varying electron-donating character of the receptor moiety in the ICT mechanism was exploited to produce logic operations such as XOR and INHIBIT, considering both Zn^{2+} and OH^- as inputs (Scheme 19c).

8.6. "IMPLICATION" Logic

IMPLICATION logic is a type of logic operation embodying a conditional statement, such as "If A, then B". If A is true (or "1") and B is false (or "0"), the output is false (or "0"). However, if A is true or B is true, or both are true (or "1"), the output will be true (or "1"). The only situation in which the IMPLICATION gate returns false (or "0") is when the first condition is true but the second condition is false.

A recent example of an IMPLICATION MLG was described by Souto and Machado via structural functionalization of ethyl(hydroxyethyl)cellulose (**EHEC**) and a silica-based xerogel (**SBX**) with a precursor of 18-crown-6-styrylpyridine **158** (Scheme 20a) [306]. The resulting materials were employed as fluorescent devices to detect Hg^{2+} in water. The precursor **158** was easily synthesized with a yield of 57% by an aldolic condensation of aldehyde **156** and methylpyridine (**157**). This compound was incorporated into the polymeric matrix via a covalent bond formed between the pyridine nitrogen and the chloropropyl groups of XSB. This covalent bond generates a positively charged pyridine group in **159**. Upon Hg^{2+} complexation by the macrocyclic moiety, there was a modification in the transfer of electronic density from the crown ether to the positive end of the molecule. Consequently, a shift in the emission from yellow to green occurred.

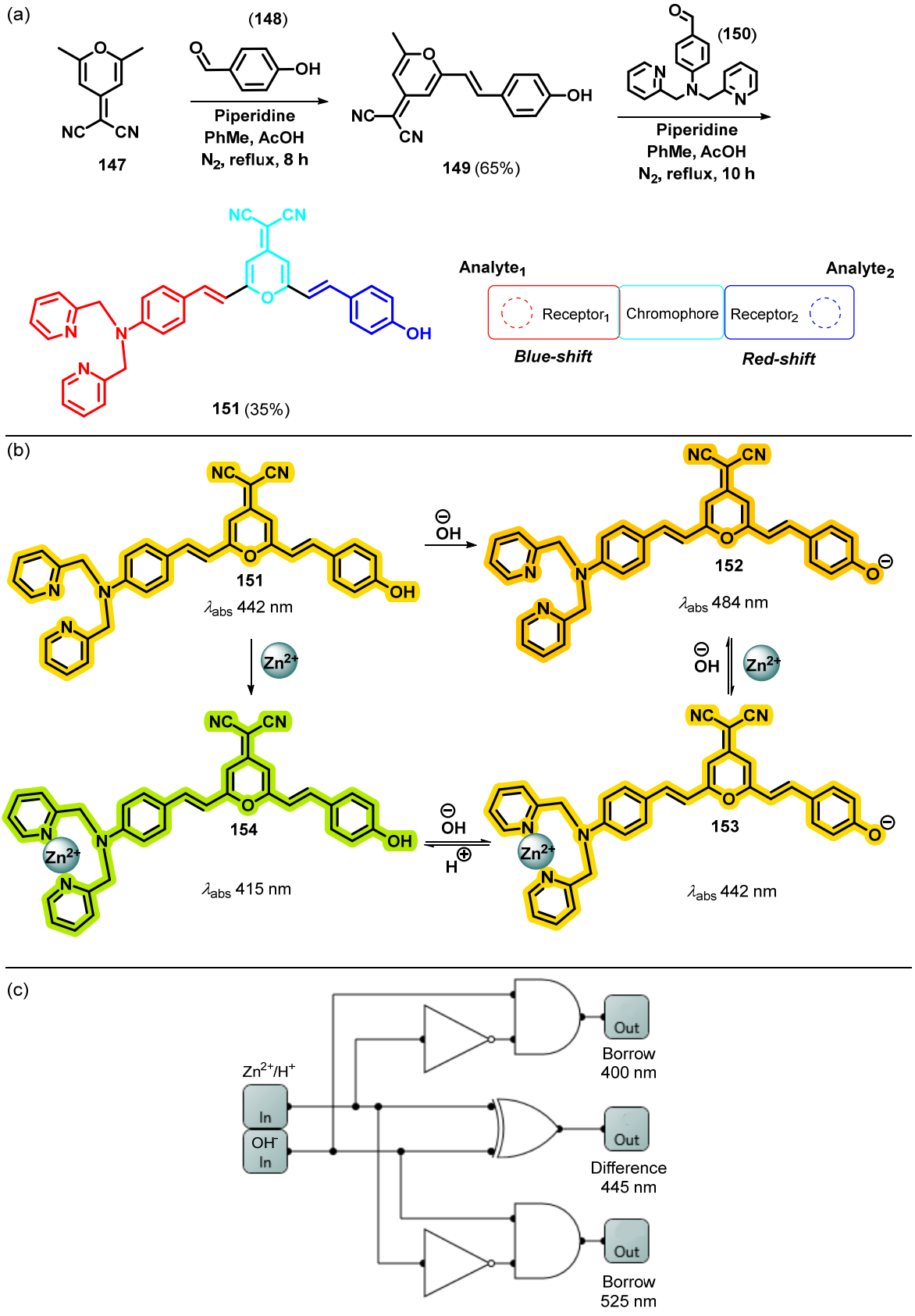

Scheme 19. (**a**) Synthesis of **151** proposed by Guo et al. [305]; (**b**) Sensing mechanism for Zn^{2+} and (**c**) logical interpretation.

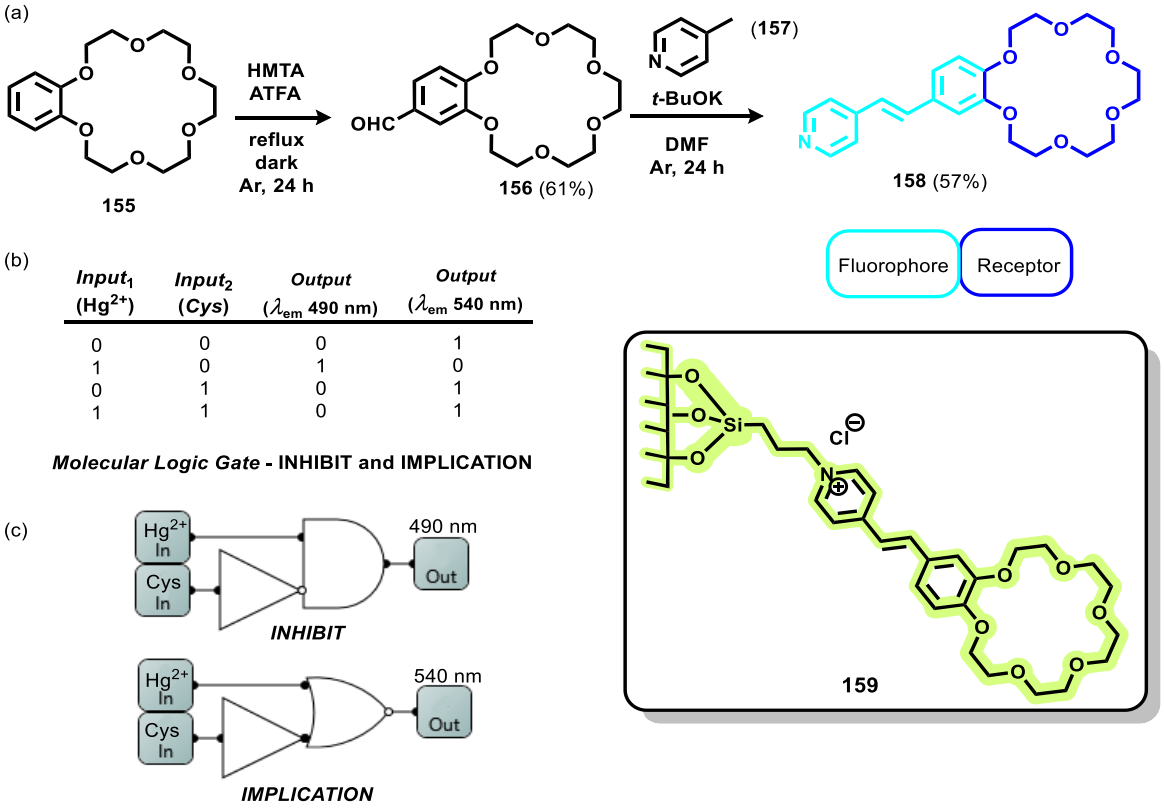

Scheme 20. (**a**) Synthesis of compound **158** and functionalized material **159**, produced by Souto and Machado; (**b**) The truth table of INHIBIT-type and (**c**) IMPLICATION-type logic [306].

The strong affinity between the Hg^{2+} and sulfur-containing ligands like cysteine (Cys) allows the design of competitive assays, and therefore, an interpretation based on INHIBIT logic (Scheme 20b,c). However, when binding Hg^{2+}, Cys displaces the material with the free macrocycle, restoring its yellow color. In other words, the presence of Cys inhibits (or suppresses) the fluorescence emission output signal at 506 nm due to the presence of Hg^{2+}. Nevertheless, considering the opposite interpretation, that is, taking the fluorescence emission at 540 nm as the output, rewriting the truth table, the authors identify an IMPLICATION logic function, i.e., the absence of both inputs (Hg^{2+} and Cys) and their combined presence result in the same output "1". INHIBIT and IMPLICATION operations are often interpreted together, since they correspond to inverse truth tables (Figure 4).

Diverse examples of MLGs bearing crown ether groups have been reported in the literature due to their suitability as chelating groups for different metals, depending on the macrocycle size and the environment in which it is inserted [294]. For example, benzo-15-crown-5 ether and benzo-18-crown-6 ether groups are often employed to recognize sodium and potassium cations, respectively [295]. Prasanna de Silva's seminal work (Figure 5) [11] already included the benzo-15-crown-5 group as a sodium ion detector unit [227].

Sharma et al. described the modification of phenothiazine-5-oxide (**160**–**162**) via Suzuki cross-coupling reaction to insert a benzaldehyde group, with behavior as the acceptor unit, to afford the MLGs (**164**–**166**) (Scheme 21) [235]. The authors have demonstrated a practical application of acidofluorochromism of MLG **164**–**166** by fabricating filter paper strips coated with them. Under UV light (λ = 365 nm), these paper strips exhibited an intense fluorescence emission, suppressed upon exposure to TFA vapors. The sequential exposition to TEA vapors recovered the fluorescence. The reversible acidofluorochromic behavior of MLG **164**–**166** toward TFA and TEA in the solid state was described as an IMPLICATION logic gate, as indicated by the truth table (Scheme 21a,b). DFT studies revealed that the reversible acidochromism is related to the protonation/deprotonation of the sulfinyl oxygen atom.

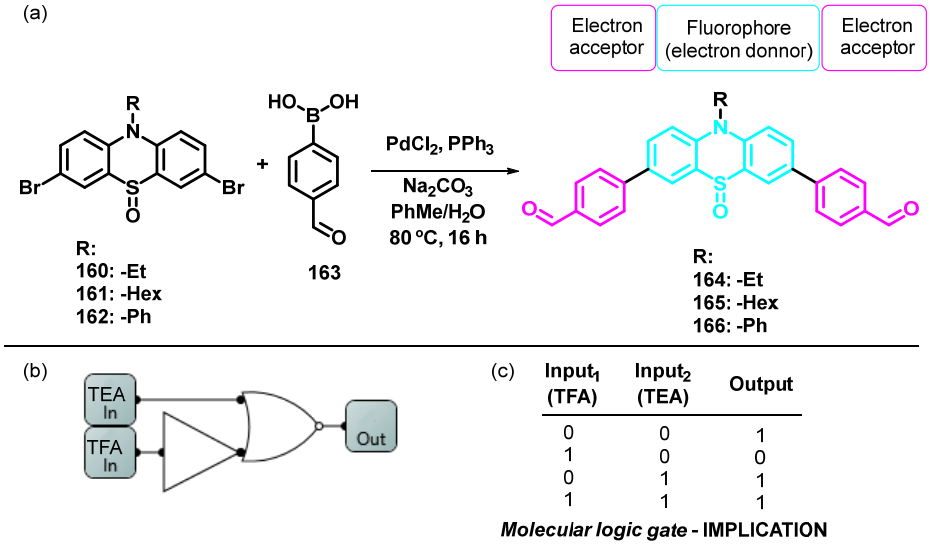

Scheme 21. (**a**) Synthetic route of MLG **164**–**166** described by Sharma et al.; (**b**) IMPLICATION logic gate and (**c**) the corresponding truth table [235].

Another example of an IMPLICATION-type logic gate was described by Tripathy et al. through the synthesis of the azo dye **168** bearing a D-π-A architecture, with salicylaldehyde as a donor group and nitrobenzene as an acceptor (Scheme 22a) [307]. Compound **168** displayed a reddish-pink color in the DMSO-water medium, attributed to the ICT from the electron-donating phenolic moiety to the electron-withdrawing nitrobenzene group. Adding Hg^{2+} as input to MLG **168** decreased the absorption at 502 nm (attributed to the ICT) with a concomitant emergence of an absorption band centered at 361 nm. This change corresponded to a color change from reddish-pink to a colorless solution (**169**). The authors have attributed this phenomenon to the partial positive charge of the oxygen atom from the hydroxyl group upon binding to Hg^{2+} (Scheme 22b). This interaction significantly decreases the conjugation of the molecular system and electron-donating ability for ICT, reducing the D-π-A phenomenon.

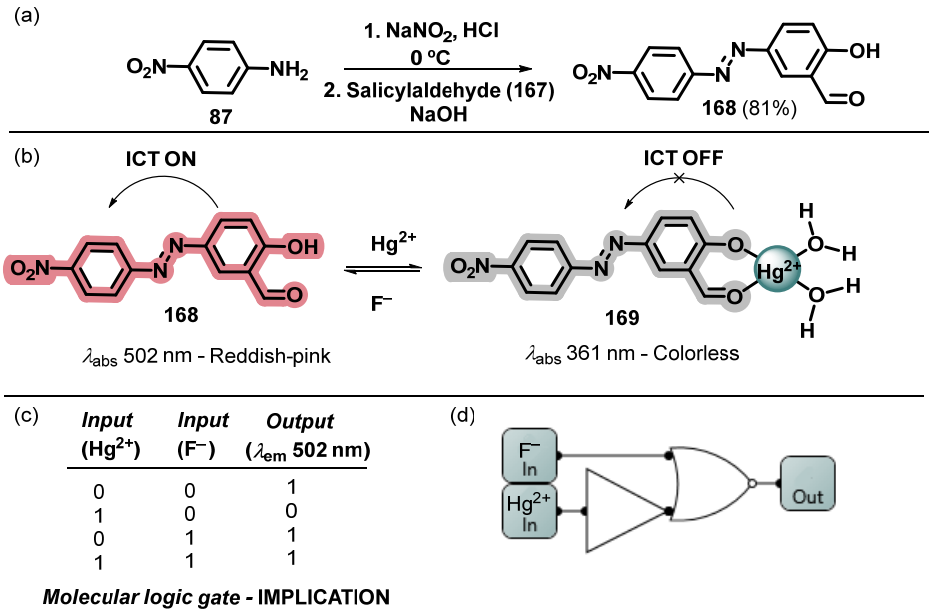

Scheme 22. (**a**) The synthetic route for **168** proposed by Thipathy et al. [307]; (**b**) Sensing mechanism for detecting Hg^{2+} and fluoride; (**c**) Corresponding truth table and (**d**) logic diagram.

Additionally, the researchers described a weaker binding of MLG **168** with Cu^{2+}, evidenced by a little hypsochromic shift with increased intensity of the shoulder peak from 405 nm to 395 nm, also associated with a decrease in absorbance at 502 nm. Sequentially adding F^- ($input_2$) to **169** recovered the reddish-pink color, and the absorption centered at 502 nm, demonstrating the system's reversibility. This anion may promote the demetallation of **169**, increasing the electron density on the phenolic oxygen atom and the consequent increase in the ICT process. This phenomenon was repeated over several cycles in a "rhythmic manner". Considering the $input_1$ (Hg^{2+}) and $input_2$ (F^-), the absorption band centered at 502 nm as output in an ON–OFF–ON input/output response, the MLG **168** was described as an IMPLICATION-type logic (Scheme 22c,d).

8.7. More Elaborated MLGs

More elaborated MLGs, such as half-adders, half-subtractors, encoders, decoders, multiplexers, and demultiplexers, can be built by combining basic MLGs [308–315]. However, a detailed discussion about them is beyond this review's scope. The growing interest in using probes to detect and quantify multiple analytes in competitive assays has motivated researchers to pursue increasingly integrated arrays.

One of these systems is "*Lab-on-a-Molecule*" [316], proposed almost twenty years ago as a device that can recognize three species in an assay and generate an output response only at the intersection of the three species. In 2019, Scerri et al. introduced device **172** as an example of *Lab-on-a-Molecule* (Scheme 23), bearing the fluorescent naphthalimide core and three receptors: (1) ferrocene, as an electron donor in the recognition of Fe^{3+}; (2) the basic site piperazine, acting as a receptor for H^+; and (3) the ether-*N*-(2-methoxyphenyl)aza-15-crown-5 group, functioning as a receptor for Na^+ ion through coordination with this ion [317]. Compound **172** exhibited a weak fluorescence quantum yield (output "0") and, as indicated by the truth table in Scheme 23, the separate addition ($inputs_{1,\ 2,}$ or $_3$ "1") of H^+, Fe^{3+}, or Na^+ (operations B, C, and E) did not significantly increase the fluorescence quantum yield (output "0"). A similar result was obtained with the combined addition of H^+ and Fe^{3+} ($input_1$ "1" and $input_2$ "1", operation D); H^+ and Na^+ ($input_1$ "1" and $input_3$ "1", operation F); or Fe^{3+} and Na^+ ($input_2$ "1" and $input_3$ "1", operation G). However, the simultaneous addition of the three ions ($inputs_{1,\ 2,}$ and $_3$ "1") increased about twenty times in fluorescence quantum yield (output "1", operation H). Since these systems are constructed to correspond to a three-input AND logic gate, it is understood as a *Lab-on-a-Molecule*.

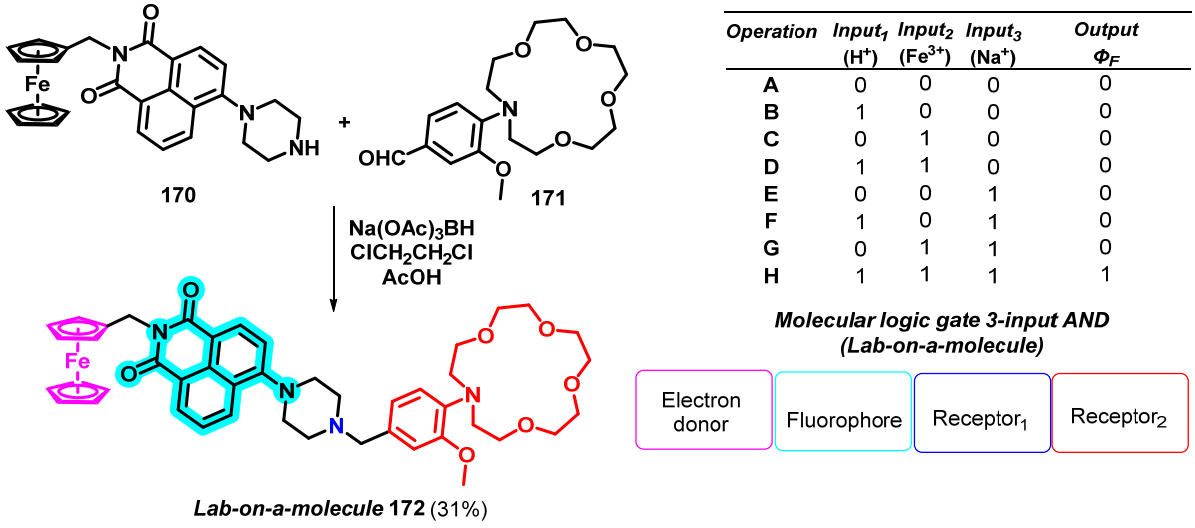

Operation	*Input*$_1$ (H^+)	*Input*$_2$ (Fe^{3+})	*Input*$_3$ (Na^+)	*Output* Φ_F
A	0	0	0	0
B	1	0	0	0
C	0	1	0	0
D	1	1	0	0
E	0	0	1	0
F	1	0	1	0
G	0	1	1	0
H	1	1	1	1

Scheme 23. Lab-on-a-molecule **172** proposed by Scerri et al. and the truth table corresponding to an AND-type gate with three inputs [317].

9. Molecular Machines as Logical Optical Devices

Rotaxanes and catenanes constitute a group of structures that can be modulated to operate as MLGs due to their inherent adherence to binary logic principles. A careful and comprehensive synthesis approach is necessary for producing rotaxanes and pseudorotaxanes. Currently, various strategies are available for creating molecular machines, including pre-organizing components using hydrogen bonding, metal coordination, hydrophobic forces, and covalent bonds [318–320]. Rotaxanes containing chelating groups designed to bind with cations/anions are good candidates for selective sensing of a particular analyte, depending on the overall construction of a mechanically interlocked system having specific cavity dimensions tailored to the desired analyte [321–325].

A remarkable structure based on a bistable[1]rotaxane (**178**) was reported by Li et al. [326]. The structure of a rotaxane features a dual operation system comprising the interaction of two receptor sites with modulating analytes: one responsive to acid/base conditions and the other to redox centers. The redox-active Fe unit is introduced as a connecting unit for two portions of the thread and provides a unit sensitive to oxidizing/reducing agents. The thread bears an amino group sensitive to pH changes and a positively charged triazole group. Depending on the environmental conditions, both groups can interact with the 24-crown-8 macrocycle, located at one end of the thread. Additionally, a 4-morpholinnaphthalimide group was selected as a terminal stopper and fluorophore, enabling the modulation of its fluorescence through a distance-dependent PET process between an electron-rich metallocene unit and an electron-deficient fluorophore.

As shown in Scheme 24, the synthetic route employed by the authors incorporates reactions previously discussed in this review. The connection of **173** and **174** groups was achieved through a 1,3-dipolar cycloaddition, resulting in the formation of a triazole using CuI in the presence of *N*,*N*-diisopropylethylamine (DIEA), resulting in a 70% yield of **175**. Subsequently, **175** underwent methylation with CH_3I and anion exchange with an aqueous NH_4PF_6 solution, providing **176** with a high yield (90%). Compound **176** was then linked to the **177** group via a 1,3-dipolar cycloaddition catalyzed by $Cu[(CH_3CN)_4]PF_6$ in dichloromethane, yielding the target [1]rotaxane (**178**) with a 74% yield.

The authors defined "active" and "inactive" signal modes for rotaxane operations. The relative mechanical movement of its ring and thread in response to external acid-base stimuli can produce an intense fluorescence signal output, representing the "active" mode when considering the amino group's deprotonation upon the base's presence (DBU input$_1$). In contrast, in the "inactive" signal mode after oxidation (Fe^{3+}, input$_2$), there was no evident change in fluorescence, which remained "locked" at its original level in the presence of $Fe(ClO_4)_3$. The fluorescence responses (output) of [1]rotaxane to the different DBU and Fe^{3+} combinations correspond to an INHIBIT logic gate, as represented in Scheme 24.

Klein et al. have described a new benzimidazole–iodotriazole motif based on halogen bonding, which has been integrated into the photoactive naphthalimide-based axle component of a bis [2]rotaxane [327]. Compound **186** was synthesized according to Scheme 25a. Initially, the naphthalimide-based precursor (**181**) was condensed to the triazole aldehyde (**180**), forming a benzimidazole core containing a **182**-functionalized end to serve as a stopper. By substituting the hydroxyl group at the opposite end of intermediate **182** with an azide moiety, followed by the subsequent addition of an isophthalamide macrocycle **185** to the system, a [2]rotaxane (**186**) is produced, representing a chloride anion template stoppering approach.

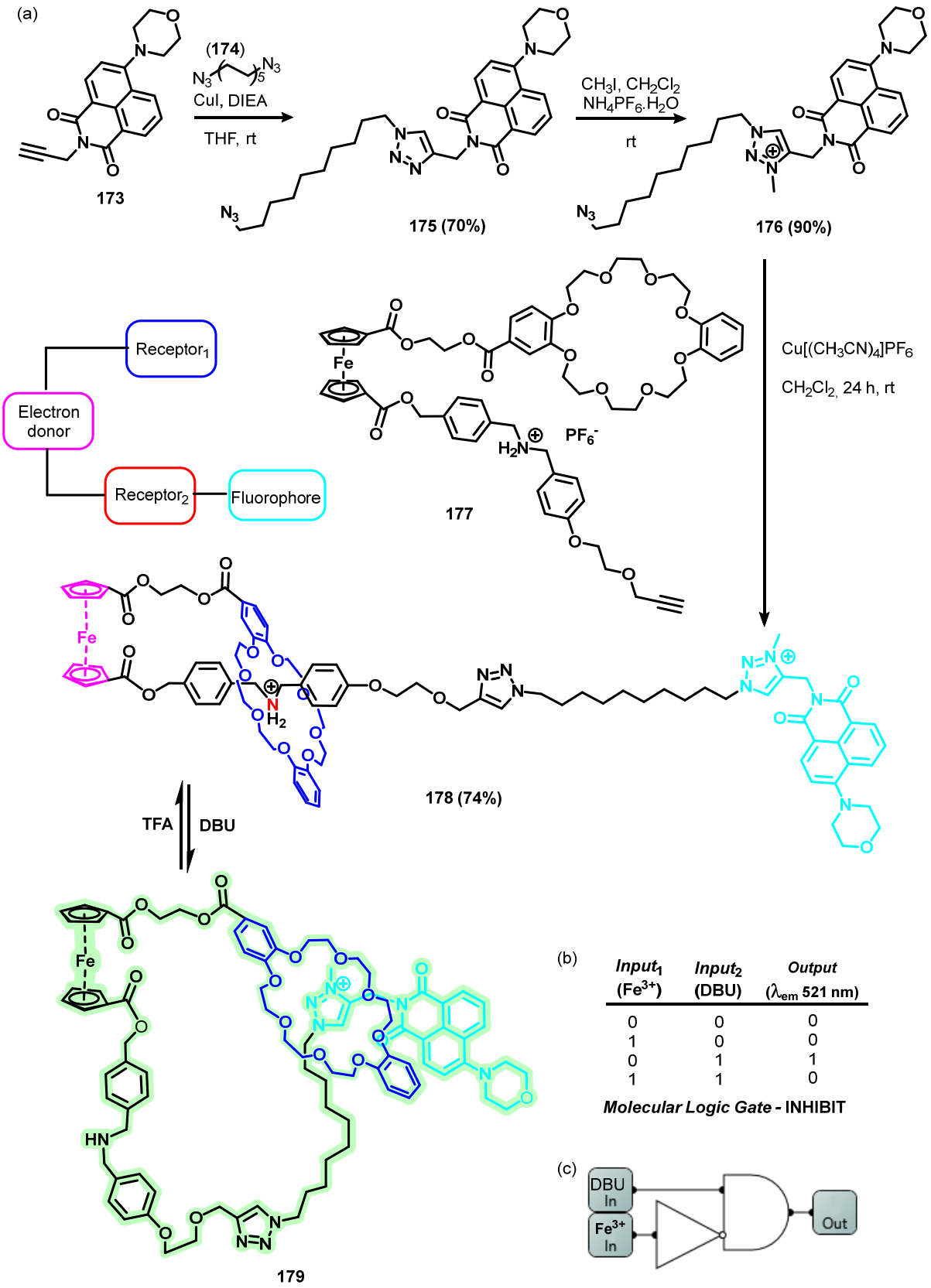

Input$_1$ (Fe^{3+})	*Input*$_2$ (DBU)	*Output* (λ_{em} 521 nm)
0	0	0
1	0	0
0	1	1
1	1	0

***Molecular Logic Gate* - INHIBIT**

Scheme 24. (**a**) Synthesis of rotaxane **178** reported by Li et al. [326]; (**b**) Corresponding truth table and (**c**) diagram.

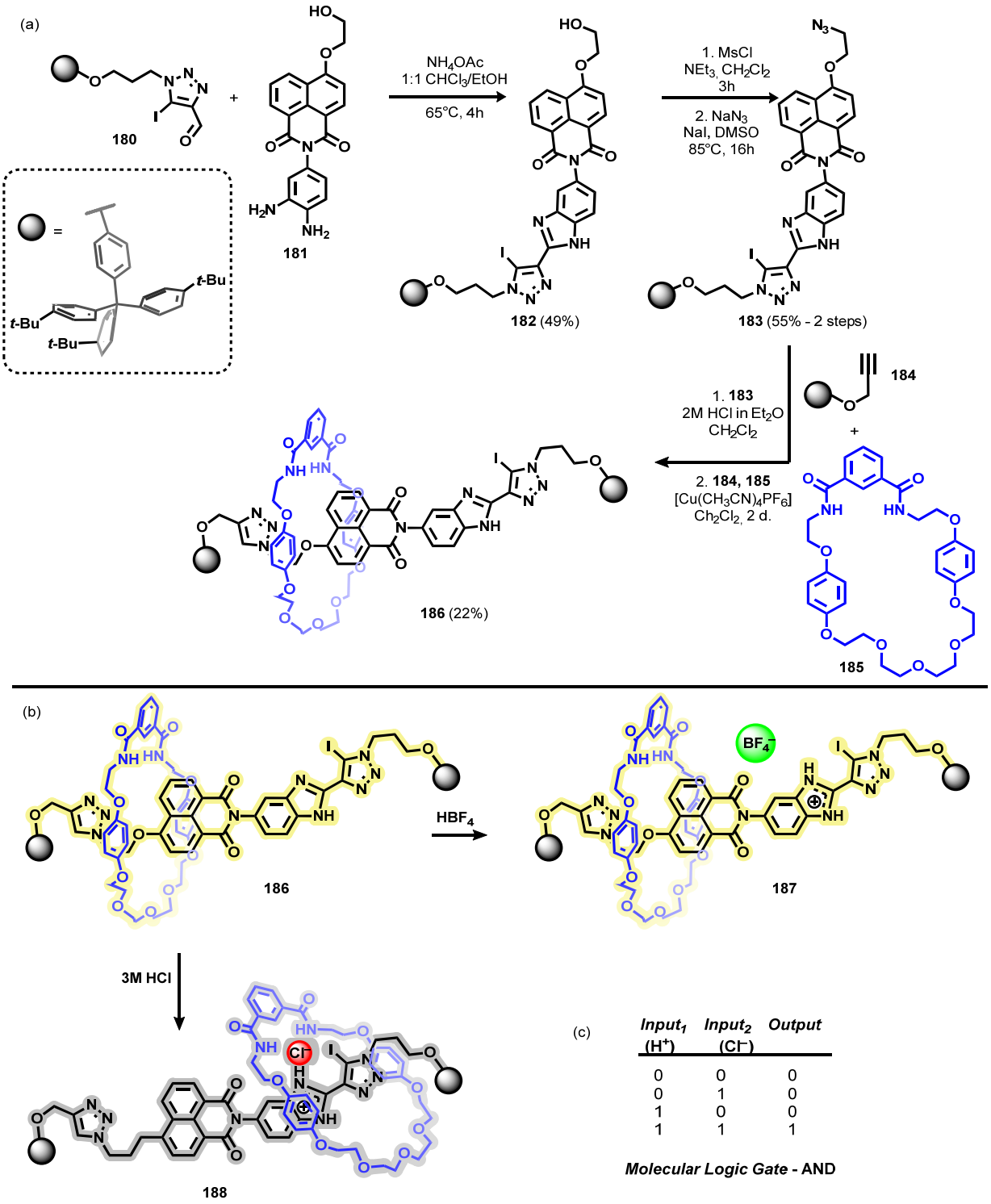

Scheme 25. (**a**) Structures proposed by Klein et al. for [2]Rotaxane **186**, (**b**) Sensing mechanism of **186** with HBF_4 and HCl; (**c**) The truth table of **186** corresponds to an AND-type molecular logic gate [327].

The neutral rotaxane **186** exhibits a yellow color in solution, attributed to the charge transfer between the electron-rich hydroquinone derivative within the macrocycle and the electron-deficient naphthalimide along the rotaxane axis. Upon the introduction of HCl, protonation of the imidazole core ensues, extinguishing this color. However, interestingly, when HBF_4 is added to the solution, no significant change in color is observed, suggesting that HCl and HBF_4 induce distinct perturbations in the rotaxane structure. Further investi-

gations through the ^{1}H-^{1}H ROESY NMR spectra of each compound demonstrated that the pronounced alteration induced by HCl is attributed to the relocation of the macrocycle from naphthalimide toward the benzimidazole nucleus, as indicated in Scheme 25b. A UV–Vis spectroscopic titration with anions was conducted after the protonation of **186** using HBF_4 to assess the significance of the counter anion's nature in inducing macrocycle translocation. Upon adding 50 equiv. of tetrabutylammonium chloride (TBACl), a notable shift in absorbance was observed, closely resembling the spectrum obtained with protonation using HCl. As a result, the authors deduced that both protonation and chloride ions as external stimuli are imperative to facilitating macrocycle translocation, exemplifying a system akin to an AND-type logic gate.

10. MLGs Based on Polymer Matrices

Integrating molecular recognition/detection mechanisms into various materials, such as silica, membranes, and polymeric films, presents an alternative approach to fabricating supramolecular systems to detect analytes.

Polymeric matrices—whether as a support solid surface for recognition molecules or polymers built from responsive monomers—offer several appealing characteristics, making them attractive in chemosensor and MLG development. Notably, they exhibit inertness against gases and liquids and have a substantial surface area in solid matrices. Furthermore, their shorter response time for efficient analyte detection and affordability render them highly attractive for optical detection device development.

An extensive possibility involves introducing a molecular chemosensor into the polymeric matrix through a physical mixture without forming or breaking chemical bonds. A second and interesting approach involves forming chemical bonds between solid support and a molecule exhibiting intrinsic photophysical properties that respond sensitively to a specific analyte.

In 2020, Bai et al. presented the fluorescent dye functionalized PEG **194** capable of recognizing Al^{3+} [328]. The synthetic strategy used by the authors consisted of a condensation reaction of 2,4-dihydroxybenzaldehyde (**189**) and furan-2-carbohydrazide (**190**), followed by the esterification of (**191**) with carboxylated PEG (**192**), as shown in Scheme 26a. Compound **193** displayed a pronounced broad absorption band at 330 nm. Upon introducing Cu^{2+}, Al^{3+}, and Ni^{2+}, a new band centered at 370 nm appeared. Solution **105** exhibits weak emission, and following the addition of 2.0 equiv. of Al^{3+}, a notable enhancement in fluorescence at λ_{em} = 436 nm (when excited at λ_{ex} = 369 nm) becomes evident. The fluorescence intensity of **193** was enhanced upon adding Al^{3+}, likely due to the complexation of the ions with the probe through CHEF. Moreover, the interaction between Al^{3+} and **193** triggers C=N isomerization, suppresses the PET effect, and contributes to the potential increase in fluorescence.

A series of detection tests were performed on the **193–Al^{3+}** complex using EDTA to explore the sensor's reversibility. Notably, in the presence of EDTA, the solution containing the material restored its optical properties to their state before complexing agent addition. This behavior revealed a reversible-type system, allowing analysis of the responses obtained for Al^{3+} and EDTA through an INHIBIT-type logic gate (Scheme 26b).

Finally, a third strategy considers the construction of a polymeric matrix from reactive monomers. In 2020, Zhou et al. reported a polymer matrix (PS)-based ratiometric fluorescent probe ($Eu(NTA)_3L$@PS, **199**) and the construction of an AND logic system with inputs of H^+ and ClO^- [329]. The preparation of the material consisted of a typical process of mini-emulsion polymerization (Scheme 27a). In the process, the reactive unit (the complex responsible for detection, **197**) is reacted with styrene (**198**) to build the polymeric matrix **199**. Concerning detection, in the absence of ClO^-, the probe exhibited a strong red emission at 618 nm, rapidly suppressed with increasing ClO^- in the presence of 3 eq H^+. At the same time, an emission at 496 nm increased. According to the authors, this response is obtained because ClO^- can swell the probe's polymer casing and allow the access of H^+, causing changes in photophysical properties. Only when the system receives

two inputs, H^+ and ClO^- together, can the output AND gate for fluorescence be activated (Scheme 27b).

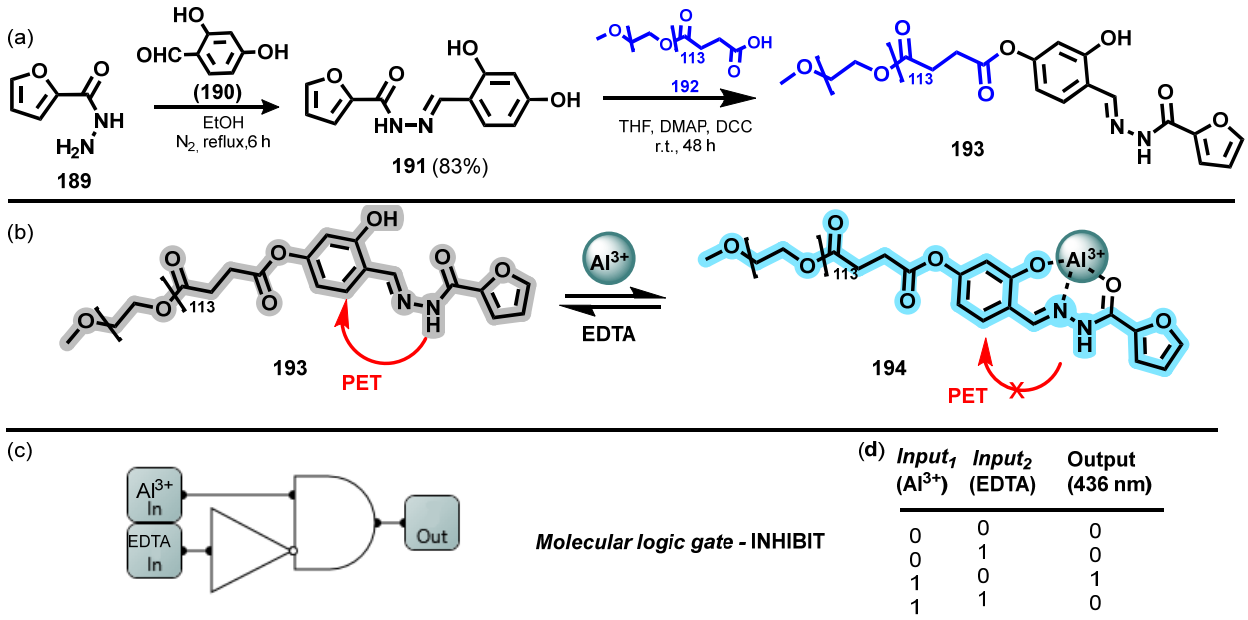

Scheme 26. (**a**) Synthesis of polymeric system **193** proposed by Bai et al.; (**b**) Sensing mechanism for recognition of Al^{3+} and EDTA; (**c**) Molecular logic gate system and (**d**) truth table Al^{3+} [328].

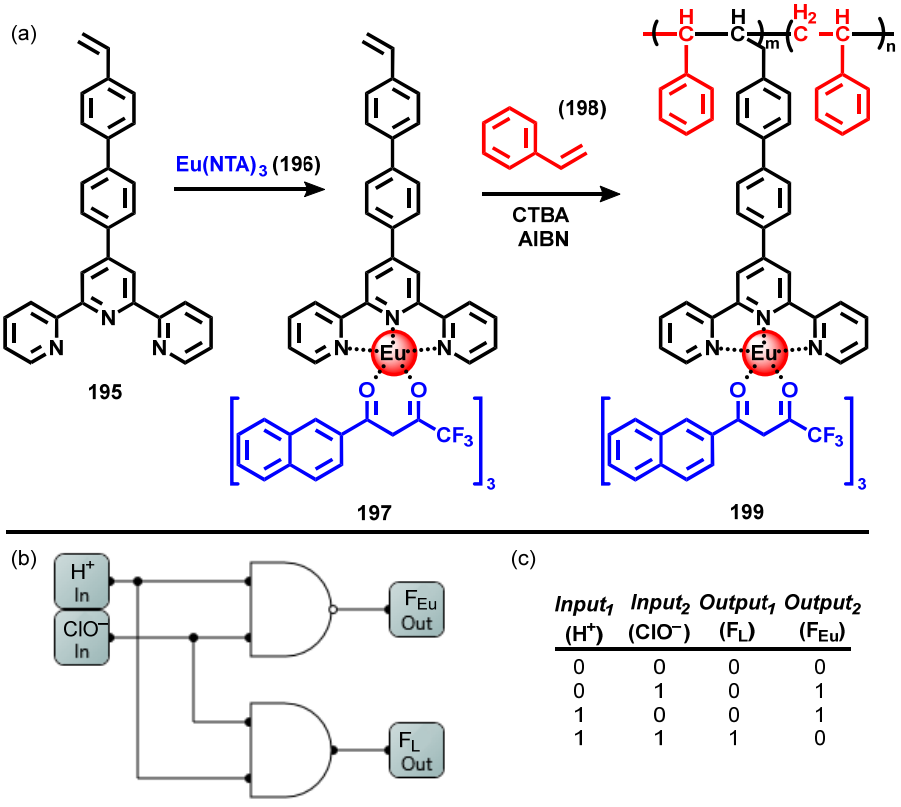

Scheme 27. (**a**) The polymerization reaction of **199** presented by Zhou et al.; (**b**) AND gate identified and (**c**) corresponding truth table [329].

11. Other Applications

Considering their potential for monitoring applications, MLGs have demonstrated their usefulness in several areas as biosensors to detect and monitor changes in cellular

processes, such as ion flux, enzyme activity, and pH [15,330,331]. They are also valuable for measuring blood electrolytes and tracking chemical species and properties in cells and tissues [332]. In addition to that, they can help detect toxic agents in aquatic environments, monitor nuclear residues, screen catalysts, and contribute to the field of theranostics [333–335]. Numerous examples of MLGs exploring the most diverse structural arrangements for various applications are reported in the literature. In addition to the examples discussed throughout the review, we present some selected examples in Table 1.

Table 1. Some other selected examples of applications of MLGs and their logic function.

	Logic Function	Analytes/Inputs	Application	Ref.
1	AND	$ONOO^-$ and mitophagy	Biological detection	[336]
2	AND	Na^+ and $H_2PO_4^-$	Ion pair detection	[337]
3	AND, OR, INHIBIT, IMPLICATION, NOR, and NAND	Cd^{2+}	Food safety	[338]
4	NOR	Hg^{2+} and Pb^{2+}	Cell imaging	[339]
5	AND	Amine and pH-based neurotransmitters	Visualization of neurotransmitter exocytosis	[340]
6	INHIBIT	TFA and TEA	Detection of neutral molecules	[341]
7	AND	Two types of miRNAs	Diagnosis and treatment of diseases	[342]
8	AND–INHIBIT–OR	H^+, Na^+ and Fe^{3+}	Cation detection	[343]
9	Lab-on-a-molecule	F^-, $H_2PO_4^-$ and AcO^-	Anion detection	[344]
10	Lab-on-a-molecule	SDS and SDBS	Differentiation of commercial surfactants	[345]
11	AND	Leucine aminopeptidase and monoamine oxidase	Hepatopathy differentiation	[346]
12	AND and INHIBIT	Protein and DNA	Medical diagnostics	[347]
13	INHIBIT	Sn^{2+} and Al^{3+}	Cation detection	[348]
14	AND, NOT, XNOR, NAND, and OR	CN^- and Cd^{2+}	Smartphone-assisted prototype	[349]
15	INHIBIT	Pb^{2+}	Food safety	[350]
16	AND	N_3–PEG and rBSA	Cell imaging	[351]
17	NOT, AND, and OR	Al^{3+} and Zn^{2+}	Intracellular detection of Al^{3+} levels in living plant tissue	[352]
18	AND	H_2S and tyrosinase	Imaging of melanoma cells	[353]
19	AND	Ag^+, Cd^{2+}, and 2,2,2-trifluoroacetic acid	Catalysis	[354]
20	AND	ORF1ab and N genes of SARS-CoV-2	Detection of SARS-CoV-2	[355]

12. Conclusions

The shift in optical device concepts from single analyte detection to multiple analyte detection has been an area of much interest in recent decades. Thirty years ago, a new field began using Boolean logic, treating molecules as logic gates. Since then, much research has been carried out aiming at the elaboration of molecular architectures capable of detecting multiple analytes in a logical/sequential way. In this context, organic synthesis has presented a set of tools capable of inspiring scientists to elaborate different molecular architectures capable of acting as various logic gates. The present review described the fundamental concepts in the architecture of MLGs by discussing examples from the litera-

ture. Despite all the advances made in the last three decades, the search for such devices is still constant, always seeking to diversify the possibilities of detections with different responses, high degrees of sensitivity and selectivity, and low cost in the preparation of MLGs. In addition, there is still a long way to go before making these compounds viable for real applications and their transposition to different matrices to enable the real application of these devices. Progress in the development of intelligent drug delivery systems, the application of chemical communication technologies in nanotechnology, and the evolution of environmental monitoring emerge as promising application areas for developing molecular logic gates. Even in the face of everything that has already been done, there is still much to be done, and we hope that this review will be a source of inspiration for expanding the state of the art in molecular logic gates.

Author Contributions: F.T.S. and G.G.D.: Conceptualization, writing—review and editing. All authors have read and agreed to the published version of the manuscript.

Funding: This research received no external funding.

Conflicts of Interest: The authors declare no conflicts of interest.

Abbreviations

ACQ	Aggregation-caused quenching
AIBN	Azobisisobutyronitrile
AIE	Aggregation-induced emission
CHEF	Chelation-enhanced fluorescence
Cys	Cysteine
CTBA	Cetrimonium bromide
DBU	1,8-Diazabicyclo[5.4.0]undec-7-ene
DIEA	*N*,*N*-Diisopropylethylamine
DMAP	4-(Dimethylamino)pyridine
EDTA	Ethylenediamine tetraacetic acid
EHEC	Ethyl(hydroxyethyl)cellulose
ESIPT	Excited state intramolecular proton transfer
ESI-MS	Electrospray ionization–mass spectrometry
FRET	Fluorescence resonance energy transfer
FT-IR	Fourier-transform infrared spectroscopy
GSH	Glutathione
Hcy	Homocysteine
HRMS	High-resolution mass spectrometry
HSAB	Hard–soft acid base
ICT	Intramolecular charge transfer
JAF	J-aggregate formation (JAF)
RIR	Intramolecular rotation restriction
SBX	Silica-based xerogel
LG	Logic gate
MLCT	Metal-to-ligand charge transfer
MLG	Molecular logic gates
NIS	*N*-Iodosuccinimide
NMR	Nuclear magnetic resonance spectroscopy
NTA	4,4,4-trifluoro-1-(naphthalen-2-yl)butane-1,3-dione
PET	Photoinduced electron transfer
ppb	Parts per billion
ppm	Parts per million
PPi	Pyrophosphate
PS	Polymer matrix
TBACl	Tetrabutylammonium chloride
TFA	Trifluoroacetic acid
TIPS	Triisopropyl silane

References

1. Umapathi, R.; Park, B.; Sonwal, S.; Rani, G.M.; Cho, Y.; Huh, Y.S. Advances in Optical-Sensing Strategies for the on-Site Detection of Pesticides in Agricultural Foods. *Trends Food Sci. Technol.* **2022**, *119*, 69–89. [CrossRef]
2. Jiang, N.; Tansukawat, N.D.; Gonzalez-Macia, L.; Ates, H.C.; Dincer, C.; Güder, F.; Tasoglu, S.; Yetisen, A.K. Low-Cost Optical Assays for Point-of-Care Diagnosis in Resource-Limited Settings. *ACS Sens.* **2021**, *6*, 2108–2124. [CrossRef] [PubMed]
3. Prodi, L. Luminescent Chemosensors: From Molecules to Nanoparticles. *New J. Chem.* **2005**, *29*, 20–31. [CrossRef]
4. Wu, D.; Sedgwick, A.C.; Gunnlaugsson, T.; Akkaya, E.U.; Yoon, J.; James, T.D. Fluorescent Chemosensors: The Past, Present and Future. *Chem. Soc. Rev.* **2017**, *46*, 7105–7123. [CrossRef] [PubMed]
5. Khan, J. Synthesis and Applications of Fluorescent Chemosensors: A Review. *J. Fluoresc.* **2023**. [CrossRef] [PubMed]
6. IUPAC. *The IUPAC Compendium of Chemical Terminology*, 2nd ed.; McNaught, A.D., Williamson, A., Eds.; International Union of Pure and Applied Chemistry (IUPAC); Research Triangle Park, Blackwell Scientific Publications: Oxford, UK, 1997; Online Version (2019); ISBN 0-9678550-9-8.
7. You, L.; Zha, D.; Anslyn, E.V. Recent Advances in Supramolecular Analytical Chemistry Using Optical Sensing. *Chem. Rev.* **2015**, *115*, 7840–7892. [CrossRef] [PubMed]
8. Valeur, B.; Berberan-Santos, M.N.; Martin, M.M. Photophysics and Photochemistry of Supramolecular Systems. In *Analytical Methods in Supramolecular Chemistry*; Wiley: Hoboken, NJ, USA, 2007; pp. 220–264. [CrossRef]
9. Anslyn, E.V. Supramolecular Analytical Chemistry. *J. Org. Chem.* **2007**, *72*, 687–699. [CrossRef] [PubMed]
10. Fukuhara, G. Analytical Supramolecular Chemistry: Colorimetric and Fluorimetric Chemosensors. *J. Photochem. Photobiol.* **2020**, *42*, 100340. [CrossRef]
11. de Silva, A.P.; Gunaratne, N.H.Q.; McCoy, C.P. A Molecular Photoionic and Gate Based on Fluorescent Signalling. *Nature* **1993**, *364*, 42–44. [CrossRef]
12. de Silva, A.P.; Gunaratne, H.Q.N.; Gunnlaugsson, T.; Huxley, A.J.M.; McCoy, C.P.; Rademacher, J.T.; Rice, T.E. Signaling Recognition Events with Fluorescent Sensors and Switches. *Chem. Rev.* **1997**, *97*, 1515–1566. [CrossRef]
13. Hou, X.; Ga, L.; Zhang, X.; Ai, J. Advances in the Application of Logic Gates in Nanozymes. *Anal. Bioanal. Chem.* **2024**, 1–22. [CrossRef] [PubMed]
14. Pawar, S.; Duadi, H.; Fleger, Y.; Fixler, D. Carbon Dots-Based Logic Gates. *Nanomaterials* **2021**, *11*, 232. [CrossRef] [PubMed]
15. Liu, L.; Liu, P.; Ga, L.; Ai, J. Advances in Applications of Molecular Logic Gates. *ACS Omega* **2021**, *6*, 30189–30204. [CrossRef] [PubMed]
16. Zhao, S.; Yu, L.; Yang, S.; Tang, X.; Chang, K.; Chen, M. Boolean Logic Gate Based on DNA Strand Displacement for Biosensing: Current and Emerging Strategies. *Nanoscale Horiz.* **2021**, *6*, 298–310. [CrossRef]
17. Chen, K.; Shu, Q.; Schmittel, M. Design Strategies for Lab-on-a-Molecule Probes and Orthogonal Sensing. *Chem. Soc. Rev.* **2015**, *44*, 136–160. [CrossRef] [PubMed]
18. Georgiev, N.I.; Bakov, V.V.; Bojinov, V.B. A Tutorial Review on the Fluorescent Probes as a Molecular Logic Circuit—Digital Comparator. *Molecules* **2023**, *28*, 6327. [CrossRef] [PubMed]
19. Kim, H.N.; Ren, W.X.; Kim, J.S.; Yoon, J. Fluorescent and Colorimetric Sensors for Detection of Lead, Cadmium, and Mercury Ions. *Chem. Soc. Rev.* **2012**, *41*, 3210–3244. [CrossRef]
20. Clevenger, W.L.; Smith, B.W.; Winefordner, J.D. Trace Determination of Mercury: A Review. *Crit. Rev. Anal. Chem.* **1997**, *27*, 1–26. [CrossRef]
21. Shuai, H.; Xiang, C.; Qian, L.; Bin, F.; Xiaohui, L.; Jipeng, D.; Chang, Z.; Jiahui, L.; Wenbin, Z. Fluorescent Sensors for Detection of Mercury: From Small Molecules to Nanoprobes. *Dye. Pigment.* **2021**, *187*, 109125. [CrossRef]
22. Chen, G.; Guo, Z.; Zeng, G.; Tang, L. Fluorescent and Colorimetric Sensors for Environmental Mercury Detection. *Analyst* **2015**, *140*, 5400–5443. [CrossRef]
23. Gidlow, D.A. Lead Toxicity. *Occup. Med.* **2015**, *65*, 348–356. [CrossRef] [PubMed]
24. Godwin, H.A. The Biological Chemistry of Lead. *Curr. Opin. Chem. Biol.* **2001**, *5*, 223–227. [CrossRef] [PubMed]
25. Hildebrand, M.P. Lead Toxicity in a Newborn. *J. Pediatr. Health Care* **2011**, *25*, 328–331. [CrossRef] [PubMed]
26. Mason, A.; Sheridan, A.; Sutherland, I.O.; Vincent, A. Selective Chromogenic Reagents for Lead. *J. Chem. Soc. Chem. Commun.* **1994**, *22*, 2627–2628. [CrossRef]
27. Satarug, S.; Vesey, D.A.; Gobe, G.C. Current Health Risk Assessment Practice for Dietary Cadmium: Data from Different Countries. *Food Chem. Toxicol.* **2017**, *106*, 430–445. [CrossRef] [PubMed]
28. Horiguchi, H.; Oguma, E.; Sasaki, S.; Miyamoto, K.; Ikeda, Y.; MacHida, M.; Kayama, F. Dietary Exposure to Cadmium at Close to the Current Provisional Tolerable Weekly Intake Does Not Affect Renal Function among Female Japanese Farmers. *Environ. Res.* **2004**, *95*, 20–31. [CrossRef]
29. Satarug, S.; Moore, M.R. Adverse Health Effects of Chronic Exposure to Low-Level Cadmium in Foodstuffs and Cigarette Smoke. *Environ. Health Perspect.* **2004**, *112*, 1099–1103. [CrossRef]
30. Greger, J.L.; Sutherland, J.E.; Yokel, R. Aluminum Exposure and Metabolism. *Crit. Rev. Clin. Lab. Sci.* **1997**, *34*, 439–474. [CrossRef]
31. Yokel, R.A.; Hicks, C.L.; Florence, R.L. Aluminum Bioavailability from Basic Sodium Aluminum Phosphate, an Approved Food Additive Emulsifying Agent, Incorporated in Cheese. *Food Chem. Toxicol.* **2008**, *46*, 2261–2266. [CrossRef]
32. Zhou, J.; Wan, X.; Li, Y. Advanced Aluminium Products and Manufacturing Technologies Applied on Vehicles Presented at the EuroCarBody Conference. In *Materials Today: Proceedings*; Elsevier: Amsterdam, The Netherlands, 2015; Volume 2, pp. 5015–5022.

33. Campbell, A. The Potential Role of Aluminium in Alzheimer's Disease. *Nephrol. Dial. Transplant.* **2002**, *17*, 17–20. [CrossRef]
34. Darbre, P.D. Aluminium, Antiperspirants and Breast Cancer. *J. Inorg. Biochem.* **2005**, *99*, 1912–1919. [CrossRef] [PubMed]
35. Goyer, R.A.; Cherian, M.G. (Eds.) *Toxicology of Metals: Biochemical Aspects*; Springer: Berlin/Heidelberg, Germany, 1995; Volume 115, ISBN 9783642791642. [CrossRef]
36. Leal, M.F.C.; Catarino, R.I.L.; Pimenta, A.M.; Souto, M.R.S. Roles of Metal Microelements in Neurodegenerative Diseases. *Neurophysiology* **2020**, *52*, 80–88.
37. Sahu, M.; Manna, A.K.; Chowdhury, S.; Patra, G.K. A Novel Dihydro Phenylquinazolinone-Based Two-in-One Colourimetric Chemosensor for Nickel(II), Copper(II) and Its Copper Complex for the Fluorescent Colourimetric Nanomolar Detection of the Cyanide Anion. *RSC Adv.* **2020**, *10*, 44860–44875. [CrossRef] [PubMed]
38. Finkelstein, M.M.; Jerrett, M. A Study of the Relationships between Parkinson's Disease and Markers of Traffic-Derived and Environmental Manganese Air Pollution in Two Canadian Cities. *Environ. Res.* **2007**, *104*, 420–432. [CrossRef] [PubMed]
39. Montgomery, E.B. Heavy Metals and the Etiology of Parkinson's Disease and Other Movement Disorders. *Toxicology* **1995**, *97*, 3–9. [CrossRef] [PubMed]
40. Chin-Chan, M.; Navarro-Yepes, J.; Quintanilla-Vega, B. Environmental Pollutants as Risk Factors for Neurodegenerative Disorders: Alzheimer and Parkinson Diseases. *Front. Cell. Neurosci.* **2015**, *9*, 124. [CrossRef] [PubMed]
41. Grattan, B.J.; Freake, H.C. Zinc and Cancer: Implications for LIV-1 in Breast Cancer. *Nutrients* **2012**, *4*, 648–675. [CrossRef] [PubMed]
42. Sensi, S.L.; Paoletti, P.; Bush, A.I.; Sekler, I. Zinc in the Physiology and Pathology of the CNS. *Nat. Rev. Neurosci.* **2009**, *10*, 780–791. [CrossRef]
43. Sadananda, D.; Mallikarjunaswamy, A.M.M.; Prashantha, C.N.; Mala, R.; Gouthami, K.; Lakshminarayana, L.; Ferreira, L.F.R.; Bilal, M.; Rahdar, A.; Mulla, S.I. Recent Development in Chemosensor Probes for the Detection and Imaging of Zinc Ions: A Systematic Review. *Chem. Pap.* **2022**, *76*, 5997–6015. [CrossRef]
44. Xu, L.H.; Wang, W.Y.; Guo, J.J.; Qin, J.; Shi, D.Q.; Li, Y.L.; Xu, J. Zinc Improves Salt Tolerance by Increasing Reactive Oxygen Species Scavenging and Reducing Na^+ Accumulation in Wheat Seedlings. *Biol. Plant* **2014**, *58*, 751–757. [CrossRef]
45. Yu, Y.; Bogliotti, N.; Maisonneuve, S.; Tang, J.; Xie, J. Fluorescent Dyad for Cooperative Recognition of Copper Cation and Halogen Anion. *Tetrahedron Lett.* **2013**, *54*, 1877–1883. [CrossRef]
46. Ruan, Y.B.; Maisonneuve, S.; Li, C.; Tang, J.; Xie, J. Cooperative Recognition of Cu^{2+} Based on Amino Acids Tethered Benzothiadiazoyl-Bistriazoles. *Front. Chem. China* **2010**, *5*, 208–213. [CrossRef]
47. Padan, E.; Landau, M. Sodium-Proton (Na^+/H^+) Antiporters: Properties and Roles in Health and Disease. In *The Alkali Metal Ions: Their Role for Life*; Metal Ions in Life Sciences Series; Sigel, A., Sigel, H., Sigel, R.K.O., Eds.; Springer: Cham, Switzerland, 2016; Volume 16, pp. 391–458. ISBN 978-3-319-21755-0. [CrossRef]
48. Pohl, H.R.; Wheeler, J.S.; Murray, H.E. Sodium and Potassium in Health and Disease. In *Interrelations between Essential Metal Ions and Human Diseases*; Metal Ions in Life Sciences; Springer: Dordrecht, The Netherlands, 2013; Volume 13, pp. 29–47. [CrossRef]
49. Crossley, R.; Goolamali, Z.; Gosper, J.J.; Sammes, P.G. Synthesis and Spectral Properties of New Fluorescent Probes for Potassium. *J. Chem. Soc. Perkin Trans.* **1994**, *2*, 513–520. [CrossRef]
50. Gao, G.; Cao, Y.; Liu, W.; Li, D.; Zhou, W.; Liu, J. Fluorescent Sensors for Sodium Ions. *Anal. Methods* **2017**, *9*, 5570–5579. [CrossRef]
51. Jaitovich, A.; Bertorello, A.M. Intracellular Sodium Sensing: SIK1 Network, Hormone Action and High Blood Pressure. *Biochim. Biophys. Acta* **2010**, *1802*, 1140–1149. [CrossRef]
52. Kofuji, P.; Newman, E.A. Potassium Buffering in the Central Nervous System. *Neuroscience* **2004**, *129*, 1043–1054. [CrossRef]
53. Sprenger, T.; Schwarze, T.; Müller, H.; Sperlich, E.; Kelling, A.; Holdt, H.J.; Paul, J.; Martos Riaño, V.; Nazaré, M. BODIPY-Equipped Benzo-Crown-Ethers as Fluorescent Sensors for PH Independent Detection of Sodium and Potassium Ions. *ChemPhotoChem* **2023**, *7*, e20220027. [CrossRef]
54. Chiu, T.C.; Huang, C.C. Aptamer-Functionalized Nano-Biosensors. *Sensors* **2009**, *9*, 10356–10388. [CrossRef]
55. Pedersen, S.F.; O'donnell, M.E.; Anderson, S.E.; Cala, P.M. Physiology and Pathophysiology of Na/H Exchange and Na-K-2Cl Cotransport in the Heart, Brain, and Blood. *Am. J. Physiol. Regul. Integr. Comp. Physiol.* **2006**, *291*, R1–R25. [CrossRef]
56. Gadsby, D.C.; Niedergerke, R.; Page, S. Do Intracellular Concentrations of Potassium or Sodium Regulate the Strength of the Heart Beat. *Nature* **1971**, *232*, 651–653. [CrossRef] [PubMed]
57. Liverani, L.; Boccardi, E.; Beltran, A.M.; Boccaccini, A.R. Incorporation of Calcium Containing Mesoporous (MCM-41-Type) Particles in Electrospun PCL Fibers by Using Benign Solvents. *Polymers* **2017**, *9*, 487. [CrossRef] [PubMed]
58. Morad, M.; Davies, N.W.; Kaplan, J.H.; Lux, H.D. Inactivation and Block of Calcium Channels by Photo-Released Ca^{2+} in Dorsal Root Ganglion Neurons. *Science* **1988**, *241*, 842–844. [CrossRef] [PubMed]
59. Mason, A.; Sutherland, I.O. A Chromogenic Reagent for Calcium. The Importance of Ion-Pairing in Cation Selection. *J. Chem. Soc. Chem. Commun.* **1994**, *9*, 1131–1132. [CrossRef]
60. Way, J.L. Cyanide Intoxication and Its Mechanism of Antagonism. *Annu. Rev. Pharmacol. Toxicol.* **1984**, *24*, 451–481. [CrossRef] [PubMed]
61. Simeonova, F.P.; Fishbein, L.; World HealthOrganization & International Programme on Chemical Safety; Inter-Organization Programme for the Sound Management of Chemicals; World Health Organization. *Hydrogen Cyanide and Cyanides: Human Health Aspects*; World Health Organization: Geneva, Switzerland, 2004; ISBN 9241530618.

62. Ballantyne, B. Acute Systemic Toxicity of Cyanides by Topical Application to the Eye. *Cutan. Ocul. Toxicol.* **1983**, *2*, 119–129. [CrossRef]
63. Xu, Z.; Chen, X.; Kim, H.N.; Yoon, J. Sensors for the Optical Detection of Cyanide Ion. *Chem. Soc. Rev.* **2010**, *39*, 127–137. [CrossRef] [PubMed]
64. Chakraborty, S.; Paul, S.; Roy, P.; Rayalu, S. Detection of Cyanide Ion by Chemosensing and Fluorosensing Technology. *Inorg. Chem. Commun.* **2021**, *128*, 108562. [CrossRef]
65. Gai, L.; Mack, J.; Lu, H.; Nyokong, T.; Li, Z.; Kobayashi, N.; Shen, Z. Organosilicon Compounds as Fluorescent Chemosensors for Fluoride Anion Recognition. *Coord. Chem. Rev.* **2015**, *285*, 24–51. [CrossRef]
66. Zhang, Y.M.; Lin, Q.; Wei, T.B.; Wang, D.D.; Yao, H.; Wang, Y.L. Simple Colorimetric Sensors with High Selectivity for Acetate and Chloride in Aqueous Solution. *Sens. Actuators B Chem.* **2009**, *137*, 447–455. [CrossRef]
67. Ho, T.Y.; Scranton, M.I.; Taylor, G.T.; Varela, R.; Thunell, R.C.; Muller-Karger, F. Acetate Cycling in the Water Column of the Cariaco Basin: Seasonal and Vertical Variability and Implication for Carbon Cycling. *Limnol. Oceanogr.* **2002**, *47*, 1119–1128. [CrossRef]
68. Manju, S.; Jose, L.; Srinivasa Gopal, T.K.; Ravishankar, C.N.; Lalitha, K.V. Effects of Sodium Acetate Dip Treatment and Vacuum-Packaging on Chemical, Microbiological, Textural and Sensory Changes of Pearlspot (*Etroplus suratensis*) during Chill Storage. *Food Chem.* **2007**, *102*, 27–35. [CrossRef]
69. Gupta, V.K.; Singh, A.K.; Gupta, N. Colorimetric Sensor for Cyanide and Acetate Ion Using Novel Biologically Active Hydrazones. *Sens. Actuators B Chem.* **2014**, *204*, 125–135. [CrossRef]
70. Han, M.S.; Kim, D.H. Naked-Eye Detection of Phosphate Ions in Water at Physiological PH: A Remarkably Selective and Easy-To-Assemble Colorimetric Phosphate-Sensing Probe. *Angew. Chem.* **2002**, *2*, 3963–3965. [CrossRef]
71. Takeda, E.; Taketani, Y.; Sawada, N.; Sato, T.; Yamamoto, H. The Regulation and Function of Phosphate in the Human Body. *BioFactors* **2004**, *21*, 345–355. [CrossRef] [PubMed]
72. Mutihac, L.; Lee, J.H.; Kim, J.S.; Vicens, J. Chromogenic and Fluorogenic Chemosensors and Reagents for Anions. A Comprehensive Review of the Year 2009. *Chem. Soc. Rev.* **2011**, *40*, 2593–2643. [CrossRef]
73. Figueroa, L.E.S.; Moragues, M.E.; Climent, E.; Agostini, A.; Martínez-Máñez, R.; Sancenón, F. Chromogenic and Fluorogenic Chemosensors and Reagents for Anions. A Comprehensive Review of the Years 2010–2011. *Chem. Soc. Rev.* **2013**, *42*, 3489–3613. [CrossRef]
74. Schmidtchen, F.P.; Berger, M. Artificial Organic Host Molecules for Anions. *Chem. Rev.* **1997**, *97*, 1609–1646. [CrossRef]
75. Mohr, G.J. New Chromogenic and Fluorogenic Reagents and Sensors for Neutral and Ionic Analytes Based on Covalent Bond Formation—A Review of Recent Developments. *Anal. Bioanal. Chem.* **2006**, *386*, 1201–1214. [CrossRef]
76. Al-Saidi, H.M.; Khan, S. Recent Advances in Thiourea Based Colorimetric and Fluorescent Chemosensors for Detection of Anions and Neutral Analytes: A Review. *Crit. Rev. Anal. Chem.* **2022**, *54*, 93–109. [CrossRef]
77. Pu, L. Fluorescence of Organic Molecules in Chiral Recognition. *Chem. Rev.* **2004**, *104*, 1687–1716. [CrossRef] [PubMed]
78. Kumar, A.; Chae, P.S. Fluorescence Tunable Thiophene-Bis(Benzimidazole)-Based Probes for a Cascade Trace Detection of Hg^{2+} and Lysine: A Molecular Switch Mimic. *Sens. Actuators B Chem.* **2019**, *281*, 933–944. [CrossRef]
79. Tavallali, H.; Espergham, O.; Deilamy-Rad, G.; Karimi, M.A.; Rostami, S.; Rouhani-Savestani, A.-R. Dye/Metal Ion-Based Chemosensing Ensemble towards L-Histidine and L-Lysine Determination in Water via Different Optical Responses. *Anal. Biochem.* **2020**, *604*, 113811. [CrossRef] [PubMed]
80. Zong, G.-Q.; Lv, G.-X. A NOR Fluorescent Logic Gate Based on *N*-(9-Anthracylmethyl)-L-Histidine. *Acta. Phys. Chim. Sin.* **2008**, *24*, 1902–1906. [CrossRef]
81. Gu, Z.; Cao, Z. Molecular Switch-Modulated Fluorescent Copper Nanoclusters for Selective and Sensitive Detection of Histidine and Cysteine. *Anal. Bioanal. Chem.* **2018**, *410*, 4991–4999. [CrossRef] [PubMed]
82. Coucouvanis, D.; Rosa, D.; Pike, J. Recognition and transport of amphiphilic molecules by a new class of inorganic ditopic receptors. The synthesis of M-^{t} Bu_4-salphen-3*n*-cr-*n* complexes and their use (M = Mn,Fe, *n* = 6) in the transport of tryptophan and serotonin across bulk liquid membranes. *Comptes Rendus Chim.* **2003**, *6*, 317–327. [CrossRef]
83. Körsten, S.; Mohr, G.J. Star-Shaped Tripodal Chemosensors for the Detection of Aliphatic Amines. *Chem. Eur. J.* **2011**, *17*, 969–975. [CrossRef] [PubMed]
84. Gräfe, A.; Haupt, K.; Mohr, G.J. Optical Sensor Materials for the Detection of Amines in Organic Solvents. *Anal. Chim. Acta* **2006**, *565*, 42–47. [CrossRef]
85. Biji, K.B.; Ravishankar, C.N.; Venkateswarlu, R.; Mohan, C.O.; Gopal, T.K.S. Biogenic Amines in Seafood: A Review. *J. Food Sci. Technol.* **2016**, *53*, 2210–2218. [PubMed]
86. Diauudin, F.N.; Rashid, J.I.A.; Knight, V.F.; Wan Yunus, W.M.Z.; Ong, K.K.; Kasim, N.A.M.; Abdul Halim, N.; Noor, S.A.M. A Review of Current Advances in the Detection of Organophosphorus Chemical Warfare Agents Based Biosensor Approaches. *Sens. Biosens. Res.* **2019**, *26*, 100305. [CrossRef]
87. Gupta, N.K.; Pashigreva, A.; Pidko, E.A.; Hensen, E.J.M.; Mleczko, L.; Roggan, S.; Ember, E.E.; Lercher, J.A. Bent Carbon Surface Moieties as Active Sites on Carbon Catalysts for Phosgene Synthesis. *Angew. Chem. Int. Ed.* **2016**, *55*, 1728–1732. [CrossRef] [PubMed]
88. Chen, L.; Wu, D.; Yoon, J. Recent Advances in the Development of Chromophore-Based Chemosensors for Nerve Agents and Phosgene. *ACS Sens.* **2018**, *3*, 27–43. [CrossRef] [PubMed]

89. Pedersen, C.J.; Frensdorff, H.K. Macrocyclic Polyethers and Their Complexes. *Angew. Chem. Int. Ed.* **1972**, *11*, 16–25. [CrossRef] [PubMed]
90. Pedersen, C.J. Cyclic Polyethers and Their Complexes with Metal Salts. *J. Am. Chem. Soc.* **1967**, *89*, 7017–7036. [CrossRef]
91. Lehn, J.M. Cryptates: Inclusion Complexes of Macropolycyclic Receptor Molecules. *Pure Appl. Chem.* **1978**, *50*, 871–892. [CrossRef]
92. Cram, D.J. Preorganization—From Solvents to Spherands. *Angew. Chem. Int. Ed.* **1986**, *25*, 1039–1057. [CrossRef]
93. Lehn, J.-M. Supramolecular Chemistry—Scope and Perspectives Molecules, Supermolecules, and Molecular Devices (Nobel Lecture). *Angew. Chem. Int. Ed.* **1988**, *27*, 89–112. [CrossRef]
94. Lehn, J.-M. From Supramolecular Chemistry towards Constitutional Dynamic Chemistry and Adaptive Chemistry. *Chem. Soc. Rev.* **2007**, *36*, 151–160. [CrossRef] [PubMed]
95. Lehn, J.-M. Design of Organic Complexing Agents Strategies towards Properties. In *Alkali Metal Complexes with Organic Ligands*; Structure and Bonding Series; Springer: Berlin/Heidelberg, Germany, 2005; Volume 16, pp. 1–69. [CrossRef]
96. Lehn, J.-M. Supramolecular Chemistry and Self-Assembly Special Feature: Toward Complex Matter: Supramolecular Chemistry and Self-Organization. *Proc. Natl. Acad. Sci. USA* **2002**, *99*, 4763–4768. [CrossRef]
97. Wang, Y.; Ping, G.; Li, C. Efficient Complexation between Pillar[5]Arenes and Neutral Guests: From Host-Guest Chemistry to Functional Materials. *Chem. Comm.* **2016**, *52*, 9858–9872. [CrossRef]
98. Guohe, X.; Jie, L.; Jinni, D.; Lv, Y.; Zhaohui, Z.; Xiaobin, D. Molecular Shuttles Based on Host-Guest Recognition Driven by External-Stimuli. *Prog. Chem.* **2015**, *27*, 1732–1742.
99. Yeung, M.C.L.; Yam, V.W.W. Luminescent Cation Sensors: From Host-Guest Chemistry, Supramolecular Chemistry to Reaction-Based Mechanisms. *Chem. Soc. Rev.* **2015**, *44*, 4192–4202. [CrossRef]
100. Long, G.L.; Winefordner, J.D. Limit of Detection: A Closer Look at the IUPAC Definition. *Anal. Chem.* **1983**, *55*, 712A–724A. [CrossRef]
101. Rajasekar, M.; Ranjitha, V.; Rajasekar, K. Recent advances in Fluorescent-based cation sensors for biomedical applications. *Results Chem.* **2023**, *5*, 100850. [CrossRef]
102. Magri, D.C. Recent Progress on the Evolution of Pourbaix Sensors: Molecular Logic Gates for Protons and Oxidants. *Chemosensors* **2018**, *6*, 48. [CrossRef]
103. Zaccheroni, N.; Palomba, F.; Rampazzo, E. Luminescent Chemosensors: From Molecules to Nanostructures. In *Applied Photochemistry: When Light Meets Molecules*; Springer: Cham, Switzerland, 2016; pp. 479–497. ISBN 978-3-319-31671-0.
104. Zimmermann-Dimer, L.; Machado, V. Chromogenic and Fluorogenic Chemosensors for Detection of Anionic Analites. *Quim. Nova* **2008**, *31*, 2134–2146. [CrossRef]
105. Martínez-Máñez, R.; Sancenón, F. Fluorogenic and Chromogenic Chemosensors and Reagents for Anions. *Chem. Rev.* **2003**, *103*, 4419–4476. [CrossRef]
106. Daly, B.; Ling, J.; de Silva, A.P. Current Developments in Fluorescent PET (Photoinduced Electron Transfer) Sensors and Switches. *Chem. Soc. Rev.* **2015**, *44*, 4203–4211. [CrossRef]
107. Escudero, D. Revising Intramolecular Photoinduced Electron Transfer (PET) from First-Principles. *Acc. Chem. Res.* **2016**, *49*, 1816–1824. [CrossRef]
108. Misra, R.; Bhattacharyya, S.P. *Intramolecular Charge Transfer: Theory and Applications*, 1st ed.; Wiley: Hoboken, NJ, USA, 2018; ISBN 978-3-527-34156-6.
109. Yuan, L.; Lin, W.; Zheng, K.; Zhu, S. FRET-Based Small-Molecule Fluorescent Probes: Rational Design and Bioimaging Applications. *Acc. Chem. Res.* **2013**, *46*, 1462–1473.
110. Zuo, Y.; Gou, Z.; Lan, Y.; Yan, M. Design Strategies of Logic Gate Sensors Based on FRET Mechanism. *Trends Anal. Chem.* **2023**, *167*, 117271. [CrossRef]
111. Varadaraju, C.; Paulraj, M.S.; Tamilselvan, G.; Enoch, I.V.M.V.; Srinivasadesikan, V.; Shyi-Long, L. Evaluation of Metal Ion Sensing Behaviour of Fluorescent Probe along with Its Precursors: PET-CHEF Mechanism, Molecular Logic Gate Behaviour and DFT Studies. *J. Incl. Phenom. Macrocycl. Chem.* **2019**, *95*, 79–89. [CrossRef]
112. Vlček, A., Jr. Mechanistic Roles of Metal-to-Ligand Charge-Transfer Excited States in Organometallic Photochemistry. *Coord. Chem. Rev.* **1998**, *177*, 219–256. [CrossRef]
113. Park, J.-K.; Shin, J.; Jang, S.; Seol, M.-L.; Kang, J.; Choi, S.; Eom, H.; Kwon, O.; Park, S.; Noh, D.-Y.; et al. Rational Design of Fluorescent/Colorimetric Chemosensors for Detecting Transition Metal Ions by Varying Functional Groups. *Inorganics* **2022**, *10*, 189. [CrossRef]
114. Han, D.Y.; Kim, J.M.; Kim, J.; Jung, H.S.; Lee, Y.H.; Zhang, J.F.; Kim, J.S. ESIPT-Based Anthraquinonylcalix[4]Crown Chemosensor for In^{3+}. *Tetrahedron Lett.* **2010**, *51*, 1947–1951. [CrossRef]
115. Guo, C.; Sedgwick, A.C.; Hirao, T.; Sessler, J.L. Supramolecular Fluorescent Sensors: An Historical Overview and Update. *Coord. Chem. Rev.* **2021**, *427*, 213560. [CrossRef] [PubMed]
116. Jayabharathi, J.; Thanikachalam, V.; Vennila, M.; Jayamoorthy, K. DFT Based ESIPT Process of Luminescent Chemosensor: Taft and Catalan Solvatochromism. *Spectrochim. Acta Part A Mol. Biomol. Spectrosc.* **2012**, *95*, 589–595. [CrossRef]
117. Paul, B.K.; Guchhait, N. Density Functional Theory (DFT) and Natural Bond Orbital (NBO) Investigation of Intramolecular Hydrogen Bond Interaction and Excited-State Intramolecular Proton Transfer (ESIPT) Reaction in a Five-Membered Hydrogen-Bonding System 2-(1*H*-Pyrazol-5-Yl)Pyridine: On the Possibility of Solvent (Water)-Assisted ESPT. *Comput. Theor. Chem.* **2011**, *972*, 1–13. [CrossRef]

118. Sakai, K.; Takemura, M.; Kawabe, Y. Lead Chloride-Based Layered Perovskite Incorporated with an Excited State Intramolecular Proton Transfer Dye. *J. Lumin.* **2010**, *130*, 2505–2507. [CrossRef]
119. Qu, W.-J.; Yan, G.-T.; Ma, X.-L.; Wei, T.-B.; Lin, Q.; Yao, H.; Zhang, Y.-M. "Cascade Recognition" of Cu^{2+} and $H_2PO_4^-$ with High Sensitivity and Selectivity in Aqueous Media Based on the Effect of ESIPT. *Sens. Actuators B Chem.* **2017**, *242*, 849–856. [CrossRef]
120. Balzani, V.; Credi, A.; Venturi, M. *Molecular Devices and Machines*, 2nd ed.; Wiley: Mörlenbach, Germany, 2008; Volume 1, ISBN 9783527313846.
121. Wang, H.; Zhao, E.; Lam, J.W.Y.; Tang, B.Z. AIE Luminogens: Emission Brightened by Aggregation. *Mater. Today* **2015**, *18*, 365–377. [CrossRef]
122. Kolanowski, J.L.; Liu, F.; New, E.J. Fluorescent Probes for the Simultaneous Detection of Multiple Analytes in Biology. *Chem. Soc. Rev.* **2018**, *47*, 195–208. [CrossRef] [PubMed]
123. Shu, Y.; Hao, J.N.; Niu, D.; Li, Y. A Smart Luminescent Metal-Organic Framework-Based Logic System for Simultaneous Analysis of Copper Ions and Hydrogen Sulfide. *J. Mater. Chem. C Mater.* **2020**, *8*, 8635–8642. [CrossRef]
124. Li, M.; Xu, X.; Cai, Q. DNA Polymerase/NEase-Assisted Signal Amplification Coupled with Silver Nanoclusters for Simultaneous Detection of Multiple MicroRNAs and Molecular Logic Operations. *Sens. Actuators B Chem.* **2021**, *327*, 128915. [CrossRef]
125. de Silva, A.P.; McClenaghan, N.D. Simultaneously Multiply-Configurable or Superposed Molecular Logic Systems Composed of ICT (Internal Charge Transfer) Chromophores and Fluorophores Integrated with One- or Two-Ion Receptors. *Chem. Eur. J.* **2002**, *8*, 4935–4945. [CrossRef] [PubMed]
126. Tavallali, H.; Parhami, A.; Karimi, M.A.; Hossein-Khezri, P. Simultaneous Detection of SO_3^{2-} and PO_4^{3-} Anions, in Aqueous Solutions Based on 4-(2-Pyridylazo) Resorcinol (PAR) as a Colorimetric Chemosensor and Analytical Applications. *Int. J. Environ. Anal. Chem.* **2020**, *102*, 3652–3671. [CrossRef]
127. Valeur, B. Design Principles of Fluorescent Molecular Sensors for Cation Recognition. *Coord. Chem. Rev.* **2002**, *205*, 3–40. [CrossRef]
128. Valeur, B. *Molecular Fluorescence: Principles and Applications*, 2nd ed.; Wiley-VCH Verlag GmbH & Co. KGaA: Weinheim, Germany, 2012; ISBN 3527600248.
129. Tjandra, A.D.; Pham, A.-H.; Chandrawati, R. Polydiacetylene-Based Sensors to Detect Volatile Organic Compounds. *Chem. Mater.* **2022**, *34*, 2853–2876. [CrossRef]
130. Qian, X.; Städler, B. Recent Developments in Polydiacetylene-Based Sensors. *Chem. Mater.* **2019**, *31*, 1196–1222. [CrossRef]
131. Lin, W.; Long, L.; Yuan, L.; Cao, Z.; Feng, J. A Novel Ratiometric Fluorescent Fe^{3+} Sensor Based on a Phenanthroimidazole Chromophore. *Anal. Chim. Acta* **2009**, *634*, 262–266. [CrossRef]
132. Kuzu, B.; Tan, M.; Ekmekci, Z.; Menges, N. A Novel Fluorescent Sensor Based on Imidazole Derivative for Fe^{3+} Ions. *J. Lumin.* **2017**, *192*, 1096–1103. [CrossRef]
133. Prakash, S.M.; Jayamoorthy, K.; Srinivasan, N.; Dhanalekshmi, K.I. Fluorescence Tuning of 2-(1H-Benzimidazol-2-Yl)Phenol-ESIPT Process. *J. Lumin.* **2016**, *172*, 304–308. [CrossRef]
134. Horak, E.; Kassal, P.; Murković Steinberg, I. Benzimidazole as a Structural Unit in Fluorescent Chemical Sensors: The Hidden Properties of a Multifunctional Heterocyclic Scaffold. *Supramol. Chem.* **2018**, *30*, 838–857. [CrossRef]
135. Gülle, S.; Çelik Erbaş, S. A Selective Fluorescence Sensor for Fe (III) Based on Phenanthroimidazole Imine Compound. *J. Fluoresc.* **2018**, *28*, 445–451. [CrossRef] [PubMed]
136. Dias, G.G.; Rodrigues, M.O.; Paz, E.R.S.; Nunes, M.P.; Araujo, M.H.; Rodembusch, F.S.; Da Silva Júnior, E.N. Aryl-Phenanthro[9,10-d]Imidazole: A Versatile Scaffold for the Design of Optical-Based Sensors. *ACS Sens.* **2022**, *7*, 2865–2919. [CrossRef] [PubMed]
137. Dias, G.G.; Paz, E.R.S.; Nunes, M.P.; Carvalho, R.L.; Rodrigues, M.O.; Rodembusch, F.S.; Da Silva Júnior, E.N. Imidazoles and Oxazoles from Lapachones and Phenanthrene-9,10-Dione: A Journey through Their Synthesis, Biological Studies, and Optical Applications. *Chem. Rec.* **2021**, *21*, 2702–2738. [CrossRef] [PubMed]
138. dos Santos, F.S.; Dias, G.G.; de Freitas, R.P.; Santos, L.S.; de Lima, G.F.; Duarte, H.A.; de Simone, C.A.; Rezende, L.M.S.L.; Vianna, M.J.X.; Correa, J.R.; et al. Redox Center Modification of Lapachones towards the Synthesis of Nitrogen Heterocycles as Selective Fluorescent Mitochondrial Imaging Probes. *Eur. J. Org. Chem.* **2017**, *2017*, 3763–3773. [CrossRef]
139. Dias, G.G.; Pinho, P.V.B.; Duarte, H.A.; Resende, J.M.; Rosa, A.B.B.; Correa, J.R.; Neto, B.A.D.; Da Silva Júnior, E.N. Fluorescent Oxazoles from Quinones for Bioimaging Applications. *RSC Adv.* **2016**, *6*, 76053–76063. [CrossRef]
140. Zhu, Q.; Li, Z.; Mu, L.; Zeng, X.; Redshaw, C.; Wei, G. A Quinoline-Based Fluorometric and Colorimetric Dual-Modal PH Probe and Its Application in Bioimaging. *Spectrochim. Acta Part A Mol. Biomol. Spectrosc.* **2018**, *188*, 230–236. [CrossRef]
141. Mikata, Y.; Nodomi, Y.; Kizu, A.; Konno, H. Quinoline-Attached Triazacyclononane (TACN) Derivatives as Fluorescent Zinc Sensors. *Dalton Trans.* **2014**, *43*, 1684–1690. [CrossRef]
142. Paisuwan, W.; Rashatasakhon, P.; Ruangpornvisuti, V.; Sukwattanasinitt, M.; Ajavakom, A. Dipicolylamino Quinoline Derivative as Novel Dual Fluorescent Detecting System for Hg^{2+} and Fe^{3+}. *Sens. Biosens.Res.* **2019**, *24*, 100283. [CrossRef]
143. Ranee, S.J.; Sivaraman, G.; Pushpalatha, A.M.; Muthusubramanian, S. Quinoline Based Sensors for Bivalent Copper Ions in Living Cells. *Sens. Actuators B Chem.* **2018**, *255*, 630–637. [CrossRef]
144. Loya, M.; Hazarika, S.I.; Pahari, P.; Atta, A.K. Fluorometric Detection of Cu^{2+} and Ni^{2+} by a Quinoline-Based Glucopyranose Derivative via the Excimer of Quinoline Subunit. *J. Mol. Struct.* **2021**, *1241*, 130634. [CrossRef]
145. Liu, Y.; Wu, M.; Zhao, J.; Wang, Y.; Zhang, Y. A Simple Salicylaldehyde-Bearing Pyrazine as a Turn-on Fluorescent Chemosensor for Al^{3+} and Zn^{2+} recognition and Its Applications. *Rev. Anal. Chem.* **2022**, *41*, 217–227. [CrossRef]

146. Lee, J.H.; Lee, S.H.; So, Y.A.; Park, G.J.; Kim, C. Simultaneous Detection of F^- and CN^- by a Simple Colorimetric Chemosensor with High Selectivity. *Bull. Korean Chem. Soc.* **2015**, *36*, 1618–1624. [CrossRef]
147. Chemate, S.; Erande, Y.; Mohbiya, D.; Sekar, N. Acridine Derivative as a "Turn on" Probe for Selective Detection of Picric Acid: Via PET Deterrence. *RSC Adv.* **2016**, *6*, 84319–84325. [CrossRef]
148. Lee, S.C.; Park, S.; So, H.; Lee, G.; Kim, K.T.; Kim, C. An Acridine-Based Fluorescent Sensor for Monitoring ClO− in Water Samples and Zebrafish. *Sensors* **2020**, *20*, 4764. [CrossRef]
149. Dai, Q.; Gao, C.; Liu, Y.; Liu, H.; Xiao, B.; Chen, C.; Chen, J.; Yuan, Z.; Jiang, Y. Highly Sensitive and Selective "Naked Eye" Sensing of Cu(II) by a Novel Acridine-Based Sensor Both in Aqueous Solution and on the Test Kit. *Tetrahedron* **2018**, *74*, 6459–6464. [CrossRef]
150. Carlos, F.S.; da Silva, L.A.; Zanlorenzi, C.; Nunes, F.S. A Novel Macrocycle Acridine-Based Fluorescent Chemosensor for Selective Detection of Cd^{2+} in Brazilian Sugarcane Spirit and Tobacco Cigarette Smoke Extract. *Inorg. Chim. Acta* **2020**, *508*, 119634. [CrossRef]
151. Carlos, F.S.; Monteiro, R.F.; da Silva, L.A.; Zanlorenzi, C.; Nunes, F.S. A Highly Selective Acridine-Based Fluorescent Probe for Detection of Al^{3+} in Alcoholic Beverage Samples. *Spectrochim. Acta Part A Mol. Biomol. Spectrosc.* **2020**, *231*, 118119. [CrossRef]
152. Nunes, M.C.; Carlos, F.S.; Fuganti, O.; Galindo, D.D.M.; de Boni, L.; Abate, G.; Nunes, F.S. Turn-on Fluorescence Study of a Highly Selective Acridine-Based Chemosensor for Zn^{2+} in Aqueous Solutions. *Inorg. Chim. Acta* **2020**, *499*, 119191. [CrossRef]
153. Kim, D.; Yamamoto, K.; Ahn, K.H. A BODIPY-Based Reactive Probe for Ratiometric Fluorescence Sensing of Mercury Ions. *Tetrahedron* **2012**, *68*, 5279–5282. [CrossRef]
154. Boens, N.; Leen, V.; Dehaen, W. Fluorescent Indicators Based on BODIPY. *Chem. Soc. Rev.* **2012**, *41*, 1130–1172. [CrossRef] [PubMed]
155. Kaur, P.; Singh, K. Recent Advances in the Application of BODIPY in Bioimaging and Chemosensing. *J. Mater. Chem. C Mater.* **2019**, *7*, 11361–11405. [CrossRef]
156. Wang, L.; Ding, H.; Ran, X.; Tang, H.; Cao, D. Recent Progress on Reaction-Based BODIPY Probes for Anion Detection. *Dye. Pigment.* **2020**, *172*, 107857. [CrossRef]
157. Shi, W.J.; Huang, Y.; Liu, W.; Xu, D.; Chen, S.T.; Liu, F.; Hu, J.; Zheng, L.; Chen, K. A BODIPY-Based "OFF-ON" Fluorescent Probe for Fast and Selective Detection of Hypochlorite in Living Cells. *Dye. Pigment.* **2019**, *170*, 107566. [CrossRef]
158. Li, Q.; Guo, Y.; Shao, S. A BODIPY Based Fluorescent Chemosensor for Cu(II) Ions and Homocysteine/Cysteine. *Sens. Actuators B Chem.* **2012**, *171–172*, 872–877. [CrossRef]
159. Elavarasan, K.; Saravanan, C.; Selvam, N.P.; Easwaramoorthi, S. Benzothiadiazole-Based Diarylamines as a Fluoride Sensor: Prevention of Fluoride Induced Decomposition of Receptor Molecule by Complex Formation with Cu^{2+}. *ChemistrySelect* **2018**, *3*, 10085–10090. [CrossRef]
160. Chen, F.; Zhang, J.; Qu, W.; Zhong, X.; Liu, H.; Ren, J.; He, H.; Zhang, X.; Wang, S. Development of a Novel Benzothiadiazole-Based Fluorescent Turn-on Probe for Highly Selective Detection of Glutathione over Cysteine/Homocysteine. *Sens. Actuators B Chem.* **2018**, *266*, 528–533. [CrossRef]
161. Lu, N.; Jiang, T.; Tan, H.; Hang, Y.; Yang, J.; Wang, J.; Qu, X.; Hua, J. A Red Fluorescent Turn-on Chemosensor for Al^{3+} Based on a Dimethoxy Triphenylamine Benzothiadiazole Derivative with Aggregation-Induced Emission. *Anal. Methods* **2017**, *9*, 2689–2695. [CrossRef]
162. Qiu, C.Q.; Li, L.Q.; Yao, S.L.; Liu, S.J.; Xu, H.; Zheng, T.F. Two Benzothiadiazole-Based Compounds as Multifunctional Fluorescent Sensors for Detection of Organic Amines and Anions. *Polyhedron* **2021**, *199*, 115100. [CrossRef]
163. Zhai, B.; Hu, Z.; Peng, C.; Liu, B.; Li, W.; Gao, C. Rational Design of a Colorimetric and Fluorescence Turn-on Chemosensor with Benzothiazolium Moiety for Cyanide Detection in Aqueous Solution. *Spectrochim. Acta Part A Mol. Biomol. Spectrosc.* **2020**, *224*, 117409. [CrossRef] [PubMed]
164. Liu, B.; Liu, J.; He, J.; Zhang, J.; Zhou, H.; Gao, C. A Novel Red-Emitting Fluorescent Probe for the Highly Selective Detection of Hg^{2+} Ion with AIE Mechanism. *Chem. Phys.* **2020**, *539*, 110944. [CrossRef]
165. Zhang, Q.; Zhang, J.; Zuo, H.; Wang, C.; Shen, Y. A Novel Colorimetric and Fluorescent Sensor for Cyanide Anions Detection Based on Triphenylamine and Benzothiadiazole. *Tetrahedron* **2016**, *72*, 1244–1248. [CrossRef]
166. Zhang, G.; Loch, A.S.; Kistemaker, J.C.M.; Burn, P.L.; Shaw, P.E. Dicyanovinyl-Based Fluorescent Sensors for Dual Mechanism Amine Sensing. *J. Mater. Chem. C Mater.* **2020**, *8*, 13723–13732. [CrossRef]
167. Cao, D.; Liu, Z.; Verwilst, P.; Koo, S.; Jangjili, P.; Kim, J.S.; Lin, W. Coumarin-Based Small-Molecule Fluorescent Chemosensors. *Chem. Rev.* **2019**, *119*, 10403–10519. [CrossRef]
168. Devendhiran, T.; Kumarasamy, K.; Lin, M.C.; Yang, Y.X. Synthesis and Physical Studies of Coumarin-Based Chemosensor for Cyanide Ions. *Inorg. Chem. Commun.* **2021**, *134*, 108951. [CrossRef]
169. Sun, X.Y.; Liu, T.; Sun, J.; Wang, X.J. Synthesis and Application of Coumarin Fluorescence Probes. *RSC Adv.* **2020**, *10*, 10826–10847. [CrossRef] [PubMed]
170. Janeková, H.; Gašpar, J.; Gáplovský, A.; Stankovičová, H. Selective Fluoride Chemosensors Based on Coumarin Semicarbazones. *J. Photochem. Photobiol. A Chem.* **2021**, *410*, 113168. [CrossRef]
171. Şenol, A.M.; Onganer, Y.; Meral, K. An Unusual "off-on" Fluorescence Sensor for Iron(III) Detection Based on Fluorescein–Reduced Graphene Oxide Functionalized with Polyethyleneimine. *Sens. Actuators B Chem.* **2017**, *239*, 343–351. [CrossRef]

172. Liu, D.; Wang, Y.; Wang, R.; Wang, B.; Chang, H.; Chen, J.; Yang, G.; He, H. Fluorescein-Based Fluorescent Sensor with High Selectivity for Mercury and Its Imaging in Living Cells. *Inorg. Chem. Commun.* **2018**, *89*, 46–50. [CrossRef]
173. Keerthana, S.; Sam, B.; George, L.; Sudhakar, Y.N.; Varghese, A. Fluorescein Based Fluorescence Sensors for the Selective Sensing of Various Analytes. *J. Fluoresc.* **2021**, *31*, 1251–1276. [CrossRef] [PubMed]
174. Rathod, R.V.; Bera, S.; Maity, P.; Mondal, D. Mechanochemical Synthesis of a Fluorescein-Based Sensor for the Selective Detection and Removal of Hg^{2+} Ions in Industrial Effluents. *ACS Omega* **2020**, *5*, 4982–4990. [CrossRef] [PubMed]
175. Rajasekar, M. Recent Development in Fluorescein Derivatives. *J. Mol. Struct.* **2021**, *1224*, 129085. [CrossRef]
176. Das, B.; Jana, A.; Das Mahapatra, A.; Chattopadhyay, D.; Dhara, A.; Mabhai, S.; Dey, S. Fluorescein Derived Schiff Base as Fluorimetric Zinc (II) Sensor via 'Turn on' Response and Its Application in Live Cell Imaging. *Spectrochim. Acta Part A Mol. Biomol. Spectrosc.* **2019**, *212*, 222–231. [CrossRef] [PubMed]
177. Hou, L.; Feng, J.; Wang, Y.; Dong, C.; Shuang, S.; Wang, Y. Single Fluorescein-Based Probe for Selective Colorimetric and Fluorometric Dual Sensing of Al^{3+} and Cu^{2+}. *Sens. Actuators B Chem.* **2017**, *247*, 451–460. [CrossRef]
178. Jiao, Y.; Liu, X.; Zhou, L.; He, H.; Zhou, P.; Duan, C.; Peng, X. A Fluorescein Derivative-Based Fluorescent Sensor for Selective Recognition of Copper(II) Ions. *J. Photochem. Photobiol. A Chem.* **2018**, *355*, 67–71. [CrossRef]
179. Yang, Y.; Gao, C.Y.; Liu, J.; Dong, D. Recent Developments in Rhodamine Salicylidene Hydrazone Chemosensors. *Anal. Methods* **2016**, *8*, 2863–2871. [CrossRef]
180. Jiao, Y.; Zhou, L.; He, H.; Yin, J.; Gao, Q.; Wei, J.; Duan, C.; Peng, X. A Novel Rhodamine B-Based "off-on" Fluorescent Sensor for Selective Recognition of Copper (II) Ions. *Talanta* **2018**, *184*, 143–148. [CrossRef]
181. Majumdar, A.; Lim, C.S.; Kim, H.M.; Ghosh, K. New Six-Membered PH-Insensitive Rhodamine Spirocycle in Selective Sensing of Cu^{2+} through C-C Bond Cleavage and Its Application in Cell Imaging. *ACS Omega* **2017**, *2*, 8167–8176. [CrossRef]
182. Cheng, J.; Yang, E.; Ding, P.; Tang, J.; Zhang, D.; Zhao, Y.; Ye, Y. Two Rhodamine Based Chemosensors for Sn^{4+} and the Application in Living Cells. *Sens. Actuators B Chem.* **2015**, *221*, 688–693. [CrossRef]
183. Arumugaperumal, R.; Srinivasadesikan, V.; Lin, M.C.; Shellaiah, M.; Shukla, T.; Lin, H.C. Facile Rhodamine-Based Colorimetric Sensors for Sequential Detections of Cu(II) Ions and Pyrophosphate ($P_2O_7^{4-}$) Anions. *RSC Adv.* **2016**, *6*, 106631–106640. [CrossRef]
184. Mwalupindi, A. Influence of Organized Media on the Absorption and Fluorescence Spectra of Auramine-O Dye. *Talanta* **1994**, *41*, 599–609. [CrossRef] [PubMed]
185. Sabnis, R.W. *Handbook of Biological Dyes and Stains—Synthesis and Industrial Applications*; John Wiley & Sons: Hoboken, NJ, USA, 2010.
186. Poulios, I.; Avranas, A.; Rekliti, E.; Zouboulis, A. Photocatalytic Oxidation of Auramine O in the Presence of Semiconducting Oxides. *J. Chem. Technol. Biotechnol.* **2000**, *75*, 205–212. [CrossRef]
187. Magde, D.; Rojas, G.E.; Seybold, P.G. Solvent Dependence of the Fluorescence Lifetimes of Xanthene Dyes. *Photochem. Photobiol.* **1999**, *70*, 737–744. [CrossRef]
188. Shabir, G.; Saeed, A.; Ali Channar, P. A Review on the Recent Trends in Synthetic Strategies and Applications of Xanthene Dyes. *Mini Rev. Org. Chem.* **2018**, *15*, 166–197. [CrossRef]
189. Padghan, S.D.; Wang, C.Y.; Liu, W.C.; Sun, S.S.; Liu, K.M.; Chen, K.Y. A Naphthalene-Based Colorimetric and Fluorometric Dual-Channel Chemodosimeter for Sensing Cyanide in a Wide PH Range. *Dye. Pigment.* **2020**, *183*, 108724. [CrossRef]
190. Muniyasamy, H.; Chinnadurai, C.; Nelson, M.; Chinnamadhaiyan, M.; Ayyanar, S. Triazole-Naphthalene Based Fluorescent Chemosensor for Highly Selective Naked Eye Detection of Carbonate Ion and Real Sample Analyses. *Inorg. Chem. Commun.* **2021**, *133*, 108883. [CrossRef]
191. Zhang, X.; Chen, S.; Jin, S.; Zhang, Y.; Chen, X.; Zhang, Z.; Shu, Q. Naphthalene Based Lab-on-a-Molecule for Fluorimetric and Colorimetric Sensing of F^- and CN^- and Nitroaromatic Explosives. *Sens. Actuators B Chem.* **2017**, *242*, 994–998. [CrossRef]
192. Zhang, W.; Zhao, X.; Gu, W.; Cheng, T.; Wang, B.; Jiang, Y.; Shen, J. A Novel Naphthalene-Based Fluorescent Probe for Highly Selective Detection of Cysteine with a Large Stokes Shift and Its Application in Bioimaging. *New J. Chem.* **2018**, *42*, 18109–18116. [CrossRef]
193. Xiao, N.; Zhang, C. Selective Monitoring of Cu(II) with a Fluorescence–on Naphthalene–Based Probe in Aqueous Solution. *Inorg. Chem. Commun.* **2019**, *107*, 107467. [CrossRef]
194. Attia, G.; Rahali, S.; Teka, S.; Fourati, N.; Zerrouki, C.; Seydou, M.; Chehimi, S.; Hayouni, S.; Mbakidi, J.P.; Bouquillon, S.; et al. Anthracene Based Surface Acoustic Wave Sensors for Picomolar Detection of Lead Ions. Correlation between Experimental Results and DFT Calculations. *Sens. Actuators B Chem.* **2018**, *276*, 349–355. [CrossRef]
195. Kaur, N.; Kaur, B. Recent Development in Anthracene Possessing Chemosensors for Cations and Anions. *Microchem. J.* **2020**, *158*, 105131. [CrossRef]
196. Kaur, B.; Gupta, A.; Kaur, N. A Novel, Anthracene-Based Naked Eye Probe for Detecting Hg^{2+} Ions in Aqueous as Well as Solid State Media. *Microchem. J.* **2020**, *153*, 104508. [CrossRef]
197. Prusti, B.; Chakravarty, M. Electron-Rich Anthracene-Based Twisted π-System as a Highly Fluorescent Dye: Easy Recognition of Solvents and Volatile Organic Compounds. *Dye. Pigment.* **2020**, *181*, 108543. [CrossRef]
198. Tümay, S.O.; Irani-nezhad, M.H.; Khataee, A. Development of Dipodal Fluorescence Sensor of Iron for Real Samples Based on Pyrene Modified Anthracene. *Spectrochim. Acta Part A Mol. Biomol. Spectrosc.* **2021**, *261*, 120017. [CrossRef] [PubMed]
199. Kathiravan, A.; Gowri, A.; Khamrang, T.; Kumar, M.D.; Dhenadhayalan, N.; Lin, K.C.; Velusamy, M.; Jaccob, M. Pyrene-Based Chemosensor for Picric Acid—Fundamentals to Smartphone Device Design. *Anal. Chem.* **2019**, *91*, 13244–13250. [CrossRef]

200. Ghorai, A.; Mondal, J.; Manna, A.K.; Chowdhury, S.; Patra, G.K. A Novel Pyrene Based Highly Selective Reversible Fluorescent-Colorimetric Sensor for the Rapid Detection of Cu^{2+} Ions: Application in Bio-Imaging. *Anal. Methods* **2018**, *10*, 1063–1073. [CrossRef]
201. Kowser, Z.; Rayhan, U.; Akther, T.; Redshaw, C.; Yamato, T. A Brief Review on Novel Pyrene Based Fluorometric and Colorimetric Chemosensors for the Detection of Cu^{2+}. *Mater. Chem. Front.* **2021**, *5*, 2173–2200. [CrossRef]
202. Xiao, T.; Wang, F.; Chen, Y.; Yang, X.; Wei, T.; Liu, C.; Chen, S.; Xu, Z.; Yoon, J.; Chen, X. Pyrene-Based Bisboronic Sensors for Multichannel Enantioselective Recognition of Tartaric Acid. *Dye. Pigment.* **2019**, *163*, 227–231. [CrossRef]
203. de Moliner, F.; Kielland, N.; Lavilla, R.; Vendrell, M. Modern Synthetic Avenues for the Preparation of Functional Fluorophores. *Angew. Chem.* **2017**, *56*, 3758–3769. [CrossRef]
204. Carvalho, R.L.; Dias, G.G.; Pereira, C.L.M.; Ghosh, P.; Maiti, D.; Da Silva, E.N. A Catalysis Guide Focusing on C-H Activation Processes. *J. Braz. Chem. Soc.* **2021**, *32*, 917–952. [CrossRef]
205. Machado, L.A.; Paz, E.R.S.; Araujo, M.H.; Almeida, L.D.; Bozzi, Í.A.O.; Dias, G.G.; Pereira, C.L.M.; Pedrosa, L.F.; Fantuzzi, F.; Martins, F.T.; et al. Ruthenium(II)-Catalyzed C−H/N−H Alkyne Annulation of Nonsymmetric Imidazoles: Mechanistic Insights by Computation and Photophysical Properties. *Eur. J. Org. Chem.* **2022**, *2022*, e202200590. [CrossRef]
206. Dias, G.G.; Paz, E.R.S.; Kadooca, J.Y.; Sabino, A.A.; Cury, L.A.; Torikai, K.; De Simone, C.A.; Fantuzzi, F.; Da Silva Júnior, E.N. Rhodium(III)-Catalyzed C-H/N-H Alkyne Annulation of Nonsymmetric 2-Aryl (Benz)Imidazole Derivatives: Photophysical and Mechanistic Insights. *J. Org. Chem.* **2021**, *86*, 264–278. [CrossRef]
207. Segawa, Y.; Maekawa, T.; Itami, K. Synthesis of Extended π-Systems through C-H Activation. *Ang. Chem.* **2015**, *54*, 66–81. [CrossRef]
208. Wang, K.; Zhang, J.; Hu, R.; Liu, C.; Bartholome, T.A.; Ge, H.; Li, B. Transition-Metal-Catalyzed C-C Bond-Forming Reactions via C-H Activation for the Development of Fluorescent Materials with Practical Value. *ACS Catal.* **2022**, *12*, 2796–2820. [CrossRef]
209. Li, B.; Ali, A.I.M.; Ge, H. Recent Advances in Using Transition-Metal-Catalyzed C–H Functionalization to Build Fluorescent Materials. *Chem* **2020**, *6*, 2591–2657. [CrossRef]
210. Ushakov, E.N.; Alfimov, M.V.; Gromov, S.P. Crown Ether-Based Optical Molecular Sensors and Photocontrolled Ionophores. *Macroheterocycles* **2010**, *3*, 189–200. [CrossRef]
211. Gokel, G.W.; Leevy, W.M.; Weber, M.E. Crown Ethers: Sensors for Ions and Molecular Scaffolds for Materials and Biological Models. *Chem. Rev.* **2004**, *104*, 2723–2750. [CrossRef]
212. Shahgaldian, P.; Pieles, U. Cyclodextrin Derivatives as Chiral Supramolecular Receptors for Enantioselective Sensing. *Sensors* **2006**, *6*, 593–615. [CrossRef]
213. Zhu, G.; Yi, Y.; Chen, J. Recent Advances for Cyclodextrin-Based Materials in Electrochemical Sensing. *Trends Anal. Chem.* **2016**, *80*, 232–241. [CrossRef]
214. Niu, X.; Mo, Z.; Yang, X.; Sun, M.; Zhao, P.; Li, Z.; Ouyang, M.; Liu, Z.; Gao, H.; Guo, R.; et al. Advances in the Use of Functional Composites of β-Cyclodextrin in Electrochemical Sensors. *Mikrochim. Acta* **2018**, *185*, 328. [CrossRef]
215. Ogoshi, T.; Harada, A. Chemical Sensors Based on Cyclodextrin Derivatives. *Sensors* **2008**, *8*, 4961–4982. [CrossRef]
216. Sayed, M. Unraveling PH-Responsive Contrasting Supramolecular Interaction of Acridine Orange with γ-Cyclodextrin. *J. Mol. Struct.* **2022**, *1261*, 132863. [CrossRef]
217. Prasad, N.; Shelar, S.; Sayed, M. PH Tolerant Metal Ion Controlled Luminescence Behaviour of Supramolecular Assembly and Its Application in Bioimaging and Supramolecular Logic Gate. *J. Mol. Liq.* **2023**, *369*, 120834. [CrossRef]
218. Lee, S.H.; Kim, J.Y.; Kim, S.K.; Lee, J.H.; Kim, J.S. Pyrene-Appended Calix[4]Crowned Logic Gates Involving Normal and Reverse PET: NOR, XNOR and INHIBIT. *Tetrahedron* **2004**, *60*, 5171–5176. [CrossRef]
219. Zhu, L.-N.; Gong, S.-L.; Gong, S.-L.; Yang, C.-L.; Qin, J.-G. Novel Pyrene-Armed Calix[4]Arenes through Triazole Connection: Ratiometric Fluorescent Chemosensor for Zn^{2+} and Promising Structure for Integrated Logic Gates. *Chin. J. Chem.* **2008**, *26*, 1424–1430. [CrossRef]
220. Kumar, R.; Sharma, A.; Singh, H.; Suating, P.; Kim, H.S.; Sunwoo, K.; Shim, I.; Gibb, B.C.; Kim, J.S. Revisiting Fluorescent Calixarenes: From Molecular Sensors to Smart Materials. *Chem. Rev.* **2019**, *119*, 9657–9721. [CrossRef]
221. Leray, I.; Valeur, B. Calixarene-Based Fluorescent Molecular Sensors for Toxic Metals. *Eur. J. Inorg. Chem.* **2009**, *2009*, 3525–3535. [CrossRef]
222. Mei, C.J.; Ahmad, S.A.A. A Review on the Determination Heavy Metals Ions Using Calixarene-Based Electrochemical Sensors. *Arab. J. Chem.* **2021**, *14*, 103303. [CrossRef]
223. Helttunen, K. Anion Responsive Molecular Switch Based on a Doubly Strapped Calix[4]Pyrrole. *Eur. J. Org. Chem.* **2022**, *2022*, e202200647. [CrossRef]
224. Peng, S.; He, Q.; Vargas-Zúñiga, G.I.; Qin, L.; Hwang, I.; Kim, S.K.; Heo, N.J.; Lee, C.-H.; Dutta, R.; Sessler, J.L. Strapped Calix[4]Pyrroles: From Syntheses to Applications. *Chem. Soc. Rev.* **2020**, *49*, 865–907. [CrossRef]
225. Lai, Z.; Zhao, T.; Sessler, J.L.; He, Q. Bis–Calix[4]Pyrroles: Preparation, Structure, Complexation Properties and Beyond. *Coord. Chem. Rev.* **2020**, *425*, 213528. [CrossRef]
226. Wagay, S.A.; Rather, I.A.; Ali, R. Functionalized Calix[4]Pyrroles: Emerging Class of Ion-Pair Receptors in Supramolecular Chemistry. *Mater. Today Proc.* **2021**, *36*, 657–678. [CrossRef]
227. Atwood, J.L.; Steed, J.W. *Supramolecular Chemistry*; John Wiley & Sons: Hoboken, NJ, USA, 2004; ISBN 0824747240.

228. Mohr, G.J. Chromo- and Fluororeactands: Indicators for Detection of Neutral Analytes by Using Reversible Covalent-Bond Chemistry. *Chem. Eur. J.* **2004**, *10*, 1082–1090. [CrossRef]
229. Ahn, S.; Kim, J.N.; Kim, Y.C. Solid State Solvation Effect of a Donor–Acceptor Type Fluorescent Molecule and Its Application to White Organic Light-Emitting Diodes. *Curr. Appl. Phys.* **2015**, *15*, S42–S47. [CrossRef]
230. Madhu, M.; Ramakrishnan, R.; Vijay, V.; Hariharan, M. Free Charge Carriers in Homo-Sorted π-Stacks of Donor–Acceptor Conjugates. *Chem. Rev.* **2021**, *121*, 8234–8284. [CrossRef]
231. Morokuma, K. Why Do Molecules Interact? The Origin of Electron Donor-Acceptor Complexes, Hydrogen Bonding and Proton Affinity. *Acc. Chem. Res.* **1977**, *10*, 294–300. [CrossRef]
232. Pond, S.J.K.; Tsutsumi, O.; Rumi, M.; Kwon, O.; Zojer, E.; Brédas, J.L.; Marder, S.R.; Perry, J.W. Metal-Ion Sensing Fluorophores with Large Two-Photon Absorption Cross Sections: Aza-Crown Ether Substituted Donor-Acceptor-Donor Distyrylbenzenes. *J. Am. Chem. Soc.* **2004**, *126*, 9291–9306. [CrossRef]
233. Mei, X.; Wen, G.; Wang, J.; Yao, H.; Zhao, Y.; Lin, Z.; Ling, Q. A Λ-Shaped Donor–π–Acceptor–π–Donor Molecule with AIEE and CIEE Activity and Sequential Logic Gate Behaviour. *J. Mater. Chem. C Mater.* **2015**, *3*, 7267–7271. [CrossRef]
234. Wan, X.; Li, C.; Zhang, M.; Chen, Y. Acceptor-Donor-Acceptor Type Molecules for High Performance Organic Photovoltaics-Chemistry and Mechanism. *Chem. Soc. Rev.* **2020**, *49*, 2828. [CrossRef]
235. Sharma, H.; Kakkar, R.; Bishnoi, S.; Milton, M.D. Synthesis of Acceptor-Donor-Acceptor Based Phenothiazine-5-Oxide Aldehydes Displaying Large Stokes Shift- "on-off-on" Acidofluorochromic Switch and Molecular Logic Gate Operation. *J. Photochem. Photobiol. A Chem.* **2022**, *430*, 113944. [CrossRef]
236. Wen, P.; Gao, Z.; Zhang, R.; Li, A.; Zhang, F.; Li, J.; Xie, J.; Wu, Y.; Wu, M.; Guo, K. A–π–D–π–A Carbazole Derivatives with Remarkable Solvatochromism and Mechanoresponsive Luminescence Turn-On. *J. Mater. Chem. C Mater.* **2017**, *5*, 6136–6143. [CrossRef]
237. Török, B.; Schäfer, C.; Kokel, A. Multicomponent Reactions. In *Heterogeneous Catalysis in Sustainable Synthesis*; Elsevier: Amsterdam, The Netherlands, 2022; pp. 443–489. ISBN 9780128178263.
238. Heravi, M.; Zadsirjan, V. Synthesis of Heterocycles via MCRs, Using a Name Reaction in Combination with Another Reaction. In *Recent Advances in Applications of Name Reactions in Multicomponent Reactions*; Elsevier: Amsterdam, The Netherlands, 2020; pp. 139–268. ISBN 978-0-12-818584-1.
239. Affeldt, R.F.; De Amorim Borges, A.C.; Russowsky, D.; Severo Rodembusch, F. Synthesis and Fluorescence Properties of Benzoxazole-1,4-Dihydropyridine Dyads Achieved by a Multicomponent Reaction. *New J. Chem.* **2014**, *38*, 4607–4614. [CrossRef]
240. Burchak, O.N.; Mugherli, L.; Ostuni, M.; Lacapère, J.J.; Balakirev, M.Y. Combinatorial Discovery of Fluorescent Pharmacophores by Multicomponent Reactions in Droplet Arrays. *J. Am. Chem. Soc.* **2011**, *133*, 10058–10061. [CrossRef] [PubMed]
241. Rocha, R.O.; Rodrigues, M.O.; Neto, B.A.D. Review on the Ugi Multicomponent Reaction Mechanism and the Use of Fluorescent Derivatives as Functional Chromophores. *ACS Omega* **2020**, *5*, 972–979. [CrossRef] [PubMed]
242. Vázquez-Romero, A.; Kielland, N.; Arévalo, M.J.; Preciado, S.; Mellanby, R.J.; Feng, Y.; Lavilla, R.; Vendrell, M. Multicomponent Reactions for de Novo Synthesis of Bodipy Probes: In Vivo Imaging of Phagocytic Macrophages. *J. Am. Chem. Soc.* **2013**, *135*, 16018–16021. [CrossRef]
243. Ahmed, F.; Xiong, H. Recent Developments in 1,2,3-Triazole-Based Chemosensors. *Dye. Pigment.* **2021**, *185*, 108905. [CrossRef]
244. Singh, G.; George, N.; Singh, R.; Singh, G.; Sushma; Kaur, G.; Singh, H.; Singh, J. Ion Recognition by 1,2,3-Triazole Moieties Synthesized via "Click Chemistry". *Appl. Organomet. Chem.* **2023**, *37*, e6897. [CrossRef]
245. Lau, Y.H.; Rutledge, P.J.; Watkinson, M.; Todd, M.H. Chemical Sensors That Incorporate Click-Derived Triazoles. *Chem. Soc. Rev.* **2011**, *40*, 2848–2866. [CrossRef]
246. Bryant, J.J.; Bunz, U.H.F. Click to Bind: Metal Sensors. *Chem. Asian J.* **2013**, *8*, 1354–1367. [CrossRef] [PubMed]
247. Ghosh, D.; Atkinson, A.; Gibson, J.; Subbaiahgari, H.; Ming, W.; Padgett, C.; Aiken, K.S.; Landge, S.M. 1,2,3-Triazoles: Controlled Switches in Logic Gate Applications. *Sensors* **2023**, *23*, 7000. [CrossRef] [PubMed]
248. Boiocchi, M.; Del Boca, L.; Esteban-Gómez, D.; Fabbrizzi, L.; Licchelli, M.; Monzani, E. Anion-Induced Urea Deprotonation. *Chem. Eur. J.* **2005**, *11*, 3097–3104. [CrossRef] [PubMed]
249. Ghosh, A.; Sengupta, A.; Chattopadhyay, A.; Das, D. A Single Probe for Sensing Both Acetate and Aluminum(Iii): Visible Region Detection, Red Fluorescence and Human Breast Cancer Cell Imaging. *RSC Adv.* **2015**, *5*, 24194–24199. [CrossRef]
250. Nguyen, B.T.; Anslyn, E.V. Indicator-Displacement Assays. *Coord. Chem. Rev.* **2006**, *250*, 3118–3127. [CrossRef]
251. Mawai, K.; Nathani, S.; Roy, P.; Singh, U.P.; Ghosh, K. Combined Experimental and Theoretical Studies on Selective Sensing of Zinc and Pyrophosphate Ions by Rational Design of Compartmental Chemosensor Probe: Dual Sensing Behaviour: Via Secondary Recognition Approach and Cell Imaging Studies. *Dalton Trans.* **2018**, *47*, 6421–6434. [CrossRef] [PubMed]
252. Nedeljko, P.; Turel, M.; Lobnik, A. Hybrid Sol-Gel Based Sensor Layers for Optical Determination of Biogenic Amines. *Sens. Actuators B Chem.* **2017**, *246*, 1066–1073. [CrossRef]
253. Buske, J.L.O.; Nicoleti, C.R.; Cavallaro, A.A.; Machado, V.G. 4-(Pyren-1-Ylimino)Methylphenol and Its Silylated Derivative as Chromogenic Chemosensors Highly Selective for Fluoride or Cyanide. *J. Braz. Chem. Soc.* **2015**, *26*, 2507–2519. [CrossRef]
254. Nandi, L.G.; Nicoleti, C.R.; Marini, V.G.; Bellettini, I.C.; Valandro, S.R.; Cavalheiro, C.C.S.; Machado, V.G. Optical Devices for the Detection of Cyanide in Water Based on Ethyl(Hydroxyethyl)Cellulose Functionalized with Perichromic Dyes. *Carbohydr. Polym.* **2017**, *157*, 1548–1556. [CrossRef]

255. Nicoleti, C.R.; Garcia, D.N.; Da Silva, L.E.; Begnini, I.M.; Rebelo, R.A.; Joussef, A.C.; Machado, V.G. Synthesis of 1,8-Naphthyridines and Their Application in the Development of Anionic Fluorogenic Chemosensors. *J. Fluoresc.* **2012**, *22*, 1033–1046. [CrossRef]
256. Bhaumik, C.; Maity, D.; Das, S.; Baitalik, S. Synthesis, structural characterization, solvatochromism, and ion-binding studies of a ditopic receptor based on 2-(4-[2,2′: 6′,2′′]terpyridin-4′-yl-phenyl)-1*H*-phenanthro[9,10-*d*] imidazole (tpy-HImzphen) unit. *RSC Adv.* **2012**, *2*, 2581–2594. [CrossRef]
257. Kim, S.Y.; Kim, M.J.; Ahn, M.; Lee, K.M.; Wee, K.R. Systematic Energy Band Gap Control of Pyrene Based Donor-Acceptor-Donor Molecules for Efficient Chemosensor. *Dye. Pigment.* **2021**, *191*, 109362. [CrossRef]
258. Yang, Y.; Zhao, Q.; Feng, W.; Li, F. Luminescent Chemodosimeters for Bioimaging. *Chem. Rev.* **2013**, *113*, 192–270. [CrossRef] [PubMed]
259. Quang, D.T.; Kim, J.S. Fluoro- and Chromogenic Chemodosimeters for Heavy Metal Ion Detection in Solution and Biospecimens. *Chem. Rev.* **2010**, *110*, 6280–6301. [CrossRef] [PubMed]
260. Souto, F.T.; Buske, J.L.d.O.; Nicoleti, C.R.; Dreyer, J.P.; Heying, R.d.S.; Bortoluzzi, A.J.; Machado, V.G. Chromogenic Chemodosimeter Based on a Silylated Azo Compound Detects Cyanide in Water and Cassava. *Spectrochim. Acta Part A Mol. Biomol. Spectrosc.* **2021**, *260*, 119950. [CrossRef] [PubMed]
261. Chen, P.; Bai, W.; Bao, Y. Fluorescent Chemodosimeters for Fluoride Ions via Silicon-Fluorine Chemistry: 20 Years of Progress. *J. Mater. Chem. C Mater.* **2019**, *7*, 11731–11746. [CrossRef]
262. Du, J.; Sheng, C.; Wang, Y.; Zhang, H.; Jiang, K. Determination of Trace Fluoride in Water Samples by Silylation and Gas Chromatography/Mass Spectrometry Analysis. *Rapid Commun. Mass. Spectrom.* **2021**, *35*, e9089. [CrossRef] [PubMed]
263. Li, Y.; Duan, Y.; Zheng, J.; Li, J.; Zhao, W.; Yang, S.; Yang, R. Self-Assembly of Graphene Oxide with a Silyl-Appended Spiropyran Dye for Rapid and Sensitive Colorimetric Detection of Fluoride Ions. *Anal. Chem.* **2013**, *85*, 11456–11463. [CrossRef] [PubMed]
264. Sánchez-Ruiz, A.; González-Alfaro, S.; García-Martínez, J.C.; Rodríguez-López, J. A Study of Silylated Tris(Styryl)Benzenes as Potential Fluorescent Sensors for Aqueous Fluoride. *Dye. Pigment.* **2020**, *182*, 108610. [CrossRef]
265. Mahapatra, A.K.; Mondal, S.; Manna, S.K.; Maiti, K.; Maji, R.; Ali, S.S.; Mandal, D.; Uddin, M.R.; Mandal, S. Reaction-Based Sensing of Fluoride Ions Using Desilylation Method for Triggering Excited-State Intramolecular Proton Transfer. *Supramol. Chem.* **2016**, *28*, 693–706. [CrossRef]
266. Nicoleti, C.R.; Nandi, L.G.; Ciancaleoni, G.; Machado, V.G. Spectrometric and Kinetics Studies Involving Anionic Chromogenic Chemodosimeters Based on Silylated Imines in Acetonitrile or Acetonitrile-Water Mixtures. *RSC Adv.* **2016**, *6*, 101853–101861. [CrossRef]
267. Song, I.H.; Yeom, G.S.; Kuwar, A.; Nimse, S.B. Elimination Reaction-Based Benzimidazole Probe for Cysteine Detection and Its Application in Serum Sample Analysis. *Biosensors* **2022**, *12*, 224.
268. Collier, C.P.; Wong, E.W.; Belohradský, M.; Raymo, F.M.; Stoddart, J.F.; Kuekes, P.J.; Williams, R.S.; Heath, J.R. Electronically Configurable Molecular-Based Logic Gates. *Science* **1999**, *285*, 391–394. [CrossRef] [PubMed]
269. Wagner, N.; Ashkenasy, G. Systems Chemistry: Logic Gates, Arithmetic Units, and Network Motifs in Small Networks. *Chem. Eur. J.* **2009**, *15*, 1765–1775. [CrossRef] [PubMed]
270. Ecik, E.T.; Atilgan, A.; Guliyev, R.; Uyar, T.B.; Gumus, A.; Akkaya, E.U. Modular Logic Gates: Cascading Independent Logic Gates via Metal Ion Signals. *Dalton Trans.* **2014**, *43*, 67–70. [CrossRef] [PubMed]
271. Magri, D.C.; de Silva, A.P. From PASS 1 to YES to AND Logic: Building Parallel Processing into Molecular Logic Gates by Sequential Addition of Receptors. *New J. Chem.* **2010**, *34*, 476–481. [CrossRef]
272. Erbas-Cakmak, S.; Kolemen, S.; Sedgwick, A.C.; Gunnlaugsson, T.; James, T.D.; Yoon, J.; Akkaya, E.U. Molecular Logic Gates: The Past, Present and Future. *Chem. Soc. Rev.* **2018**, *47*, 2228–2248. [CrossRef]
273. Balzani, V.; Credi, A.; Venturi, M. The Bottom-up Approach to Molecular-Level Devices and Machines. *Chem. Eur. J.* **2002**, *8*, 5524–5532. [CrossRef]
274. de Silva, A.P. *Molecular Logic-Based Computation*, 1st ed.; RSC Publishing: Cambridge, UK, 2012; ISBN 9781849731485.
275. de Silva, A.P.; Uchiyama, S. Molecular Logic Gates and Luminescent Sensors Based on Photoinduced Electron Transfer. In *Luminescence Applied in Sensor Science*; Prodi, L., Montalti, M., Zaccheroni, N., Eds.; Springer Science & Business Media: Berlin, Germany, 2010; Volume 300, pp. 1–28. [CrossRef]
276. Souto, F.T.; Dias, G.G. Input Selection Drives Molecular Logic Gate Design. *Analytica* **2023**, *4*, 456–499. [CrossRef]
277. Daly, B.; Silverson, V.A.D.; Yao, C.Y.; Chen, Z.Q.; de Silva, A.P. *Molecular Logic Gates as Fluorescent Sensors*, 2nd ed.; Elsevier: Amsterdam, The Netherlands, 2017; Volume 8, ISBN 9780128031988.
278. Budyka, M.F. Design Principles and Action of Molecular Logic Gates. *Russ. Chem. Bull.* **2015**, *63*, 1656–1665. [CrossRef]
279. Dhir, A.; Bhalla, V.; Kumar, M. Ratiometry of Monomer/Excimer Emissions of Dipyrenyl Thiacalix[4]Arene for Cu^{2+} Detection: A Potential Cu^{2+} and K^{+} Switched INHIBIT Logic Gate with NOT and YES Logic Functions. *Tetrahedron Lett.* **2008**, *49*, 4227–4230. [CrossRef]
280. Torawane, P.; Sahoo, S.K.; Borse, A.; Kuwar, A. A New Schiff Base as a Turn-off Fluorescent Sensor for Cu^{2+} and Its Photophysical Properties. *Luminescence* **2017**, *32*, 1426–1430. [CrossRef] [PubMed]
281. Maurya, N.; Singh, A.K. Indirect Approach for CN^{-} Detection via Cu^{2+} Induced Turn-off Sensor: Using Novel AIEE Fluorophore with Logic Gate and Antimicrobial Application. *Dye. Pigment.* **2017**, *147*, 484–490. [CrossRef]

282. Lee, K.S.; Kim, T.K.; Lee, J.H.; Kim, H.J.; Hong, J.I. Fluorescence Turn-on Probe for Homocysteine and Cysteine in Water. *Chem. Commun.* **2008**, 6173–6175. [CrossRef] [PubMed]
283. Kumar, V.; Anslyn, E. A Selective Turn-on Fluorescent Sensor for Sulfur Mustard Simulants. *J. Am. Chem. Soc.* **2013**, *135*, 6338–6344. [CrossRef] [PubMed]
284. Wu, S.; Zhang, K.; Wang, Y.; Mao, D.; Liu, X.; Yu, J.; Wang, L. A Novel Cr^{3+} Turn-on Probe Based on Naphthalimide and BINOL Framework. *Tetrahedron Lett.* **2014**, *55*, 351–353. [CrossRef]
285. Wang, W.; Yan, Y.; Wang, Q. A Fluorescence Turn-on Probe for Al(III) Based on a Naphthaldehyde Derivative. *Chem. Lett.* **2017**, *46*, 1605–1607. [CrossRef]
286. Beatty, M.A.; Borges-González, J.; Sinclair, N.J.; Pye, A.T.; Hof, F. Analyte-Driven Disassembly and Turn-On Fluorescent Sensing in Competitive Biological Media. *J. Am. Chem. Soc.* **2018**, *140*, 3500–3504. [CrossRef]
287. Zhang, S.; Sun, M.; Yan, Y.; Yu, H.; Yu, T.; Jiang, H.; Zhang, K.; Wang, S. A Turn-on Fluorescence Probe for the Selective and Sensitive Detection of Fluoride Ions. *Anal. Bioanal. Chem.* **2017**, *409*, 2075–2081. [CrossRef]
288. Gupta, R.C.; Dwivedi, S.K.; Razi, S.S.; Singh, P.; Koch, B.; Misra, A. A Chemodosimeter Exhibiting Fluorescence Turn-On Response to Detect Copper(II) Ions: Cell Imaging and Logic Function. *ChemistrySelect* **2019**, *4*, 2761–2765. [CrossRef]
289. Mohanasundaram, D.; Kumar, G.G.V.; Kumar, S.K.; Maddiboyina, B.; Raja, R.P.; Rajesh, J.; Sivaraman, G. Turn-on Fluorescence Sensor for Selective Detection of Fluoride Ion and Its Molecular Logic Gates Behavior. *J. Mol. Liq.* **2020**, *317*, 113913. [CrossRef]
290. Li, X.; Huo, F.; Yue, Y.; Zhang, Y.; Yin, C. A Coumarin-Based "off-on" Sensor for Fluorescence Selectivily Discriminating GSH from Cys/Hcy and Its Bioimaging in Living Cells. *Sens. Actuators B Chem.* **2017**, *253*, 42–49. [CrossRef]
291. Shukla, S.; Singh, S.; Mitra, M.D. Photosensitizer Modulated Turn-off Fluorescence System and Molecular Logic Functions for Selective Detection of Arsenic(III). *ChemistrySelect* **2020**, *5*, 13609–13618. [CrossRef]
292. Musib, D.; Devi, L.R.; Raza, M.K.; Chanu, S.B.; Roy, M. A New Thiophene-Based Aggregation-Induced Emission Chemosensor for Selective Detection of Zn^{2+} Ions and Its Turn Off. *Chem. Lett.* **2020**, *49*, 473–476. [CrossRef]
293. Midya, G.C.; Paladhi, S.; Bhowmik, S.; Saha, S.; Dash, J. Design and Synthesis of an On-off "Click" Fluorophore That Executes a Logic Operation and Detects Heavy and Transition Metal Ions in Water and Living Cells. *Org. Biomol. Chem.* **2013**, *11*, 3057–3063. [CrossRef] [PubMed]
294. Noushija, M.K.; Shanmughan, A.; Mohan, B.; Shanmugaraju, S. Selective Recognition and Reversible "Turn-Off" Fluorescence Sensing of Acetate (CH_3COO^-) Anion at Ppb Level Using a Simple Quinizarin Fluorescent Dye. *Chemistry* **2022**, *4*, 1407–1416.
295. Gauci, G.; Magri, D.C. Solvent-Polarity Reconfigurable Fluorescent 4-Piperazino-N-Aryl-1,8-Naphthalimide Crown Ether Logic Gates. *RSC Adv.* **2022**, *12*, 35270–35278. [CrossRef] [PubMed]
296. Tang, Z.; Yin, Z.-X.; Sun, X.; Cui, J.-Z.; Yang, J.; Wang, R.-S. Dynamically NAND Gate System on DNA Origami Template. *Comput. Biol. Med.* **2019**, *109*, 112–120. [CrossRef]
297. Fang, C.J.; Zhu, Z.; Sun, W.; Xu, C.H.; Yan, C.H. New TTF Derivatives: Several Molecular Logic Gates Based on Their Switchable Fluorescent Emissions. *New J. Chem.* **2007**, *31*, 580–586. [CrossRef]
298. Gunnlaugsson, T.; Mac Donail, D.A.; Parker, D. Luminescent Molecular Logic Gates: The Two-Input Inhibit (INH) Function. *Chem. Commun.* **2000**, *2000*, 93–94. [CrossRef]
299. Kim, H.N.; Lee, M.H.; Kim, H.J.; Kim, J.S.; Yoon, J. A New Trend in Rhodamine-Based Chemosensors: Application of Spirolactam Ring-Opening to Sensing Ions. *Chem. Soc. Rev.* **2008**, *37*, 1465–1472. [CrossRef] [PubMed]
300. Bai, C.B.; Qiao, R.; Liao, J.X.; Xiong, W.Z.; Zhang, J.; Chen, S.S.; Yang, S. A Highly Selective and Reversible Fluorescence "OFF-ON-OFF" Chemosensor for Hg^{2+} Based on Rhodamine-6G Dyes Derivative and Its Application as a Molecular Logic Gate. *Spectrochim. Acta Part A Mol. Biomol. Spectrosc.* **2018**, *202*, 252–259. [CrossRef] [PubMed]
301. Jilal, I.; el Barkany, S.; Bahari, Z.; Sundman, O.; el Idrissi, A.; Abou-Salama, M.; Romane, A.; Zannagui, C.; Amhamdi, H. New Quaternized Cellulose Based on Hydroxyethyl Cellulose (HEC) Grafted EDTA: Synthesis, Characterization and Application for Pb(II) and Cu(II) Removal. *Carbohydr. Polym.* **2018**, *180*, 156–167. [CrossRef] [PubMed]
302. Mondal, A.; Roy Chowdhury, A.; Bhuyan, S.; Mukhopadhyay, S.K.; Banerjee, P. A Simple Urea-Based Multianalyte and Multichannel Chemosensor for the Selective Detection of F^-, Hg^{2+} and Cu^{2+} in Solution and Cells and the Extraction of Hg^{2+} and Cu^{2+} from Real Water Sources: A Logic Gate Mimic Ensemble. *Dalton Trans.* **2019**, *48*, 4375–4386. [CrossRef] [PubMed]
303. Kumar, R.; Ravi, S.; David, C.I.; Nandhakumar, R. A Photo-Induced Electron Transfer Based Reversible Fluorescent Chemosensor for Specific Detection of Mercury (II) Ions and Its Applications in Logic Gate, Keypad Lock and Real Samples. *Arabian J. Chem.* **2021**, *14*, 102911. [CrossRef]
304. Li, Y.-P.; Yang, H.-R.; Zhao, Q.; Song, W.-C.; Han, J.; Bu, X.-H. Ratiometric and Selective Fluorescent Sensor for Zn^{2+} as an "off-on-off" Switch and Logic Gate. *Inorg. Chem.* **2012**, *51*, 9642–9648. [CrossRef] [PubMed]
305. Guo, Z.; Zhao, P.; Zhu, W.; Huang, X.; Xie, Y.; Tian, H. Intramolecular Charge-Transfer Process Based on Dicyanomethylene-4H-Pyran Derivative: An Integrated Operation of Half-Subtractor and Comparator. *J. Phys. Chem. C* **2008**, *112*, 7047–7053. [CrossRef]
306. Souto, F.T.; Machado, V.G. Hybrid Films Composed of Ethyl(Hydroxyethyl)Cellulose and Silica Xerogel Functionalized with a Fluorogenic Chemosensor for the Detection of Mercury in Water. *Carbohydr. Polym.* **2022**, *304*, 120480. [CrossRef]
307. Tripathy, M.; Subuddhi, U.; Patel, S. An Azo Dye Based D-π-A Chromogenic Probe for Selective Naked-Eye Detection of Hg^{2+} Ion: Application in Logic Gate Operation. *ChemistrySelect* **2020**, *5*, 4803–4815. [CrossRef]

308. Andréasson, J.; Straight, S.D.; Kodis, G.; Park, C.-D.; Hambourger, M.; Gervaldo, M.; Albinsson, B.; Moore, T.A.; Moore, A.L.; Gust, D. All-Photonic Molecular Half-Adder. *J. Am. Chem. Soc.* **2006**, *128*, 16259–16265. [CrossRef]
309. Qu, D.-H.; Wang, Q.-C.; Tian, H. A Half Adder Based on a Photochemically Driven [2]Rotaxane. *Angew. Chem.* **2005**, *117*, 5430–5433. [CrossRef]
310. Suresh, M.; Ghosh, A.; Das, A. Half-Subtractor Operation in PH Responsive N-Heterocyclic Amines. *Tetrahedron Lett.* **2007**, *48*, 8205–8208. [CrossRef]
311. Wang, S.; Zang, L.; Zhao, L.; Wang, X.; Hou, Q.; Jiang, S. A Molecular Half-Subtractor with Zn^{2+} and UV-Light as Inputs. *Spectrochim. Acta Part A Mol. Biomol. Spectrosc.* **2010**, *77*, 226–231. [CrossRef] [PubMed]
312. Zong, G.; Lu, G. A Molecular Half-Subtractor Based on a Fluorescence and Absorption Dual-Modal Sensor for Copper Ions. *Tetrahedron Lett.* **2008**, *49*, 5676–5679. [CrossRef]
313. Mondal, D.; Bar, M.; Maity, D.; Baitalik, S. Anthraimidazoledione-Terpyridine-Based Optical Chemosensor for Anions and Cations That Works as Molecular Half-Subtractor, Key-Pad Lock, and Memory Device. *J. Phys. Chem. C* **2015**, *119*, 25429–25441. [CrossRef]
314. Andréasson, J.; Straight, S.D.; Moore, T.A.; Moore, A.L.; Gust, D. Molecular All-Photonic Encoder−Decoder. *J. Am. Chem. Soc.* **2008**, *130*, 11122–11128. [CrossRef] [PubMed]
315. Andréasson, J.; Pischel, U. Smart Molecules at Work—Mimicking Advanced Logic Operations. *Chem. Soc. Rev.* **2010**, *39*, 174–188. [CrossRef] [PubMed]
316. Magri, D.C.; Brown, G.J.; McClean, G.D.; Prasanna De Silva, A. Communicating Chemical Congregation: A Molecular AND Logic Gate with Three Chemical Inputs as a "Lab-on-a-Molecule" Prototype. *J. Am. Chem. Soc.* **2006**, *128*, 4950–4951. [CrossRef] [PubMed]
317. Scerri, G.J.; Spiteri, J.C.; Mallia, C.J.; Magri, D.C. A Lab-on-a-Molecule with an Enhanced Fluorescent Readout on Detection of Three Chemical Species. *Chem. Comm.* **2019**, *55*, 4961–4964. [CrossRef]
318. Nepogodiev, S.A.; Stoddart, J.F. Cyclodextrin-Based Catenanes and Rotaxanes. *Chem. Rev.* **1998**, *98*, 1959–1976. [CrossRef]
319. Fioravanti, G. Benzylic Amide Rotaxanes: A Versatile Architecture. *Curr. Org. Synth.* **2012**, *9*, 199–214. [CrossRef]
320. Gavina, P.; Tatay, S. Synthetic Strategies for the Construction of Threaded and Interlocked Molecules. *Curr. Org. Synth.* **2010**, *7*, 24–43. [CrossRef]
321. García-Río, L.; Otero-Espinar, F.J.; Luzardo-Alvarez, A.; Blanco-Méndez, J. Cyclodextrin Based Rotaxanes, Polyrotaxanes and Polypseudorotaxanes and Their Biomedical Applications. *Curr. Top. Med. Chem.* **2014**, *14*, 478–493. [CrossRef] [PubMed]
322. Miyagawa, S.; Kimura, M.; Kagami, S.; Kawasaki, T.; Tokunaga, Y. Utilization of a Crown Ether/Amine-Type Rotaxane as a Probe for the Versatile Detection of Anions and Acids by Thin-Layer Chromatography. *Chem. Asian J.* **2020**, *15*, 3044–3049. [CrossRef]
323. Fielden, S.D.P.; Leigh, D.A.; McTernan, C.T.; Perez-Saavedra, B.; Vitorica-Yrezabal, I.J. Spontaneous Assembly of Rotaxanes from a Primary Amine, Crown Ether and Electrophile. *J. Am. Chem. Soc.* **2018**, *140*, 6049–6052. [CrossRef]
324. Langton, M.J.; Beer, P.D. Rotaxane and Catenane Host Structures for Sensing Charged Guest Species. *Acc. Chem. Res.* **2014**, *47*, 1935–1949. [CrossRef]
325. Ashton, P.R.; Baldoni, V.; Balzani, V.; Credi, A.; Hoffmann, H.D.A.; Martinez-Diaz, M.V.; Raymo, F.M.; Stoddart, J.F.; Venturi, M. Dual-Mode "Co-Conformational" Switching in Catenanes Incorporating Bipyridinium and Dialkylammonium Recognition Sites. *Chem. Eur. J.* **2001**, *7*, 3482–3493. [CrossRef]
326. Li, H.; Zhang, J.-N.; Zhou, W.; Zhang, H.; Zhang, Q.; Qu, D.-H.; Tian, H. Dual-Mode Operation of a Bistable [1]Rotaxane with a Fluorescence Signal. *Org. Lett.* **2013**, *15*, 3070–3073. [CrossRef] [PubMed]
327. Klein, H.A.; Kuhn, H.; Beer, P.D. Anion and PH Dependent Molecular Motion by a Halogen Bonding [2]Rotaxane. *Chem. Commun.* **2019**, *55*, 9975–9978. [CrossRef]
328. Bai, L.; Xu, Y.; Li, L.; Tao, F.; Wang, S.; Wang, L.; Li, G. An Efficient Water-Soluble Fluorescent Chemosensor Based on Furan Schiff Base Functionalized PEG for the Sensitive Detection of Al^{3+} in Pure Aqueous Solution. *New J. Chem.* **2020**, *44*, 11148–11154. [CrossRef]
329. Zhou, Z.; Wu, H.; Li, F.; Ma, L.; Qiao, X. Hypochlorite Responsive Ratiometric Fluorescent Switch and Logic Gates Based on Lanthanide Functionalized Polymer Nanosphere. *Dye. Pigment.* **2020**, *174*, 108033. [CrossRef]
330. Barnoy, E.A.; Popovtzer, R.; Fixler, D. Fluorescence for Biological Logic Gates. *J. Biophotonics* **2020**, *13*, e202000158. [CrossRef] [PubMed]
331. Schneider, H.J. Logic-Gate Functions in Chemomechanical Materials. *ChemPhysChem* **2017**, *18*, 2306–2313. [CrossRef] [PubMed]
332. Yin, F.; Wang, F.; Fan, C.; Zuo, X.; Li, Q. Biosensors Based on DNA Logic Gates. *View* **2021**, *2*, 20200038. [CrossRef]
333. Tregubov, A.A.; Nikitin, P.I.; Nikitin, M.P. Advanced Smart Nanomaterials with Integrated Logic-Gating and Biocomputing: Dawn of Theranostic Nanorobots. *Chem. Rev.* **2018**, *118*, 10294–10348. [CrossRef] [PubMed]
334. Raynal, M.; Ballester, P.; Vidal-Ferran, A.; van Leeuwen, P.W.N.M. Supramolecular Catalysis. Part 1: Non-Covalent Interactions as a Tool for Building and Modifying Homogeneous Catalysts. *Chem. Soc. Rev.* **2014**, *43*, 1660–1733. [CrossRef] [PubMed]
335. Ballester, P.; Vidal-Ferran, A.; van Leeuwen, P.W.N.M. *Modern Strategies in Supramolecular Catalysis*, 1st ed.; Elsevier Inc.: Amsterdam, The Netherlands, 2011; Volume 54, ISBN 978-0-12-387772-7.
336. Liu, Z.; Sun, Q.; Yan, M.; Zhang, C.; Yuan, H.; He, W. Activity-Based Fluorescent Molecular Logic Gate Probe for Dynamic Tracking of Mitophagy Induced by Oxidative Stress. *Anal. Chem.* **2021**, *93*, 3502–3509. [CrossRef] [PubMed]
337. de Silva, A.P.; McClean, G.D.; Pagliari, S. Direct Detection of Ion Pairs by Fluorescence Enhancement. *Chem. Commun.* **2003**, *16*, 2010–2011. [CrossRef] [PubMed]

338. Chen, J.; Pan, J.; Liu, C. Versatile Sensing Platform for Cd^{2+} Detection in Rice Samples and Its Applications in Logic Gate Computation. *Anal. Chem.* **2020**, *92*, 6173–6180. [CrossRef]
339. Muthusamy, S.; Rajalakshmi, K.; Zhu, D.; Zhu, W.; Wang, S.; Lee, K.B.; Xu, H.; Zhao, L. Dual Detection of Mercury(II) and Lead(II) Ions Using a Facile Coumarin-Based Fluorescent Probe via Excited State Intramolecular Proton Transfer and Photo-Induced Electron Transfer Processes. *Sens. Actuators B Chem.* **2021**, *346*, 130534. [CrossRef]
340. Klockow, J.L.; Hettie, K.S.; Glass, T.E. ExoSensor 517: A Dual-Analyte Fluorescent Chemosensor for Visualizing Neurotransmitter Exocytosis. *ACS Chem. Neurosci.* **2013**, *4*, 1334–1338. [CrossRef]
341. Sachdeva, T.; Milton, M.D. Novel Push-Pull Based Phenothiazine-Benzothiazole Derivatives Integrated with Molecular Logic Gate Operation for Reversible Volatile Acid Detection. *J. Mol. Struct.* **2021**, *1243*, 130768. [CrossRef]
342. Matsuura, S.; Ono, H.; Kawasaki, S.; Kuang, Y.; Fujita, Y.; Saito, H. Synthetic RNA-Based Logic Computation in Mammalian Cells. *Nat. Commun.* **2018**, *9*, 4847. [CrossRef] [PubMed]
343. Magri, D.C.; Spiteri, J.C. Proof of Principle of a Three-Input AND-INHIBIT-OR Combinatorial Logic Gate Array. *Org. Biomol. Chem.* **2017**, *15*, 6706–6709. [CrossRef] [PubMed]
344. Chen, K.; Schmittel, M. A Triple-Channel Lab-on-a-Molecule for Triple-Anion Quantification Using an Iridium(III)–Imidazolium Conjugate. *Chem. Commun.* **2014**, *50*, 5756–5759. [CrossRef]
345. Sandhu, S.; Kumar, R.; Tripathi, N.; Singh, H.; Singh, P.; Kumar, S. Lab-on-a-Molecule Elaboration for Fluorescence Based Discrimination of Commercial Surfactants Sodium Dodecyl Sulfate and Sodium Dodecylbenzenesulfonate. *Sens. Actuators B Chem.* **2017**, *241*, 8–18. [CrossRef]
346. Chen, M.; Wang, C.; Ding, Z.; Wang, H.; Wang, Y.; Liu, Z. A Molecular Logic Gate for Developing "AND" Logic Probes and the Application in Hepatopathy Differentiation. *ACS Cent. Sci.* **2022**, *8*, 837–844. [CrossRef]
347. Konry, T.; Walt, D.R. Intelligent Medical Diagnostics via Molecular Logic. *J. Am. Chem. Soc.* **2009**, *131*, 13232–13233. [CrossRef]
348. Singh, G.; Gupta, S.; Priyanka; Puspa; Rani, B.; Kaur, H.; Vikas; Yadav, R.; Sehgal, R. Designing of Bis-Organosilanes as Dual Chemosensor for Sn(II) and Al(III) Ions: Antibacterial Activity and in Silico Molecular Docking Study. *Spectrochim. Acta Part A Mol. Biomol. Spectrosc.* **2024**, *305*, 123435. [CrossRef]
349. Paul, S.; Mondal, U.; Nag, S.; Seth, M.; Banerjee, P. Unveiling of a Smartphone-Mediated Ratiometric Chemosensor towards the Nanomolar Level Detection of Lethal CN^{-}: Combined Experimental and Theoretical Validation with the Proposition of a Molecular Logic Circuitry. *RSC Adv.* **2022**, *12*, 12564–12572. [CrossRef]
350. Prabakaran, G.; Vickram, R.; Velmurugan, K.; Immanuel David, C.; Prince Makarios Paul, S.; Suresh Kumar, R.; Almansour, A.I.; Perumal, K.; Abiram, A.; Prabhu, J.; et al. A Lead Selective Dimeric Quinoline Based Fluorescent Chemosensor and Its Applications in Milk and Honey Samples, Smartphone and Bio-Imaging. *Food Chem.* **2022**, *395*, 133617. [CrossRef] [PubMed]
351. Tang, Y.; Liu, S.; Hao, X.; Wang, Z.; Liang, M.; Lu, Y.; Zhou, X. Near-Infrared Molecular Logic Gate for In Situ Construction and Quantification of Cell–Macromolecule Conjugates. *Anal. Chem.* **2023**, *95*, 15818–15825. [CrossRef] [PubMed]
352. Das, G.C.; Kumar Das, A.; Das, D.; Raj Maity, T.; Samanta, A.; Ali Alasmary, F.; Salem Almalki, A.; Iqbal, A.; Dolai, M. Ortho-Vanillin Based Multifunctional Scaffold for Selective Detection of Al^{3+} and Zn^{2+} Employing Molecular Logic with DFT Study and Cell Imaging with Live Grass Pea. *J. Photochem. Photobiol. A Chem.* **2023**, *440*, 114663. [CrossRef]
353. Almammadov, T.; Dirak, M.; Saymaz, A.; Acari, A.; Kolemen, S. A Hydrogen Sulfide and Tyrosinase Responsive Dual-Locked Fluorophore for Selective Imaging of Melanoma Cells. *Chem. Commun.* **2023**, *59*, 9972–9975. [CrossRef] [PubMed]
354. Kundu, S.; Mondal, D.; Rajasekaran, V.V.; Goswami, A.; Schmittel, M. Three-Input Logic AND Gate Drives Sequential Three-Step Catalysis by Parallel Activation of H^{+} and Ag^{+} as a Catalyst Duo. *Inorg. Chem.* **2022**, *61*, 17007–17011. [CrossRef]
355. Chen, T.; Liu, P.; Wang, H.; Su, Y.; Li, S.; Ma, S.; Xu, X.; Wen, J.; Zou, Z. Dumbbell-Type Triplex Molecular Switch-Based Logic Molecular Assays of SARS-CoV-2. *Sens. Actuators B Chem.* **2022**, *371*, 132579. [CrossRef]